DOCTORAL THESIS

Presented to the Department of Pharmacy
Graduate School of Pharmaceutical Science, XXXIII Cycle

University of Naples Federico II

Self-assembling nanoparticles for drug delivery in tumors: insights for novel applications and industrial development.

Ph.D. Thesis
LORENA SCOTTI

Approved by
Ph.D. Supervisor: Prof. Giuseppe De Rosa
Ph.D. Program Coordinator: Prof. Maria Valeria D'Auria

ABSTRACT

Hybrid self-assembling nanoparticles (SANPs) have been previously designed as novel drug delivery system, with an easy scale-up, that overcome stability issues following long-term storage. This system has been successfully used to deliver anionic-charged agents, e.g. bisphosphonates, in different types of tumors, such as glioblastoma. Here, further insights have been provided for SANPs to promote the technology transfer and to found novel potential applications for this technology.

More in details, the Ph.D. activity has been organized in two different directions. The first one aimed to support the industrial development of SANPs encapsulating zoledronic acid. More in details, following a deep characterization of each component, namely PEGylated liposomes, human transferrin, calcium-phosphate nanoparticles and zoledronic acid solution, the preparation protocol of SANPs encapsulating zoledronic acid was modified to adapt the formulation to the preparation in the plant of the company owner of a license agreement on the SANPs technology. Finally, a first kit of the formulation, named as EDROMA, was entirely prepared by the company and assembled to obtain the first “industrial” batch of EDROMA. Thus, this part of the work demonstrated the industrial transferability of the SANPs technology. In the second phase of this first part of the Ph.D. activity, the development of a formulation strategy, able to simplify the preparation protocol of the product, was investigated. In particular, the study was focused on the development of a strategy to freeze-dry SANPs-containing zoledronic acid. More in details, a thermodynamic study was carried out to select the cryoprotectants able to preserve the product during the lyophilization process. The dried product was analyzed in term of physical-chemical characteristics. Moreover, *in vitro* and *in vivo* studies were set up to demonstrate that SANPs encapsulating zoledronic acid, reconstituted following freeze-drying, maintained the ability to inhibit glioblastoma (GBM) cell viability and tumor regression.

A second direction of the Ph.D. thesis has been focused on the research of novel applications for SANPs. In particular, in the first project of this second part of the Ph.D. activity, the SANPs technology has been optimized for

encapsulation and delivery of miRNA. To this aim, SANPs with different lipids were prepared and characterized, in terms of size, polydispersity index, zeta potential, miRNA encapsulation, stability in bovine serum albumin (BSA), serum and hemolytic activity. Then, SANPs were tested *in vitro* on two different cell lines of GBM. Finally, miRNA biodistribution was tested *in vivo* in an orthotopic model of GBM. The majority of the formulations showed good technological characteristics and were stable in BSA and serum with a low hemolytic activity. Cell cloture studies showed that SANPs allowed enhance the miRNA intracellular delivery. Finally, *in vivo* biodistribution studies demonstrated that the optimized SANP formulations were able to deliver miRNA in different organs, e.g. the brain.

Finally, in the last part of the Ph.D. activity, the modification of SANPs surface with hyaluronic acid (HA) for targeting of CD44-overexpressing cells was investigated. More in details, SANPs including different molecular weight HA were prepared by two different protocols and with or without PEGylated lipid. Zoledronic acid was encapsulated as model drug. SANPs were fully characterized and the selected formulations were investigated on cell culture to investigate the CD44 targeting.

LIST OF PUBLICATIONS

- **Urotensin-II-Targeted Liposomes as a New Drug Delivery System towards Prostate and Colon Cancer Cells.** Silvia Zappavigna, Marianna Abate, Alessia Maria Cossu, Sara Lusa, Virginia Campani, Lorena Scotti, Amalia Luce, Ali Munaim Yousif, Francesco Merlino, Paolo Grieco, Giuseppe De Rosa, and Michele Caraglia. Journal of Oncology. **2019** Dec 17; doi: 10.1155/2019/9293560

- **Skin permeation and thermodynamic features of curcumin-loaded liposomes.** Virginia Campani, Lorena Scotti, Teresa Silvestri, Marco Biondi and Giuseppe De Rosa. Journal of Materials Science: Materials in Medicine. **2020** Jan 21; JMSM-D-19-00386R1; doi:10.1007/s10856-019-6351-6

- **ABCA1/ABCB1 Ratio Determines Chemo- and Immune-Sensitivity in Human Osteosarcoma.** Dimas Carolina Belisario, Muhlis Akman, Martina Godel, Virginia Campani, Maria Pia Patrizio, Lorena Scotti, Claudia Maria Hattinger, Giuseppe De Rosa, Massimo Donadelli, Massimo Serra, Joanna Kopecka and Chiara Riganti. Cells **2020** Mar 6, 9, 647; doi:10.3390/cells9030647

- ***In Vitro* Biophysical and Biological Characterization of Lipid Nanoparticles Co-Encapsulating Oncosuppressors miR-199b-5p and miR-204-5p as Potentiators of Target Therapy in Metastatic Melanoma.** Luigi Fattore, Virginia Campani, Ciro Francesco Ruggiero, Valentina Salvati, Domenico Liguoro, Lorena Scotti, Gerardo Botti, Paolo Antonio Ascierto, Rita Mancini, Giuseppe De Rosa and Gennaro Ciliberto. Int. J. Mol. Sci. **2020** Mar 12, 21(6), 1930; doi:10.3390/ijms21061930

- **Hybrid lipid self-assembling nanoparticles for brain delivery of microRNA.** Virginia Campani, Silvia Zappavigna, Lorena Scotti, Marianna Abate, Manuela Porru, Carlo Leonetti, Michele Caraglia, Giuseppe De Rosa. International Journal of Pharmaceutics Volume 588, **2020** Ago 2; doi: 10.1016/j.ijpharm.2020.119693

- **Freeze-drying of self-assembling nanoparticles: physical-chemical and biological characterization.** Lorena Scotti, Silvia Zappavigna, Marianna Abate, Manuela Porru, Virginia Campani, Michele Caraglia, Carlo Leonetti, Giuseppe De Rosa. **Manuscript in preparation.**

LIST OF ABBREVIATIONS

∆H	Enthalpy
ABS	Absorbance
BBB	Blood-brain barrier
BSA	Bovine serum albumin
BSD	Backscatter detector
$CaCl_2$	Calcium chloride
CaP NPs	Calcium-Phosphate nanoparticles
CaPZ	Calcium-Phosphate nanoparticles complexed with Zoledronic acid
CD44	Cluster of differentiation 44
cer-PEG	N-palmitoyl-sphingosine-1 {succinyl[methoxy(polyethylene glycol)$_{2000}$]} (PEG_{2000}-Cer^{16})
CHOL	Cholesterol
CNS	Central nervous system
Cryo	Cryoprotectant
CQAs	Critical quality attributes
Ct	Cross-threshold
DA	Degree of association
DC-chol	3ß-[N-(N',N'-dimethylaminoethane)-carbamoyl]cholesterol hydrochloride
DLS	Dynamic light scattering
DMSO	Dimethyl sulfoxide
DNA	Deoxyribonucleic acid
DOPE	Dioleoylphosphatidylethanolamine
DOTAP	1,2-dioleoyl-3-trimethylammonium-propane chloride
DOTMA	N-[1-(2,3-dioleyloxy)propyl]-N,N,N-trimethylammonium chloride
DSC	Differential scanning calorimeter
DSPE-PEG	1,2-distearoyl-sn-glycero-3-phosphoethanolamine-N-[amino(polyethylene glycol)-2000]
EE	Encapsulation efficiency
EMA	European medicine agency
EPR	Permeation and retention effect

FDA	Food and drug administration
FPPS	Farnesyl pirophosphate synthase
GC	Gas-chromatography
GBM	Glioblastoma multiforme
GMP	Good manufacturing practices
HA	Hyaluronic acid
HBS	HEPES buffer solution
HPLC	High performance liquid chromatography
ICAM-1	Intercellular adhesion molecule-1
K_2HPO_4	Potassium phosphate dibasic
KCl	Potassium chloride
MGMT	O^6-methylguanine-methyl transferase
microRNA	Micro riboNucleic acid
miRNA	Micro riboNucleic acid
Na_2HPO_4	Sodium phosphate dibasic
NaCl	Sodium Chloride
NaOH	Sodium hydroxide
NBP	Amino-bisphosphonate
nc-RNA	Non-coding RNA
NPs	Nanoparticles
NTA	Nanoparticle tracking analysis
O-Met	5'-O-methyl nucleotides
PBS	Phosphate buffer solution
PCS	Photon correlation spectroscopy
PI	Polydispersity index
PLs	PEGylated liposomes
ppH_2O	Partial pressur of water
R&D	Research and development
RHAMM	Receptor for HA-mediated motility
SANPs	Self assembling nanoparticles
sd	Standard deviation
SED	Secondary electron detector
SEM	Scanning electron microscope
SRB	Sulphorhodamine B

Teu	Eutectic temperature
Tf	Human transferrin
TFF	Tangential flow filtration
Tg	Transition glass temperature
TJs	Tight junctions
TMZ	Temozolomide
UHPLC	Ultra-high performance liquid chromatography
USP	United states pharmacopeia
WHO	World health organization
wt	Wild type
ζ	Zeta potential
Zol	Zoledronic acid

LIST OF FIGURES

LIST OF TABLES

TABLE OF CONTENTS

CHAPTER 4

Self-assembling nanoparticles for delivery of microRNA to the brain to revert chemoresistance in therapy against glioblastoma

CHAPTER 5

SANPs modification with hyaluronic acid for targeting of CD44-overexpressing cell

CHAPTER 1

General introduction

1.1 Nano-carriers based formulations as drug delivery system in anticancer therapy

Cancer is one of the major causes of death worldwide. According to WHO (World Health Organization) new cancer diagnoses are about 18 million each year. Currently, cancer represents the second cause of death after cardiovascular diseases [Siegel *et al.*, 2020]. Surgery, chemotherapy, immunotherapy and radiotherapy, in combination, simultaneously or sequentially, are different possibilities for the treatment of cancer.

In particular, chemotherapy is based on the use of antineoplastic drugs able to kill tumor cells. Ideally, an anticancer drug should perform its cytotoxicity selectively against the tumoral tissue. However, the majority of the anticancer agents have low therapeutic indexes and poor specificity. Indeed, chemotherapeutics cause damage to cancer cells as well as to normal cells, with consequent serious side effects. Therefore, it is necessary that administrated drugs act on the cancerous tissue without affecting other normal cells and maintain stable state *in vivo* microenvironments until they are delivered [Lee *et al*., 2020]. In the last years, innovative therapeutic strategies, such as gene therapy, immunotherapy, targeted therapy, neoadjuvant therapy, and natural products, have become valid alternatives to replace classic anticancer drugs [Falzone *et al.*, 2018]. However, these approaches require often the use of biomacromolecules such as proteins, peptides, nucleic acids, etc. characterized by a poor biopharmaceutical profile, due to the rapid degradation in biological fluids, inability to cross the intact endothelia and poor uptake into the cells.

In this context, over the past two decades, nano-carriers based formulations for drug delivery and targeting have emerged as tool to overcome the limitations of the common chemotherapy [Shi *et al*., 2017]. The growing number of publications on nanotechnology and drug delivery contributed to the development of a new science named nanomedicine, in which drug

administration, pharmacokinetic and pharmacodynamic, is affected by the use of materials organized in nanoscale structures. A number of nanotechnology-based pharmaceutical products are today on the market for different applications, especially for cancer [Bisso and Leroux, 2020; Crommelin *et al.*, 2020; He *et al.*, 2019]. A well-designed nano-system, in terms of size and circulation half-life, could promote a controlled release of the loaded drug(s), thus facilitating a better clinical result with reduced aggression compared to classical chemotherapeutics. Moreover, these systems are able to protect encapsulated drugs from the premature chemical/enzymatic degradation, improving their bioavailability into target sites and thus their therapeutic efficacy. Finally, one of the most challenging tasks in the design of nano-carriers is an efficient drug accumulation into target sites. Indeed, they can passively accumulate into tumors taking advantage of enhanced permeation and retention effect (EPR) [Fang *et al*., 2020], associated with increased permeability of blood vessels in the tumor area. This, in principle, increases the chance of drug accumulation in solid tumor tissues. The particles properties are the key parameter in this case; after administration, size, surface behaviours and composition are crucial for the solubility and stability of the loaded drug(s), as well as for the interactions with cells [Aktaş *et al*., 2005; Au *et al*., 2001; Ruoslahti *et al*., 2010]. On the other hand, drugs can be selectively delivered to the target site by an active targeting. This strategy provides the functionalization of the carriers surface with specific ligands, such as proteins, antibodies and nucleic acids, able to recognize and bind specific receptors overexpressed by cancer cells, thus allowing a greater accumulation into tumor [Kommareddy *et al*., 2005].

1.2 Glioblastoma Multiforme (GBM)

One of the opened challenges in cancer therapy remains the treatment of tumors affecting central nervous system (CNS). Nowadays, primary malignant tumors affecting CNS represent about 2% of all cancers [Buckner 2007]. One of the most spread of these cancers is the astrocytoma, a tumor that affects the neuroglia cells. In Europe, about 27,000 new cases of malignant astrocytic tumors are diagnosed per year. The most common astrocytic tumor is

glioblastoma multiforme (GBM), representing alone slightly more than 50% of the total astrocytomas [Sant, 2012].

GBM is the most malignant of all astrocytic tumors and is characterised by poorly differentiated neoplastic astrocytes. Its histopathological features include cellular polymorphism, nuclear atypia, mitotic activity, vascular thrombosis, microvascular proliferation and necrosis [Louis 2007]. GBM is a highly aggressive brain tumor with poor prognosis, indeed the median survival period for patients harbouring GBM, currently treated with radiotherapy in combination with chemotherapy with temozolomide (TMZ), remains less than 15 months [Stupp 2009]. Moreover, the viability of patients affected by GBM does not exceed 9-15 months and, only in 9-25% of cases, it reaches 2 years [Zhang 2016].

GBM and anaplastic tumors are often irregular in shape and frequently they have a necrotic centre. In particular, the glioblastoma multiforme usually exhibits a "ring" or "ring-like" zone around a dark central area of necrosis. Several groups have identified correlations between the expression of particular molecularly defined oncogenic pathways in the GBM and malignant phenotypes. Therefore, among genetic alterations, hypermethylation of the O^6-methylguanine-methyl transferase (MGMT) promoter is rather frequent; it causes MGMT gene silencing and reduce DNA repair. MGMT specifically removes mutagenic, carcinogenic and cytotoxic O^6-alkylguanine DNA adducts. This explains that MGMT promoter hypermethylation correlates with increased sensitivity to alkylating chemotherapy in tumors. MGMT promoter hypermethylation is associated with up to 50% of the diffuse astrocytomas [Weller 2012].

Although chemotherapy provides only modest benefit for many patients with brain tumors, it plays an increasingly important role in palliation and can have an adjuvant effect in combination with surgery and radiation therapy. The most commonly used agent is the temozolomide, which penetrates the intact blood-brain barrier and produces benefit in many patients with glioma [Buckner 2007].

1.3 Issues of the development of nanocarriers based formulations and self-assembling nanoparticles

The treatment of neurological disease, such as brain cancer or neurodegenerative diseases, is one of the most difficult challenges in medicine. The main limit of conventional chemotherapy in the treatment of brain tumors is the inability of most of the anti-cancer agents to reach effective concentrations within brain parenchyma, when these agents were intravenously administrated. The drug transport from the bloodstream to the CNS is hindered by the presence of an endothelium characterized by low permeability, and by the blood brain barrier (BBB), whose cells are linked by tight junctions (TJs) that hindered the passage of non-lipophilic solutes from blood to brain and *vice versa* [Patel *et al*., 2009; Korfel *et al*., 2007].

In addition to the TJs, other structural features, namely the absence of fenestrations, the deficiency in pinocytosis vesicles, the high metabolic capacity of cerebral endothelial cell [Reese 1967] and the presence of perivascular elements such as astrocytes and pericytes [Bodor 1999] contribute to the lack of permeability of the BBB.

For this reasons, nanotechnologies have been proposed to enhance drug delivery into the CNS [De Rosa *et al*., 2012; Alphandéry, 2020].

However, systems based on nano-carriers can be affecting by several problems. A drawback for the nanomedicine is their instability due to the colloidal characteristics of these carriers. For this reason, the preparations based on nanocarriers have to assemble before use. This issue leads to another drawback: the difficult scale-up of laboratory scale formulations.

Pharmaceutical manufacturing development is centred on quality and cost. Quality includes the manufacturing process and stability of the formulation, so the nano-systems manufacturing being challenged by potential issues related to: poor quality control, scalability complexities, lack of consistency and of storage stability of the final product, low production yield, insufficient batch-to-batch reproducibility, lack of infrastructure and/or in-house expertise, chemical instability or denaturation of the encapsulated compound during the manufacturing process [Teli *et al*., 2010; Narang *et al*., 2013; Hafner *et al*.,

2014; Tinkle *et al*., 2014]. Therefore, to achieve clinical translation of nanocarriers, the complexity in their design and development needs to be minimized as much as possible to create reproducible and fully characterized systems [Lammers, 2013; Barz *et al*., 1999].

To address some of above mentioned issues, a novel formulation based on hybrid self-assembling nanoparticles (SANPs) for the delivery of anionic drugs, e.g. bisphosphonates, in the treatment of glioblastoma (GBM), has been developed [Salzano *et al.,* 2011] and patented (WO/2012/042024 A1, EP2621539A1, US20140086979). This formulation overcome scale-up issues because the components are already available in pharmaceutical grade; moreover, the self-assembling process allows overcoming the instability issues of colloidal systems. Then, the introduction of specific ligands, such as transferring, on the surface of nanocarriers offers the possibility of improving the efficacy and specificity of therapeutics in certain diseases as well as enhancing the access of the nanocarriers to impermeable barriers, such as the BBB [Patel *et al*., 2009; Korfel *et al*., 2007; Jones *et al*., 2007]. The formulation is obtained by mixing lipid and inorganic components with Zoledronic acid (Zol), together with transferrin. A significant tumor regression in the brain of the mice treated with SANPs encapsulating Zoledronic acid was observed in an experiemental orthotopic model of GBM [Porru, 2014]. The experimental results obtained with this formulation (also named as EDROMA) contributed to achieve the designation of orphan drug recently granted by European Medicine Agency (EMA) and (29/08/2016- EU/3/16/1735) and Food and Drug Administration (FDA - 29/11/2016) for the glioma's treatment. The industrial interest for this product is also suggested by a license agreement with a pharmaceutical company Lisapharma s.p.a.

1.4 Aim of the thesis

This research activity is organized in two main directions, each contributing to different features of the SANPs technology.
Briefly, in the second chapter, a study to provide insights on the preparation of SANPs encapsulating zoledronic acid supporting the industrial development of

SANPs is reported. In the third chapter, a strategy to simplify the SANPs preparation protocol is investigated. Finally, in the fourth and fifth chapters, novel applications for SANPs are proposed.

More in details, in the first step of the research an additional development of the formulation has been planned to adapt the SANPs preparation to the industrial manufacturing process (Chapter 2). In this perspective, the single characteristics of the four components, namely PEGylated liposomes, human transferrin, calcium-phosphate nanoparticles and zoledronic acid solution, were investigated. Moreover, the preparation protocol of each component of the SANPs was modified to adapt the formulation to an industrial manufacturing process. Finally, the scale-up of the formulation was investigated and the first kit of the industrial formulation, named EDROMA, was set up and also assembled to obtain the first EDROMA.

Then, a strategy to freeze-dry SANPs-containing Zoledronic acid has been investigated to facilitate the preparation of the final product in hospital setting (Chapter 3). In this context, the inclusion of different cryoproctectants in the formulation and their influence on the characteristics of the formulation was evaluated to select additive to be used during the lyophilization process. The freeze-dried and reconstituted product was then analyzed in term of physical-chemical characteristics, *in vitro* and *in vivo* activity on cell lines and experimental orthotopic model of GBM, respectively.

Novel applications for SANPs have been also investigated. In particular, the formulation was modified for encapsulation and delivery of nucleic acids, namely microRNA (miRNA), with potential use in therapy of GBM (Chapter 4). More in details, in the case of formulations encapsulating miRNA, SANPs with different lipids were prepared and characterized, in terms of size, polydispersity index, zeta potential, miRNA encapsulation, stability in BSA, serum and hemolytic activity. Then, SANPs were tested *in vitro* on two different cell lines of GBM. Finally, miRNA biodistribution was tested *in vivo* in an orthotopic model of GBM.

Finally, the possibility to modify SANPs with hyaluronic acid for targeting of CD44-overexpressing cells has been investigated (Chapter 5). Thus, self-assembling nanoparticles modified with HA were prepared two different

preparation protocol, with or without PEGylation. Then, zoledronic acid was added in these complexes and the physical-chemical characteristics of these formulations were investigated in term of size, polydispersity index, zeta potential and HA and Zol encapsulation. Finally, tests on different cell lines, characterized by overexpression of CD44 receptors, have been carried out.

REFERENCES

Aktaş Y, Andrieux K, Alonso M.J., Calvo P, Gürsoy R.N., Couvreur P, Capan Y. Preparation and in vitro evaluation of chitosan nanoparticles containing a caspase inhibitor. Int J Pharm, 298:378-383 (2005).

Alphandéry E. Nano-Therapies for Glioblastoma Treatment. Cancers (Basel). 19;12(1):242 (2020).

Au J.L., Jang S.H., Zheng J, Chen C.T., Song S, Hu L, Wientjes M.G. Determinants of drug delivery and transport to solid tumors. J Contr Rel, 74:31-46 (2001).

Barz, M., Luxenhofer, R., and Schillmeier, M. Quo vadis nanomedicine? Nanomedicine 10, 3089–3091 (2015). doi: 10.2217/nnm.15.156

Bisso S, Leroux J.C. Nanopharmaceuticals: A focus on their clinical translatability. Int J Pharm. 30;578:119098 (2020).

Bodor, N.; Buchwald, P. Recent advances in the brain targeting of neuropharmaceuticals by chemical delivery systems, Adv. Drug Deliv. Rev., 36, 229-254 (1999).

Buckner J.C., Brown P.D., O'Neill B.P., Meyer F.B., Wetmore C.J., Uhm J.H., Central nervous system tumors, in Mayo Clin Proc, vol. 82, n. 10, pp. 1271-86, (2007). doi:10.4065/82.10.1271.

Crommelin D.J.A., Van Hoogevest P., Storm G. The role of liposomes in clinical nanomedicine development. What now? Now what? J Control Release; 318:256-263 (2020).

De Rosa G., Salzano G., Caraglia M., Abbruzzese A. Nanotechnologies: a strategy to overcome blood-brain barrier. Curr Drug Metab. 13:61-69 (2012).

De Rosa G., Misso G., Salzano G. and Caraglia M. Bisphosphonates and Cancer: What Opportunities from Nanotechnology? Nanotechnologies in Cancer (2013).

Falzone L., Salomone S., Libra M. Evolution of Cancer Pharmacological Treatments at the Turn of the Third Millennium. Front. Pharmacol. (2018). doi.org/10.3389/fphar.2018.01300.

Fang J, Islam W, Maeda H. Exploiting the dynamics of the EPR effect and strategies to improve the therapeutic effects of nanomedicines by using EPR effect enhancers. Adv Drug Deliv Rev. 157:142-160 (2020).

Hafner, A., Lovric, J., Lakos, G. P., and Pepic, I. Nanotherapeutics in the EU: an overview on current state and future directions. Int. J. Nanomedicine. 9, 1005–1023 (2014). doi: 10.2147/IJN.S55359.

He H., Liu L., Morin E.E., Liu M., Schwendeman A. Survey of Clinical Translation of Cancer Nanomedicines-Lessons Learned from Successes and Failures. Acc Chem Res. 17;52(9):2445-2461 (2019).

Jones A.R., Shusta E.V. Blood-brain barrier transport of therapeutics via receptor-mediation. Pharm Res. 24:1759-1771 (2007).

Kommareddy S, Tiwari S.B., Amiji M.M. Long-circulating polymeric nanovectors for tumor-selective gene delivery. Technol Cancer Res Treat, 4:615-625 (2005).

Korfel A., Thiel E.. Targeted therapy and blood-brain barrier. Recent Results Cancer Res; 176:123-33 (2007).

Lammers, T. Smart drug delivery systems: back to the future vs. clinical reality. Int. J. Pharm. 454, 527–529 (2013). doi: 10.1016/j.ijpharm.2013.02.046.

Lee S.Y., Kang, M.S., Jeong W.Y., Han D.W. and Kim K.S. Hyaluronic Acid-Based Theranostic Nanomedicines for Targeted Cancer Therapy. Cancers. 12, 940 (2020). doi:10.3390/cancers12040940.

Louis D.N., Ohgaki H., Wiestler O.D. The 2007 WHO classfication of tumors of the central nervous system. Acta Neuropathol; 114(2): 97-109 (2007).

Mattheolabakis, G.; Rigas, B.; Constantinides, P.P. Nanodelivery strategies in cancer chemotherapy: Biological rationale and pharmaceutical perspectives. Nanomedicine, 7, 1577–1590 (2012).

Narang, A. S., Chang, R. K., and Hussain, M. A. Pharmaceutical development and regulatory considerations for nanoparticles and nanoparticulate drug delivery systems. J. Pharm. Sci. 102, 3867–3882 (2013). doi: 10.1002/jps.23691.

Patel M.M., Goyal B.R., Bhadada S.V., Bhatt J.S., Amin A.F. Getting into the brain: approaches to enhance brain drug delivery. CNS Drugs; 23:35-58 (2009).

Porru M., Zappavigna S., Salzano G., Luce A., Stoppacciaro A., Balestrieri M. L., Artuso S., Lusa S., De Rosa G., Leonetti C. and Caraglia M.. Medical treatment of orthotopic glioblastoma with transferrin conjugated nanoparticles encapsulating Zoledronic acid. Oncotarget. 5(21): 10446–10459 (2014). doi: 10.18632/oncotarget.2182.

Reese, T.S.; Karnovsky, M.J. Fine structural localization of a blood-brain barrier to exogenous peroxidase, J. Cell Biol., 34, 207-217 (1967).

Ruoslahti E, Bhatia S.N., Sailor M.J. Targeting of drugs and nanoparticles to tumors. J Cell Biol, 188:759-768 (2010).

Salzano G., Marra M., Porru M., Zappavigna S., Abbruzzese A., La Rotonda M.I., Leonetti C., Caraglia M., De Rosa G.. Self-assembly nanoparticles for the delivery of bisphosphonates into tumors. Int J Pharm. 403(1-2):292-7 (2011).

Sant M., Minicozzi P., Lagorio S., Børge Johannesen T., Marcos-Gragera R., Francisci S.; EUROCARE Working Group. Survival of European patients with central nervous system tumors. Int J Cancer; 131(1): 173-85 (2012).

Shi J., Kantoff P.W., Wooster R., Farokhzad O.C. Cancer nanomedicine: progress, challenges and opportunities. Nat Rev Cancer. 17(1):20-37 (2017).

Siegel R. L., Miller K.D., Jemal A. Cancer statistics, 2020. Ca cancer J. clin. 70:7–30 (2020).

Stupp R., Hegi M.E., Mason W.P., Van den Bent M.J., Taphoorn M.J., Janzer R.C., Ludwin S.K., Allgeier A., Fisher B., Belanger K., Hau P., Brandes A.A., Gijtenbeek J., Marosi C., Vecht C.J., Mokhtari K., Wesseling P., Villa S., Eisenhauer E., Gorlia T., Weller M., Lacombe D., Cairncross J.G., Mirimanoff R.O.; Effects of radiotherapy with concomitant and adjuvant temozolomide versus radiotherapy alone on survival in glioblastoma in a randomised phase III study: 5-year analysis of the EORTC-NCIC trial. Lancet Oncol. 10(5):459-466 (2009).

Teli, M. K., Mutalik, S., and Rajanikant, G. K. Nanotechnology and nanomedicine: going small means aiming big. Curr. Pharm.Des. 16, 1882–1892 (2010). doi: 10.2174/138161210791208992.

Tinkle, S., McNeil, S. E., Muhlebach, S., Bawa, R., Borchard, G., Barenholz, Y. C. Nanomedicines: addressing the scientific and regulatory gap. Ann. N. Y. Acad. Sci. 1313, 35–56 (2014). doi: 10.1111/nyas. 12403.

Weller M., Stupp R., Hegi M.E. Personalized care in neuro-oncology coming of age: why we need MGMT and 1p/19q testing for malignant glioma patients in clinical practice. Neuro Oncol; 14 Suppl 4: iv100-8 (2012).

Zhang X., Wang X., Xu R., Ji J., Xu Y., Han M., Wei Y., Huang B., Chen A., Zhang Q. YM155 decreases radiation induced invasion and reverses epithelial–mesenchymal transition by targeting STAT3 in glioblastoma. Journal of Translational Medicine. 30(8):930-934 (2016).

CHAPTER 2

Hybrid self-assembling nanoparticles encapsulating zoledronic acid: optimization of the formulation for industrial development.

2.1 Zoledronic acid

Zoledronic acid (Zol) (Figure 2.1.1) is the most widely used amino-bisphosphonate (NBP) in clinical practice for its potent anti-resorptive activity [Wang, 2020] and it represents the standard treatment for different diseases, such as osteoporosis, Paget's disease and bone metastases [Cheer *et al*.,2001]; in addition, it inhibits the differentiation and the apoptosis of osteoclasts [Qiao *et al*., 2016; Li *et al*., 2017] by inhibition of farnesyl pirophosphate synthase (FPPS), an enzyme of the mevalonate pathway involved in regulation of proliferation invasive properties and pro-angiogenic activity of human tumor cells [Schafer *et al*., 1992; Dunford *et al*., 2001]. Numerous studies have demonstrated that Zol induces apoptosis in a variety of cancer cell types, including prostate cancer [Lee *et al.*, 2001], melanoma [Riebeling *et al.*, 2002], osteosarcoma [Mackie *et al.*, 2001] and multiple myeloma [Shipman *et al.*, 1997; Aparicio *et al.*, 1998; Tassone *et al.*, 2000] thus showing a direct anti-proliferative action on human tumor cells *in vitro* [Caraglia *et al.*, 2004]. Anticancer effects of Zoledronic acid have been reported *in vivo* [Morii *et al*., 2015]; these effects include suppression of bone metastasis [Peng *et al*., 2007, Hiraga *et al*., 2004], the inhibition of the angiogenesis [Gao *et al*., 2017], and the synergistic antiproliferative effect with other anticancer drugs [Qiao *et al*., 2016, Morii *et al*., 2015, Yamakawa *et al*., 2017].

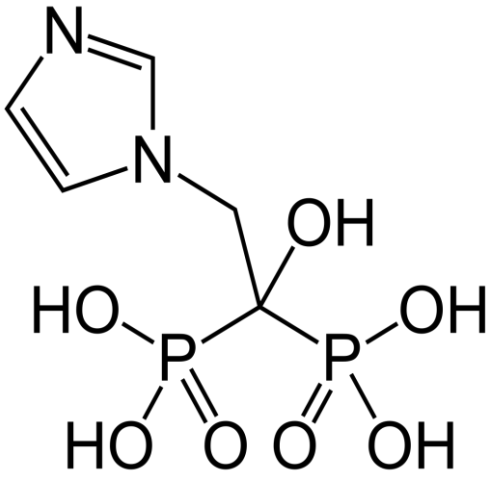

Figure 2.1.1: Zoledronic acid structure.

One of the most important limits of Zol is the lack of clear evidence *in vivo* of Zol-induced anti-cancer effects that is likely due to its unfavourable pharmacokinetic profile. In fact, it accumulates almost exclusively in the bone and it has a short serum half-life (only 15 min) not reaching active antitumor concentrations [Caraglia *et al*., 2010].

Research group of Prof. De Rosa has demonstrated that the use of nanotechnology-based formulations overcomes these limitations by changing Zol biodistribution and increasing its bioavailability in extra-skeletal tumor sites. This approach allowed transforming Zol in a powerful anticancer agent in different kinds of tumor [Marra *et al*., 2011, Marra *et al*., 2012].

2.2 Self-assembling nanoparticles (SANPs)

A novel formulation based on nanocarriers for the delivery of Zol in solid tumors has been developed [Salzano *et al*., 2011] and patented (WO/2012/042024) by the research group of Prof. De Rosa. In detail, Zol was firstly complexed with a mixture of calcium phosphate NPs (CaP NPs) and the resulting CaPZ NPs were then mixed with PEGylated cationic liposomes (PLs). The developed formulation exhibited optimal physical characteristics in terms of size, Zol encapsulation and Zol delivery in different cancer cell lines [Salzano *et al*., 2011]. Moreover, these NPs can be prepared immediately before use, overcoming problems of stability during the storage which often hampers the

scale-up of many promising drug delivery systems based on nanotechnology. In addition, in different experimental models of solid and circulating tumors, a significant inhibition of the tumor growth was demonstrated [Marra *et al*., 2011, Marra *et al*., 2012].

Self-assembling NPs have also been modified to target brain tumor, such as glioblastoma (GBM). In particular, to improve the delivery of Zol into the brain, the previous developed self-assembling NPs were updated by introducing human transferrin (Tf) as a ligand on the surface of the NPs. Zol-containing NPs, functionalized with Tf, were able to bind specific receptors on endothelial cells of BBB. The Tf insertion on the NPs surface aimed to improve the efficacy and selectivity of therapeutics towards Tf-overexpressing cells. Therefore, the overexpression of Tf receptor on the surface of GBM cells could allow using these newly developed NPs to actively target GBM cells as well as to enhance the access of the nanocarriers to BBB [Salzano *et al*., 2016; Porru *et al*., 2014]. For these reasons, a fourth component, e.g. an aqueous solution of transferrin, was included in the self-assembling process [Salzano *et al*., 2016; Porru *et al*., 2014]. In an orthotopic animal model of GBM, the use of transferrin-targeted SANPs encapsulating Zol resulted in a significant anticancer activity, while the tumors remained unaffected with free temozolomide, considered the gold standard in the treatment of GBM [Salzano *et al*., 2016 Stupp *et al.* 2005].

These results, namely the stabilization of the tumor in all the animals and complete regression in one out of eight [Porru *et al*., 2014], opened a new scenario in which it could have a strong impact for the treatment of brain tumors, for which a paucity of effective treatments exists.

All together these data support the further work on transferrin-targeted SANPs for future industrial development of the formulation.

2.3 Aim of the work

Due to the encouraging results previously described for the treatment of GBM, additional development of the formulation has been planned to adapt the SANPs preparation to the industrial manufacturing process.

It is worthy of note that the self-assembling nanoparticles encapsulating Zol have been designed to facilitate the scale-up phase. In this context, the Italian

pharmaceutical company Lisapharma s.p.a. signed a license agreement finalized to the industrial development of the product based on Zol-encapsulating SANPs. Actually, a part of this Ph.D. activity has been carried out at Lisapharma production plant located in Erba (CO), Italy, and has been focused on changes of the formulation's components needed for the SANPs component manufacturing. In particular, for supporting the industrial development of SANPs encapsulating zoledronic acid, all SANPs components, namely PEGylated liposomes, human transferrin, calcium-phosphate nanoparticles and zoledronic acid solution, were fully characterized in order to control physical-chemical changes during the manufacturing into the plant. One of the required formulation changes was the volume increase of the Zol solution. Moreover, the replacement of the component transferrin in HBS solution with transferrin in freeze-dried form was highly suggested to overcome issues encountered with protein stability. Thus, the influence of these changes on the physical-chemical characteristics, as well as with the delivery efficiency (measured as pharmacological activity of Zol) has been investigated. Finally, the preparation methods of CaP NPs and liposomes have been changed to meet technical needs of the Lisapharma plant.

Once fixed the novel experimental conditions and manufacturing methods to prepared the novel version of the SANPs components, the kit EDROMA was assembled and SANPs were characterized to evaluate correspondance with the formulations previously developed [Salzano *et al*. 2016].

2.4 Materials and methods

2.4.1 Materials

Zoledronic acid (Zol) kindly provided by Lisapharma S.p.a. (Erba, Italy). 1,2-dioleoyl-3-trimethylammonium-propane chloride (DOTAP) was kindly providedby Lipoid GmbH (Ludwigshafen, Germany). Cholesterol (CHOL), 1,2-distearoyl-sn-glycero-3-phosphoethanolamine-N-[amino(polyethylene glycol)-2000] (DSPE-PEG_{2000}) were purchased from Avanti Polar (Alabama, Usa). Sodium chloride, sodium hydroxide (NaOH), calcium chloride ($CaCl_2$), sodium phosphate dibasic (Na_2HPO_4), potassium chloride, Kit Sigma Calcium

Colorimetric Assay, ammonium molybdate, acid amino naphthol sulfonic, sodium bisulphate, sodium sulphite anhydrous, human transferrin (Tf), absolute ethanol HPLC grade were obtained from Sigma-Aldrich Co. (Milan, Italy).

2.4.2 Methods

2.4.2.1 Liposomes preparation

PEGylated cationic liposomes (PLs) (DOTAP/chol/DSPE-PEG_{2000} 1:1:0.5 weight ratio) were prepared by hydration of a thin lipid film, followed by extrusion. Briefly, the lipid mixture was dissolved in 1 ml of a mixture chloroform/methanol (2:1 v/v). The organic solution was removed by rotavapor. Then the lipid film was hydrated with 1 ml of water, and the resulting dispersion was extruded using a thermobarrel extruder system, through polycarbonate membranes with progressively lower porosity from 0.4 to 0.1 μm. The liposomes were stored at 4 °C before use.

2.4.2.2 CaP nanoparticles (CaP NPs) and CaP NPs/Zol complex (CaPZ) preparation

An aqueous solution of dibasic hydrogen phosphate (10.8 mM) was added, dropwise and under magnetic stirring, to an aqueous solution of calcium chloride (18 mM). The pH of both solutions was adjusted beforehand to 9.5 with NaOH 0.1 M. The resulting dispersion (CaP NPs) was filtered twice through a 0.22 μm filter and stored at 4 °C before use. 500 μl of this dispersion were then mixed for 15 minutes with 91 μl (0.4 mg) of an aqueous solution of Zol (0.125 M) in phosphate buffer at pH 9.5, resulting in formation of a colloidal dispersion, here named CaPZ.

2.4.2.3 SANPs-Zol preparation

One milliliter of PEGylated cationic liposomes (2.5 mg/ml) was mixed with 5 mg of human Tf, at room temperature for 15 minutes, obtaining a colloidal dispersion here named PL-Tf. SANPs-Zol (Figure 2.4.2.3.1) were prepared by

mixing PL-Tf complex with CaPZ, at room temperature for 15 min and then filtered through a 0.22 µm filter.

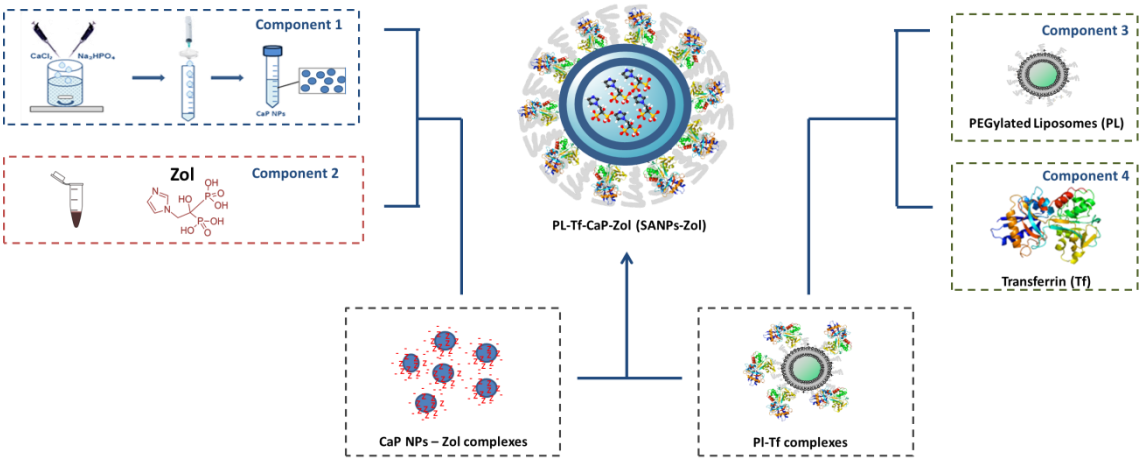

Figure 2.4.2.3.1: Preparation of hybrid self-assembling NPs encapsulating Zol (SANPs-Zol).

2.4.2.4 Particle size

PLs and SANPs were characterized in terms of mean diameter and polydispersity index (PI). In particular, mean diameter was determined at 20°C by photon correlation spectroscopy (PCS) (N5, Beckman Coulter, Miami, USA). For these measurements, each sample was analyzed with detector at 90° angle. Polydispersity index (PI) was used as measure of the particle size distribution. For each batch, mean diameter and size distribution were the average of three measures, while for each formulation; the mean diameter and PI were calculated as the values averaged over three different batches.

The Nanoparticle Tracking Analysis (NTA) technique was used to evaluate the diameter of CaP NPs by NS300 – Malvern Analytical. A patented optical element illuminates the chamber containing the sample with a laser beam at a specific angle. The suspended particles diffuse the light and this makes them perfectly visible under the microscope (x20). A camera mounted on the microscope records a video in which the particles appear individually as moving light points under the effect of the Brownian motion and where the small

particles move faster than the large ones. The NTA software automatically follows them, analyzes their movements and calculates the diffusion coefficient of many particles simultaneously. Finally, the hydrodynamic diameter of each particle identified was obtained by the Stokes-Einstein equation.

2.4.2.5 Zeta potential

The zeta-potential (ζ) of the NPs surface was measured in water by means of a Zetasizer Nano Z (Malvern, UK). For each batch, data of ζ were collected as the average of 20 measurements, while for each formulation the ζ was calculated as the average of ζ over three different batches.

2.4.2.6 Zol encapsulation efficiency

Encapsulation efficiency of Zol was determined by ultra-high performance liquid chromatography (UHPLC). A UHPLC system consisting of an isocratic pump UHPLC LC-10AD (Shimadzu, Milano, Italia), equipped with injection valve 7725i (Rheodyne) and detector at λ= 220 nm, was used. The chromatograms were collected and analyzed by PC with Lab Solution software. The analysis was carried out by Gemini 5 µm C18 (250 X 4.60 mm, 110 Å Phenomenex, Klwid, USA) column with guard column. A mobile phase consisting of a mixture of acetonitrile and an aqueous solution 20:80 v/v (8 mM K_2HPO_4, 2 mM Na_2HPO_4 e 7 mM tetra-N-Butyl ammonium sulphate hydroxide, pH 7,0) was used. Previously, Zol-containing formulations were alkalized to pH 14 by the addition of NaOH (51.69 mg/ml). Analyses were carried out on supernatants under isocratic conditions, with a mobile phase flow of 1 ml/min at room temperature. The supernatants were obtained by ultracentrifugation (Optima Max E, Beckman Coulter, USA) at 80000 rpm, at 4 °C, for 40 minutes. The results obtained from the chromatogram analysis were expressed as encapsulation efficiency, calculated as:

[(theoretical Zol concentration in SANPs - Zol concentration in supernatants) / theoretical Zol concentration in SANPs] x 100.

2.4.2.7 Gravimetric determination of CaP NPs

One milliliter of CaP NPs was prepared as reported in paragraph 2.4.1.2. After preparation the CaP NPs, unfiltered and filtered twice, were lyophilized and weighted. The result was compared with the theoretical weight of CaP NPs.

2.4.2.8 Scanning Electron Microscope (SEM)

The CaP NPs images were obtained by Scanning electron microscope (SEM) (PhenomXL – Thermo Fisher Scientific) using both Backscatter Detector (BSD) and Secondary Electron Detector (SED) with magnification between 160-200000x, resolution <10 nm and voltage range between 4.8 kV-20.5 kV.

2.4.2.9 Colorimetric assay of $CaCl_2$

Kit Sigma Calcium Colorimetric Assay was used to evaluate the quantity of $CaCl_2$ into the CaP NPs. The method was adopted with some modifications and the tests were carried out on three different batch. For the determination of $CaCl_2$ the assay was carried out by taking 50 µl of the sample, previously diluted 1/50, subsequently placed in the well of a multiwell plate; 90µl of chromogenic agent were added on the sample (from Kit Sigma Calcium Colorimetric Assay) and the content of the well was mixed. Then, 60 µl of Calcium Assay Buffer (from Kit Sigma Calcium Colorimetric Assay) were added to the mixture and mixed and left to react in a dark place for 10 minutes. The calcium concentration in the resulting solution was obtained by spectrophotometric analysis (using the Thermo Fisher Scientific 1510 Multiskan Go spectrophotometer) at a wavelength of 575 nm, using a calibration line that was prepared keeping constant the phosphate concentration at 228 µg/ml and changing only the calcium concentration between 1.5 µg/ml e 300µg/ml.

2.4.2.10 Colorimetric assay of Na_2HPO_4

Bartlett assay [Bartlett *et al*., 1959] was used to evaluate the quantity of Na_2HPO_4 into the CaP NPs. The method was adopted with some modifications

and the tests were carried out on three different batches. The test was carried out by preparing a calibration curve with a Na_2HPO_4 stock solution of 0.76 mg/ml and preparing diluted standard solutions at different concentrations (0.038 mg/ml to 0.76 mg/ml). The assay was carried out by mixing 300 µl of sample with 1200 µl of water, 200 µl of ammonium molybdate (0.05 mg/ml) and 50 µl of Fiske reagent (62.5 mg of amino naphthol sulfonic acid, sodium bisulphite 15%, 125 mg of anhydrous sodium sulphite per 25 ml of final product). The resulting solution was mixed by vortex and then incubated in water at 100 °C for 7 minutes. After cooling at room temperature, the samples were analyzed by spectrophotometer (UV-1800, UV Spectrophotometer) at the wavelength of 830 nm.

2.4.2.11 Gaschromatographic analysis

The gaschromatografic method was performed by GC – Agilent 7820 A with head space 7697 A to evaluate the yield of diafiltration method in terms of ppm of ethanol into the retentate liposome. The method was performed following the US Pharmacopeia (USP) method [USP 467].

2.5 Results and discussion

2.5.1 Optimization of SANPs preparation protocol to facilitate the technology transfer from the lab to the manufacturing plant

In this study, we modified the formulation of the previously developed hybrid self-assembling nanoparticles (SANPs) [Salzano *et al*., 2011], to meet some manufacturing requirements in agreement with the pharmaceutical company Lisapharma s.p.a. and to facilitate the future scale-up.

More in details, in the previously formulation protocol, the human transferrin was dissolved in HBS buffer solution at pH 8.0. Unfortunately, the transferrin dissolved in HBS buffer showed a reduced stability (change of the colour solution and precipitation) if not used immediately (data not showed). A first approach to address this issue is the design of a kit in which the transferrin is provided separately from the buffer. However, this should increase the

complexity of the SANPs preparation requiring the mixing of five components. Thus, to guarantee the stability of the Tf without affecting the complexity of the preparation protocol, freeze-dried transferrin has been dissolved directly with the liposomes dispersion; consequently, the volume of liposome dispersion (5 mg lipid/ml in the previously developed formulation) was diluted with water at a final liposome concentration 2.5 mg/ml, thus maintaining unaltered the final volume.

Another formulation change was on the solution of zoledronic acid. In particular, according to the previously developed protocol, the volume of the Zol solution in the final kit should be 100 µl, that is a volume not suitable for manufacturing in the Lisapharma plant where a minimum volume of 1 ml is required. For this reason, the volume of zoledronic acid was adjusted adding water to Zol (4 mg of Zol in the component of the final kit) until the final volume of 1 ml. The characteristics of the newly developed formulations are described in Figure 2.5.1.1. In this figure, the SANPs prepared following the previously developed protocol (here reported as SANPs 1), the SANPs prepared from freeze-dried Tf (reported as SANPs 2) and the SANPs prepared from the increased volume of the aqueous solution of Zol (reported as SANPs 3) were compared to the SANPs-Zol formulation containing both the modifications of SANPs 2 and SANPs 3 (reported as SANPs 4).

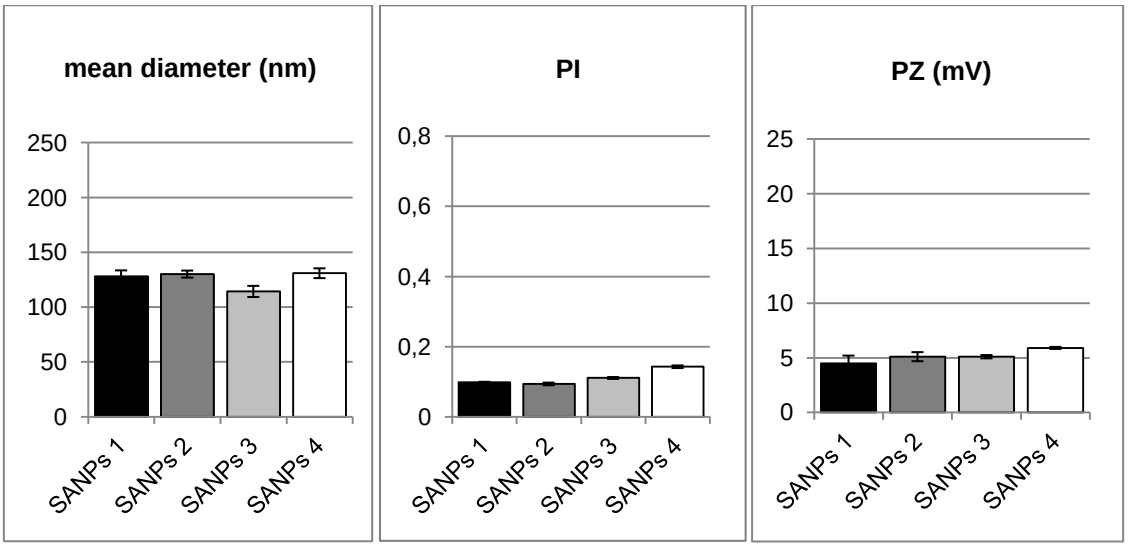

*standard deviation calculated on average of three batches

SANPs 1	A*: 500µl PLs [5mg/ml] + 500µl Tf in HBS 8.0 [10mg/ml] B*: 10µl Zol (0.4mg) + 500µl CaP NPs
SANPs 2	A*: 1000µl PLs [2.5mg/ml] + 5mg Tf B*: 10µl Zol (0.4mg) + 500µl CaP NPs
SANPs 3	A*: 500µl PLs [5mg/mL] + 500µl Tf in HBS 8.0 [10mg/ml] B*: 91µl Zol (0.4mg) + 500µl CaP NPs
SANPs 4	A*: 1000µl PLs [2.5mg/ml] + 5mg Tf B*: 91µl Zol (0.4mg) + 500µl CaP NPs

Figure 2.5.1.1: Characterization of new hybrid self-assembling NPs encapsulating Zol (SANPs). *volume used at the laboratory scale.

We found that the changes in the SANPs formulation did not significantly affect the physical-chemical characteristics of SANPs. Finally, the encapsulation efficiency (EE%) of Zol was determined by ultra high performance liquid chromatography (UHPLC). As reported in Table 2.5.1.1 the results showed a high encapsulation efficiency for all SANPs, suggesting that the Zol encapsulating in to the SANPs was not significantly affected by the formulation changes.

Formulation	Encapsulation Efficiency (EE%) ± sd*
SANPs 1	93% ± 0.7*
SANPs 2	94% ± 1.1*
SANPs 3	92% ± 2.0*
SANPs 4	93% ± 2.2*

*standard deviation calculated on average of three batches

Table 2.5.1.1: Encapsulation efficiency (EE%) of Zol in SANPs. SANPs prepared following the previously developed protocol (SANPs 1), SANPs prepared from freeze-dried Tf (SANPs 2), SANPs prepared from the increased volume of the aqueous solution of Zol (SANPs 3) and SANPs-Zol formulation containing both the modifications of SANPs 2 and SANPs 3 (SANPs 4).

2.5.2 CaP NPs characterization and industrial development

CaP NPs are certainly the SANPs component for which some features are still unclear and worthy of investigation. Indeed, CaP NPs are prepared by mixing of two aqueous solution followed by two filtration steps on 0.22 μm membranes. Thus, the exact composition of the resulting CaP NPs dispersion remains to be determined to support the future industrial development and scale-up of the product. Moreover, the stability of this colloidal dispersion during the storage was studied. Thus, to fill the gap, two different tests have been developed or adapted to determine the amount of $CaCl_2$ and Na_2HPO_4 actually present into the CaP NPs after preparation and filtration

In the Figure 2.5.2.1, an image of CaP NPs obtained by scanning electron microscope (SEM) was reported. Large CaP crystals are visible certainly due to CaP NPs aggregation during drying and thus not considered indicative of the CaP NPs size.

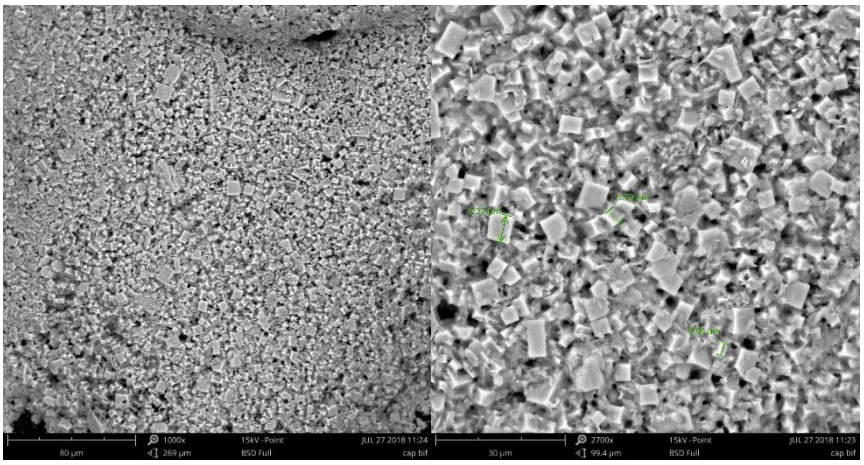

Figure 2.5.2.1: Image of CaP NPs obtained by Scanning electron microscope (SEM).

Then, the gravimetric measure of dried CaP NPs was carried out. Compared to the theoretical weight of 1.76 mg/ml, a dry residue of about 1.21 mg was obtained following double filtration, corresponding to a 68.8% ± 7.4 of the theoretical value (Table 2.5.2.1).

Sample	CaP NPs solid residue (mg/ml after lyophilization ± sd*)	Yield (%) ± sd*
CaP NPs after preparation	1.71 ± 0.08*	97.4 ± 4.3*
CaP NPs filtered twice	1.21 ± 0.13*	68.8 ± 7.4*

The theoretical solid residue is 1.76 mg/ml

*standard deviation calculated on average of three batches

Table 2.5.2.1: Gravimetric determination of dried CaP NPs.

Subsequently, two colorimetric assays were carried out to evaluate the actual concentration of $CaCl_2$ and of Na_2HPO_4 into the final CaP NPs; the analysis was carried out using the Kit Sigma Calcium Colorimetric Assay and the Bartlett

assay [Bartlett *et al*., 1959], respectively, with some modifications as reported in paragraphs 2.4.1.8 and 2.4.1.9.

The $CaCl_2$ concentration was obtained by spectrophotometric analysis, using the calibration curve reported in Figure 2.5.2.2.

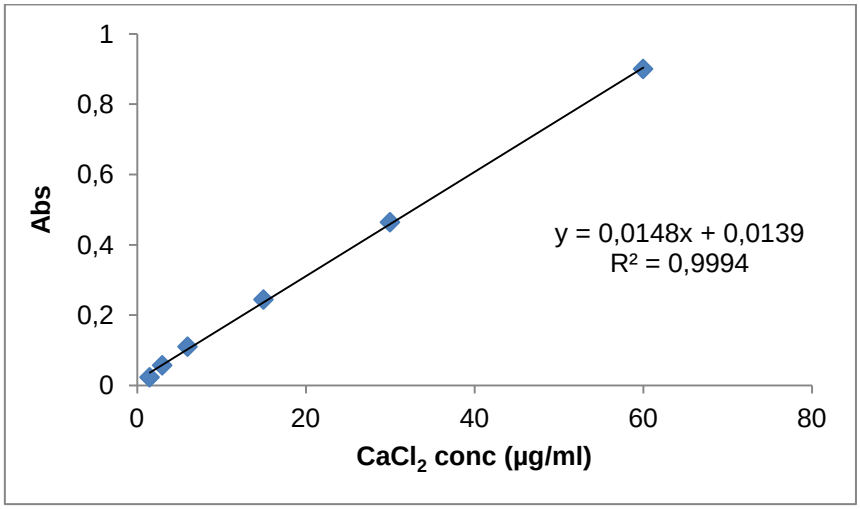

Figure 2.5.2.2: Calibration line of $CaCl_2$ obtained by colorimetric assay.

Analysis showed that, in the dispersion CaP NPs, $CaCl_2$ had a concentration of 0.56 mg/ml ± 0.05 (5.05mM) corresponding to a concentration of Ca^{2+} of 1.82 mM. This concentration is equivalent to 56.3% of the theoretical calcium concentration (3.25 mM). The determination of Na_2HPO_4 was obtained by spectrophotometric analysis, using the calibration curve reported in Figure 2.5.2.3.

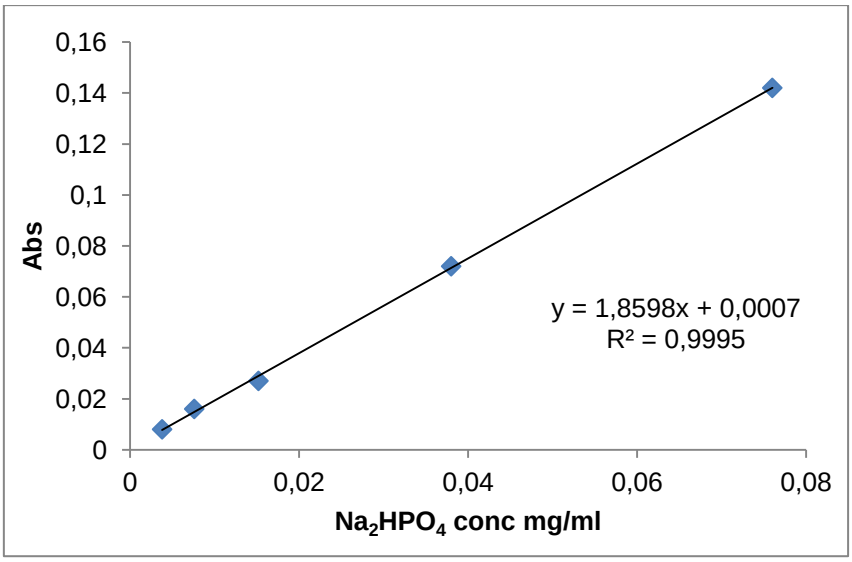

Figure 2.5.2.3: Calibration line of Na_2HPO_4 obtained by Bartlett assay.

Analysis showed that Na_2HPO_4 in CaP NPs had a concentration of 0.25 ± 0.03 mg/ml (1.76 mM) corresponding to a concentration of PO_4^{3-} of 1.18 mM. This concentration is equivalent to 32.9% of the theoretical phosphate concentration (3.58 mM). Due to the discrepancy between data obtained by gravimetric and colorimetric assays, the latter was taken into account as test for characterization of Ca^{2+} and PO_4^{3-} that was found be more selective for analytical purposes in the following phase of the study.

In the second step of the work, the protocol to prepare CaP NPs was modified to be adapted to a large-scale manufacturing. In particular, at laboratory scale the phosphate buffer and the calcium chloride buffer were mixed dropwise. However, this protocol should result too complex and expensive at large-scale production. Indeed, three separated bags and two pumps for the control of the flow should be considered. To simplify this process, we evaluated the possibility to pour the whole phosphate buffer solution all at once into the solution of calcium chloride buffer; this reduces the number of required bags and eliminated the need of two pumps. Thus, CaP NPs were prepared with both the methods and compared in terms of Ca^{2+} and PO_4^{3-} content and size. The stability of the CaP dispersion was also evaluated by monitoring the size upon storage a 2-4°C. Colorimetric assay showed that the Ca^{2+} and PO_4^{3-} content did

not significantly changed when preparing the CaP NPs by using the rapid mixing of the two solutions. The mean diameter of CaP NPs as well as CaP NPs concentration expressed as particles/ml and particles/frame dispersion prepared with both methods was investigated by Nanoparticle Tracking Analysis (NTA) technique.

The results, reported in Figure 2.5.2.4, showed that the characteristics of CaP NPs prepared following the modified protocol were comparable to the characteristics of CaP NPs prepared as previously reported. Furthermore, the stability at 2-4°C of the CaP NPs prepared by the rapid mixing was tested until 4 months. A moderate decrease of the mean diameter was found, considered a “maturation” of the dispersion. Since no aggregations were found it is possible confirm that the mean diameter of CaP NPs maintains (colloidal) dimension during 4 months of storage, that is a suitable time for preparing and deliver the nanoparticles for their clinical use. The results of this analysis are reported in Figure 2.5.2.4.

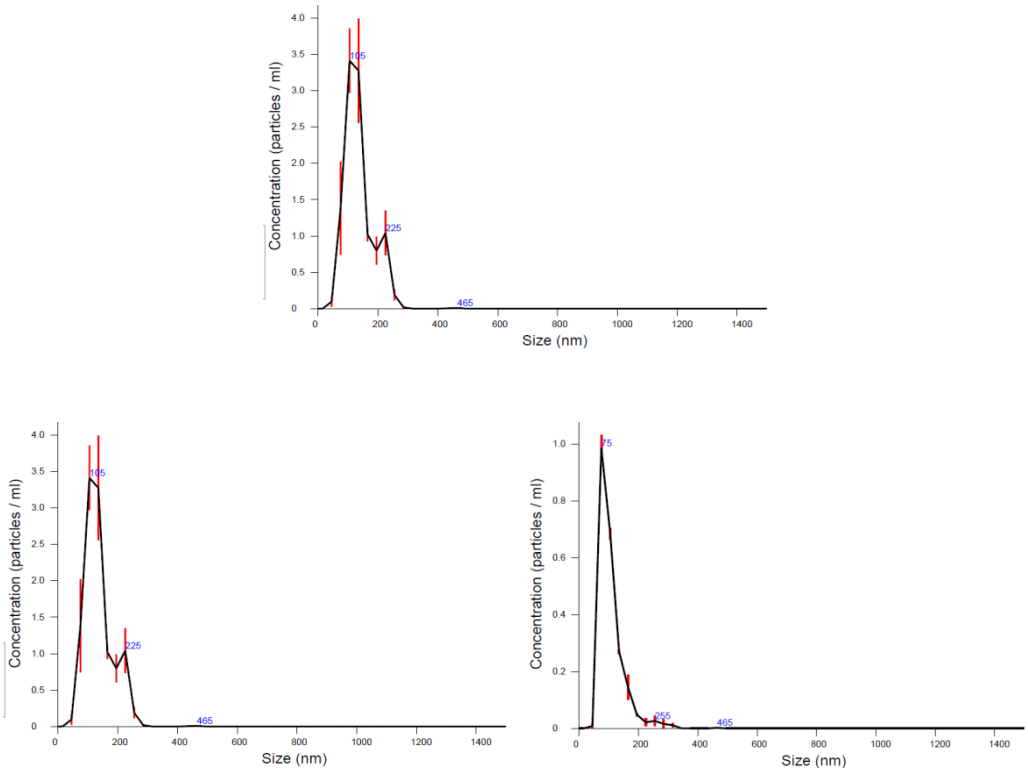

CaP NPs	Method 1	Method 2	Method 2 following 4 months of storage at 4°C
Mean diameter (nm) ± sd*	137 ± 2.5*	138 ± 1.1*	107 ± 1.9*
Particles/ml	2.13×10^{12}	2.69×10^{12}	2.22×10^{12}
Particles/frame	35.0	35.1	27.9

*standard deviation on almost three different batches

Figure 2.5.2.4: Characteristics of CaP NPs measured by NTA analysis. The CaP NPs were prepared by mixing the dibasic hydrogen phosphate (10.8 mM) to an aqueous solution of calcium chloride (18 mM) dropwise under magnetic stirring (method 1) and pouring the whole phosphate buffer solution all at once into the solution of calcium chloride buffer under magnetic (method 2).

2.5.3 Industrial development of PEGylated Liposomes (PLs)

In this part of the work, the protocol to prepare PLs was modified to adapt them to a preparation in R&D laboratory of Lisapharma S.p.a. (Erba (CO), Italy) for future large scale manufacturing. The protocol previously developed was based on liposomes obtained starting from the lipids dissolution in chloroform and methanol and formation of a thin lipid film by rotary evaporator followed by extrusion. However, this protocol was judged not convenient for large-scale manufacturing; indeed, rotary evaporator is in general not recommended for large scale production; moreover, chloroform and methanol either are considered dangerous solvents for the operators or can represent a risk factor for the product's injection into the patient [ATSDR, 1997; Tephly, 1991]. Therefore, an alternative liposome preparation method, namely "ethanol-injection", was investigated. In a preliminary phase of the study, different experimental parameters were tested, namely the solubility of lipids in ethanol, the ratio between ethanol and water, the rate of injection, the stirring rate and the time of the incubation. The experimental conditions selected are reported in Table 2.5.3.1.

Ratio EtOH/H2O	7.5% v/v
RPM	950
Time of reaction	10 minutes
Lipid concentration	2.5 mg/ml

Table 2.5.3.1: Optimized experimental conditions to prepare liposomes by "ethanol injection" method.

For moving more easily toward a large scale preparation of PLs, the Allegro High Performance Mixer by Pall Corporation (Figure 2.5.3.1), has been used to prepare liposomes. Briefly, Allegro Mixer is composed by a mixing chamber where is possible insert a disposable bag provided with a turbine, five input/output placed at the base (to control parameters as temperature, pH etc.)

and another input on the top. This instrument has been used to prepare the lipids mix in ethanol and also to inject this mix in water to obtain the final liposomes. More in details, in the first step the ethanol has been placed in the mixer under stirring and the mix of lipids has been injected inside the chamber from the top. The final mix has been collected into a bag. In the second step, the water will be placed into the chamber at 950 RPM to create a vortex and the ethanol/lipids mix will be inserted by the bottom of the vortex and the stirring will be maintained for 10 minutes. Finally, the liposomes will be collected into a disposable bag.

Figure 2.5.3.1: Allegro High Performance Mixer - Pall Corporation.

Finally, to remove the ethanol by the formulation, a diafiltration protocol was investigated using a CentraMate 500 S (CM500) Tangential Flow Filtration (TFF) system - Pall Corporation (Figure 2.5.3.2).

Figure 2.5.3.2: CentraMate 500 S (CM500) Tangential Flow Filtration (TFF) system - Pall Corporation.

Briefly, Tangential Flow Filtration (TFF) is a separation process that is characterized by a feed stream that passes parallel to the membrane face. One portion passes through the membrane (permeate) while the remainder (retentate) is recirculated back to the feed reservoir. In continuous diafiltration, the diafiltration solution (water) is added to the sample feed reservoir at the same rate of the generated filtrate. In this way the volume in the sample reservoir remains constant but the ethanol, which can freely permeate through the membrane, is washed away (see Figure 2.5.3.3). In this experiment, we used 7 diafiltration volumes to reduce the ethanol concentration by ~98% using continuous diafiltration through a Minimate TFF Capsule of 5K Omega.

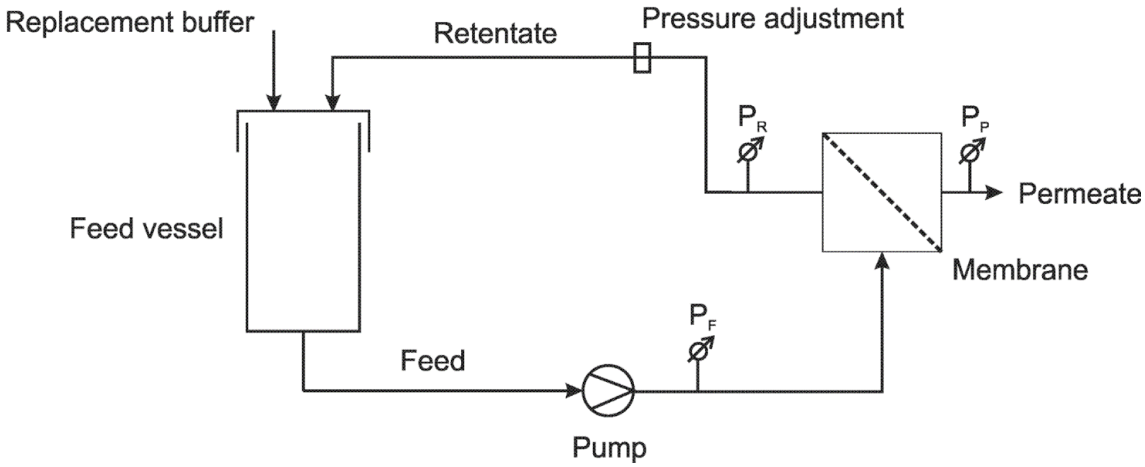

Figure 2.5.3.3: Tangential Flow Filtration (TFF) scheme.

Thereafter the retentate liposomes were characterized to evaluate mean diameter, polydispersity index and zeta potential. Also the diavolumes of permeate were analyzed to confirm the absence of liposomes in this phase; the pH of retentate and permeate were analyzed (see Table 2.5.3.2).

Sample	Mean diameter (nm)	PI	Z Potential (mV)	pH
Liposomes (pre-diafiltration)	49.33	0.340	31.6	4.51
Liposomes retentate	53.03	0.391	48.9	6.00
I-VII diavolumes	259.3 to 690.0	0.246 to 0.639	17.8 to -27.2	n.a.

Table 2.5.3.2: Mean diameter, Polydispersity index, Zeta potential, pH liposomes before and after TFF.

Finally, a gas-chromatographic method by GC - Agilent 7820 A with head space 7697 A was performed, following the method reported in USP [USP 467], to evaluate the yield of the TFF process in term of concentration of ethanol, expressed as % into the liposomes or ppm. Indeed, the maximum value permitted for the ethanol to injectable product is 5000 ppm [USP 467]. The ethosomes (liposomes before TFF) showed a concentration of ethanol around

52000 ppm; after 7 diafiltration volumes this concentration dropped to 1122 ppm, a value much lower than limit of the guidelines reported in USP (see Figure 2.5.3.4).

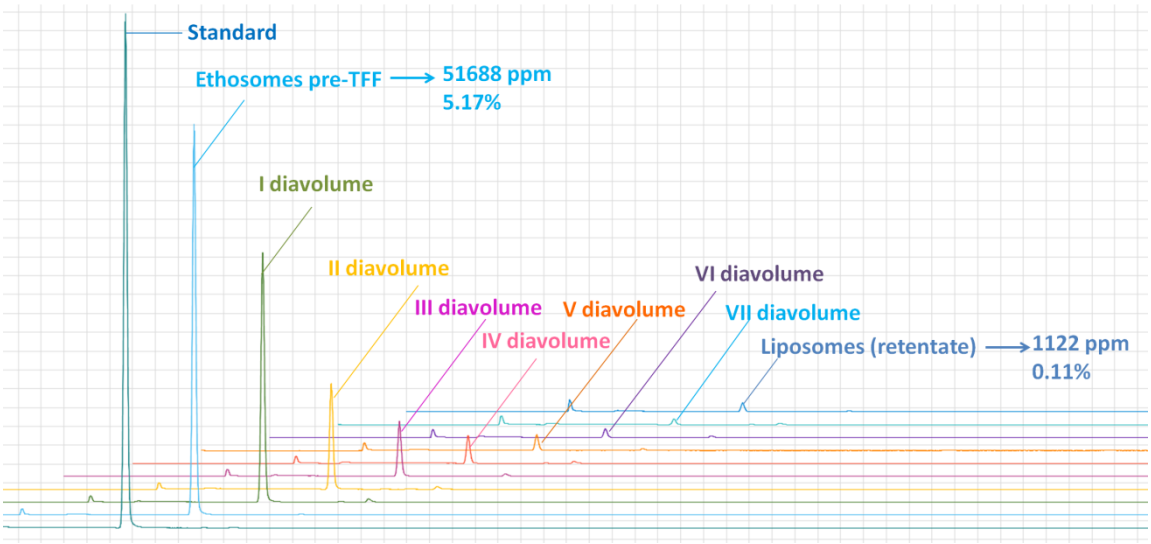

Samples	% EtOH - ppm
Liposomes pre-diafiltration	5.17% - 51688 ppm
Liposomes retentate	0.11% - 1122 ppm

Figure 2.5.3.4: Yield of TFF process evaluated by Gas-chromatographic analysis.

2.5.4 Kit EDROMA preparation

The last step of this work was based on the preparation of a kit for the preparation of the final product (to whom the name EDROMA has been given) based on SANPs encapsulating Zol. The kit is composed by components prepared starting from totally prepared in Lisapharma, with the exception of the only component transferrin that was bought in lyophilized form by Sigma Aldrich. Therefore, using CaP NPs and liposomes prepared following the new methods set up in Lisapharma and adding zoledronic acid dissolved in PBS 9.5, the first kit of EDROMA was assembled in Lisapharma in final volume designed for the clinical use. The complete kit of EDROMA is shown in Figure 2.5.4.1.

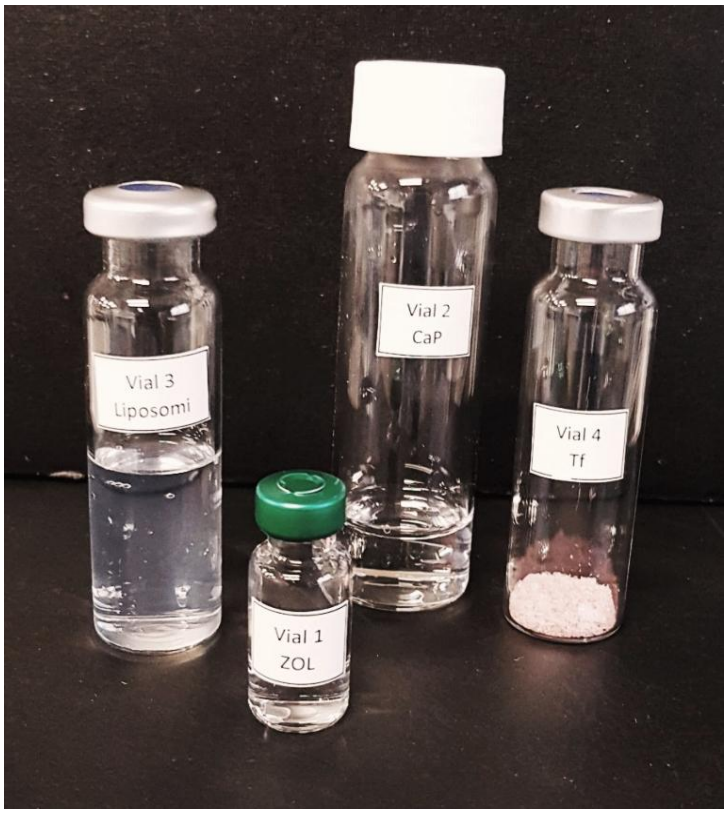

KIT EDROMA	**Vial 1**: Zoledronic acid, 4mg in 1 ml PBS 9.5 **Vial 2**: Calcium-phosphate nanoparticles, 6ml **Vial 3**: Pegylated liposomes, 12 ml [2.5 mg/ml] **Vial 4**: Human Transferrin dried shape, 60 mg

Figure 2.5.4.1: EDROMA kit assembled in Lisapharma S.p.a.

Moreover, the kit was assembled by component mixing (final vial: vial 2 in the figure 2.5.4.1) thus preparing the first batch of EDROMA (see Figure 2.5.4.2).

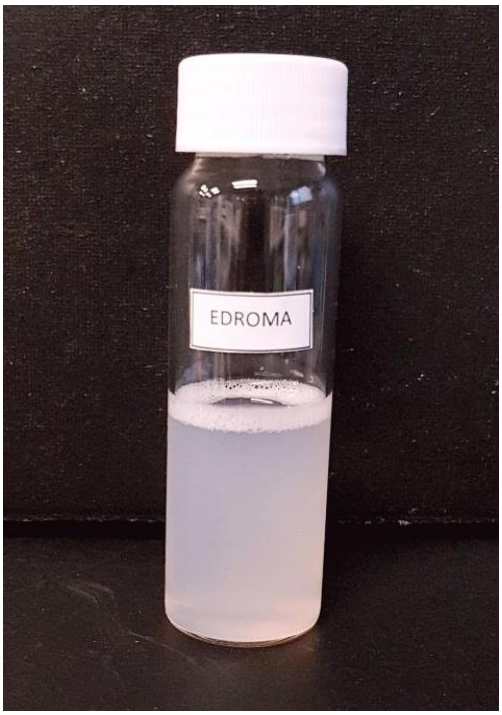

Figure 2.5.4.2: EDROMA assembled in Lisapharma S.p.a.

The result of this analysis showed that EDROMA, although had some difference in the characteristics (in term of mean diameter, polydispersity index and zeta potential) compared to the laboratory scale formulation. In particular, this first batch of EDROMA is characterized by SANPs that are significantly lower in diameter, with a higher PI and reduced zeta potential (see Table 2.5.4.1).

	Laboratory scale formulation	**EDROMA assembled in Lisapharma**
Mean (nm)	110.8	60.07
PI	0.165	0.265
PZ (mV)	+8.2	+4.85

Table 2.5.4.1: Mean diameter, polydispersity index, zeta potential of EDROMA compared to laboratory scale formulation.

EDROMA has been prepared following significant changes in preparation protocol. These changes have been necessary to adapt the preparation carried

out in the research lab at the Department of Pharmacy of Naples to the production in the plant of Lisapharma S.p.a. In particular, the higher volume of the Zol aqueous solution has been considered, together with an increase of the volume of the liposome dispersion; finally, transferrin has been used in freeze-dried form. Moreover, the preparation method of CaP NPs as well as of the liposomes has been changed to meet technical needs of the Lisapharma plant. Despite all these changes, three of the four components were prepared in Lisapharma and characterized. While the CaP NPs have characteristics comparable to the prepared in the research lab, liposomes with a significantly lower mean diameter were produced in Lisapharma. It is worthy of note that, once that the four components are mixed to prepare the SANPs, liposomes should disassemble, reorganizing the lipids for the two bilayers surrounding the CaP core, as previously found [Ristori *et al.*, 2018]. Once assembled, the SANPs prepared into the company plant sill showed physical-chemical characteristics that make the product suitable for intravenous injection, although with a significant reduction of the SANPs size and slight increase of the polydispersity index. These modifications in the final SANPs product should also be due to the change of the preparation of liposome/transferrin mixing, as suggested by the slight change in the SANPs zeta potential. Further batches are needed to confirm the characteristics of the SANPs prepared within the company plant. Moreover, *in vitro* and *in vivo* studies must be carried out to investigate if the modified formulation maintains the ability to deliver Zol in tumor and, in particular, in glioblastoma. These studies are mandatory before further scale-up experiments for large scale-production of the two components CaP NPs and liposomes that are certainly the most sensitive to the preparation conditions.

2.6 Conclusions

Due to the encouraging results previously described for the treatment of GBM, additional development of the formulation has been planned to adapt the SANPs preparation to the industrial manufacturing process.

In this context, for manufacturing purposing, all components were individually considered and, when requested, fully characterized. Then, the preparation protocol of each component was changed to be adapted them to facilities available into the Lisapharma s.p.a. plant, where part of this Ph.D. activity has been carried out. More in details, before moving toward the scale up process, some modification have been required for three of the components. In detail, to increase the chemical-physical stability of the transferrin, its lyophilization was proposed, followed by dissolution in the liposomes dispersion during the self-assembling procedure. Of course, the volume of the liposome dispersion was increased maintaining unaltered the final volume of the liposome/transferrin mixing. Furthermore, the volume of zoledronic acid was reduced to allow the vial filling in the company plant.

Other issues to address before the scale up were the methods to prepare some of the components that required to be adapted to the preparation in the company plant. Preliminarily, the exact CaP NPs composition used in the previously used SANPs preparation protocol was investigated. Moreover, the CaP NPs preparation protocol was modified and, once more, adapted to the facilities of the company plant. Despite these modifications, CaP NPs have no significant changes in the composition and chemical-physical characteristics CaP NPs; moreover, CaP NPs were stable for 4 months, which is a suitable period to allow their large-scale preparation and distribution.

The technical requirements of the company plant also lead to change the liposome preparation. More in details, the “ethanol-injection method” was set up to prepare liposomes; in this case a purification process for liposome as well as a test to detect ethanol residual content was set-up.

Finally, once the different components were prepared into the company plant (Cap NPs, Zol solution and liposomes dispersion) or obtained from other producers (e.g. freeze-dried transferrin), the first batch of SANPs-encapsulating Zol was assembled taking into account the volumes, the Zol concentration and

the final Zol dose scheduled for the future clinical use. Some physical-chemical characteristics of EDROMA are different compared to the product prepared into the research lab requiring pharmacological validation *in vitro* and *in vivo*. However, this part of the Ph.D. activity laid the foundation for the future transfer of the SANPs technology to the industrial production. It is worthy of note that the company plant in which this part of the work has been carried out is not specialized for the manufacturing of products based on nanotechnology-based formulation. Despite this, the whole kit for preparation of the final product EDROMA was produced “in house”. As expected, some changes in the physical-chemical characteristics occurred when reproducing the “industrial” SANPs. However, this work demonstrates that the development of self-assembling nanoparticles can represent a strategy to accelerate the technology transfer, avoiding the need of dedicated manufacturing equipments and facilities that are still not commons in the pharmaceutical companies.

REFERENCES

Agency for Toxic Substances and Disease Registry (ATSDR). Toxicological Profile for Chloroform. (1997), US Department of Health and Human Services: Atlanta, US.

Aparicio A., Gardner A., Tu Y., Savage A., Berenson J., Lichtenstein A. *In vitro* cytoreductive effects on multiple myeloma cells induced by bisphosphonates. Leukemia; 12:220-229 (1998).

Bartlett, G.R. Phosphorus Assay in Column Chromatography. J. Biol. Chem. 234, 466–468 (1959).

Caraglia M., Marra M., Naviglio S., Botti G., Addeo R., Abbruzzese A. Zoledronic acid: an unending tale for an antiresorptive agent. Expert Opin Pharmacother. 11: 141-154 (2010).

Caraglia M., D'Alessandro A.M., Marra M., Giuberti G., Vitale G., Viscomi C., Colao A., Prete S.D., Tagliaferri P., Tassone P., Budillon A., Venuta S., Abbruzzese A. The farnesyl transferase inhibitor R115777 (Zarnestra) synergistically enhances growth inhibition and apoptosis induced on epidermoid cancer cells by Zoledronic acid (Zometa) and Pamidronate. Oncogene; 23:6900-6913 (2004).

Cheer S.M., Noble S. Zoledronic acid. Drugs; 61:799-805; discussion 806 (2001).

Dunford J.E., Thompson K., Coxon F.P., Luckman S.P., Hahn F.M., *et al*. Structure-activity relationships for inhibition of farnesyl diphosphate synthase *in vitro* and inhibition of bone resorption in vivo by nitrogen-containing bisphosphonates. J Pharmacol Exp Ther; 296:235–242 (2001).

Gao S.Y., Zheng G.S., Wang L., Liang Y.J., Zhang S.E., Lao X.M. Zoledronate suppressed angiogenesis and osteogenesis by inhibiting osteoclasts formation and secretion of PDGF-BB. Plos One.12(6):e0179248 (2017).

Hiraga T., Williams P.J., Ueda A., Tamura D., Yoneda T. Zoledronic acid inhibits visceral metastases in the 4T1/luc mouse breast cancer model. Clin Cancer Res. 10(13):4559–67 (2004).

Lee M.V., Fong E.M., Singer F.R., Guenette R.S.Bisphosphonate treatment inhibits the growth of prostate cancer cells. Cancer Res; 61:2602-2608 (2001).

Li P., Yang H., Jia N., Jin X., Xu D., Shen Y. Experimental study on inhibitory effect of Zoledronic acid on the action style of the osteoclast. Sheng wu yi xue gong cheng xue za zhi; 34(1):78–82 (2017).

Mackie P.S., Fisher J.L., Zhou H., Choong1 P.F.M. Bisphosphonates regulate cell growth and gene expression in the UMR 106-01 clonal ratosteoarcoma cell line British Journal of Cancer; 84(7):951-958 (2001).

Marra M., Salzano G., Leonetti C., Tassone P., Scarsella M., Zappavigna S., Calimeri T., Franco R., Liguori G., Cigliana G., Ascani R., La Rotonda M.I., Abbruzzese A.. Nanotechnologies to use bisphosphonates as potent anticancer agents: the effects of Zoledronic acid encapsulated into liposomes. Nanomedicine. 7: 955- 967 (2011).

Marra M., Salzano G., Leonetti C., Porru M., Franco R., Zappavigna S., Liguori G., Botti G., Chieffi P., Lamberti M., Vitale G., Abbruzzese A., La Rotonda M.I. New self-assembly nanoparticles and stealth liposomes for the delivery of Zoledronic acid: a comparative study. Biotechnol Adv. 30: 302-309 (2012).

Morii K., Aoyama Y., Nakamura S., Okushin H. Synergistic anti-tumor effects of Zoledronic acid and radiotherapy against metastatic hepatocellular carcinoma. Int Med. 54(20):2609–13 (2015).

Peng H., Sohara Y., Moats R.A., Nelson M.D. Jr., Groshen S.G., Ye W. The activity of Zoledronic acid on neuroblastoma bone metastasis involves inhibition of osteoclasts and tumor cell survival and proliferation. Cancer Res.;67(19):9346–55 (2007).

Porru M., Zappavigna S., Salzano G., Luce A., Stoppacciaro A., Balestrieri M. L., Artuso S., Lusa S., De Rosa G., Leonetti C.and Caraglia M.. Medical treatment of orthotopic glioblastoma with transferrin conjugated nanoparticles encapsulating Zoledronic acid. Oncotarget. 5(21): 10446–10459. (2014) doi: 10.18632/oncotarget.2182.

Qiao H., Wang T.Y., Yu Z.F., Han X.G., Liu X.Q., Wang Y.G. Structural simulation of adenosine phosphate via plumbagin and Zoledronic acid competitively targets JNK/Erk to synergistically attenuate osteoclastogenesis in a breast cancer model. Cell Death Dis. 7:e2094 (2016).

Riebeling C., Forsea A.M., Raisova M., Orfanos C.E., Geilen C.C. The bisphosphonate pamidronate induces apoptosis in human melanoma cells in vitro. Br J Cancer. 87(3):366-71 (2002).

Ristori S., Grillo I., Lusa S., Thamm J., Valentino G., Campani V., Caraglia M., Steiniger F., Luciani P. and De Rosa G., Mol. Pharmaceutics, 15, 3, 1258–1265 (2018). doi.org/10.1021/acs.molpharmaceut.7b01085

Salzano G., Marra M., Porru M., Zappavigna S., Abbruzzese A., La Rotonda M.I., Leonetti C., Caraglia M., G. De Rosa. Self-assembly nanoparticles for the delivery of bisphosphonates into tumors. Int J Pharm. Jan 17;403(1-2):292-7 (2011).

Salzano G., Zappavigna S., Luce A., D'Onofrio N., Balestrieri M.L., Grimaldi A., Lusa S., Ingrosso D., Artuso S., Porru M., Leonetti C., Caraglia M., DeRosa G. Transferrin-Targeted Nanoparticles containing Zoledronic Acid as a potential tool to inhibit Glioblastoma growth. J. Biomed. Nanotechnol. 12:1–20 (2016).

Schafer W.R., Rine J. Protein prenylation: genes, enzymes, targets, and functions. Annu Rev Genet; 26:209-237 (1992).

Shipman C.M., Rogers M.J., Apperley J.F., Russell R.G., Croucher P.I. Bisphosphonates induce apoptosis in human myeloma cell lines: a novel anti-tumor activity. Br J Haematol; 98:665-672 (1997).

Stupp R., Mason W.P., Van den Bent M.J., Weller M., Fisher B., Taphoorn M.J., Belanger K., Brandes A.A., Marosi C., Bogdahn U., Curschmann J., Janzer R.C., Ludwin S.K. Radiotherapy plus concomitant and adjuvant temozolomide for glioblastoma. N Engl J Med. 352: 987-996 (2005).

Tassone P., Forciniti S., Galea E., Morrone G., Turco M.C., Martinelli V., Tagliaferri P., Venuta S. Growth inhibition and synergistic induction of apoptosis by Zoledronate and dexamethasone in human myeloma cell lines. Leukemia. 14(5):841-4 (2000).

Tephly T.R. The toxicity of methanol. Life Sciences Volume 48, Issue 11, Pages 1031-1041 (1991). doi.org/10.1016/0024-3205(91)90504-5

USP 467, Residual Solvent Method – Procedure A – HS Set 2.

Wang L., D. Fang, J. Xu and R. Luo. Various pathways of Zoledronic acid against osteoclasts and bone cancer metastasis: a brief review. BMC Cancer. 20:1059 (2020). doi.org/10.1186/s12885-020-07568-9.

Yamakawa Y., Tazawa H., Hasei J., Osaki S., Omori T., Sugiu K. Role of Zoledronic acid in oncolytic virotherapy: promotion of antitumor effect and prevention of bone destruction. Cancer Sci. 108(9):1870–80 (2017).

CHAPTER 3

Hybrid self-assembling nanoparticles encapsulating zoledronic acid: a simplification strategy for fostering clinical use.

3.1 Issues related to preparation protocol of hybrid self-assembling nanoparticles encapsulating zoledronic acid.

In the design of SANPs technology, the possibility of a rapid transferability to large-scale manufaturing has been taken into account. The SANPs formulation need to be prepared immediately before use on patients, thus overcoming the stability issues generally encountered with nanomedicine [Hua *et al.,* 2018]. Thus, SANPs are assembled by ordered mixing of four components [Salzano *et al*. 2016] already present on the market or easily produced in GMPs quality. Despite the self-assembling strategy should facilitate the technology transfer, the complexity of the preparation protocol of SANPs in clinical setting could represent the downside, raising concerns on the high probability of “human” mistakes. Indeed, SANPs preparation requires the rigorous respect for the order of component mixing, while ensuring an incubation time enough long for nanoparticles assembling (at least 15 min following each mixing). The reconstitution of parenteral antineoplastic preparations requires centralization in a hospital pharmacy equipped with an area for such activities, not present in all the hospitals. Moreover, national/international recommendations/guidelines for the preparation of parenteral antineoplastic drugs point out on measures aimed to avoid errors in the reconstitution of products for human use [Goldspiel *et al.*, 2015]. This is particularly important in the case of formulations with a complex reconstitution, where multiple sources of errors can be found. In this context, SANPs preparation obtained mixing of 4 components, in a predetermined order, can certainly represent a “minefield”.

3.2 Aim of the work

In this context, a formulation strategy able to simplify the preparation of SANPs has been investigated to facilitate the preparation of the final product in view of

a clinical use. Thus, we investigated the possibility to freeze-dry the SANPs following preparation, thus leading to a single component in powder to be reconstituted with water before the use. The removal of water should also guaranty a higher chemical stability of all the components.

The freeze-drying of lipid-based colloidal dispersion represents a challenge in the case of liposomes requiring the use of cryoprotectants. Indeed, it is necessary protect the double lipid layers from damage caused by ice crystals during the freezing, because the formation of ice inside the membrane is fatal for the vesicle [Crowe *et al*., 1987]. A cryoprotectant hampers the phase transition and protects liposomes from the damage due to ice aggregation [Chengiun *et al*., 2010]. To prevent these issues, the freeze-drying of SANPs dispersion was investigated in presence of cryoprotectants. In particular, in this work, mannitol, trehalose and sucrose were studied as potential cryoprotectant for SANPs lyophilization.

Lyophilization, also known as freeze drying or cryodesiccation, is a low temperature dehydration process carried out in three steps: freezing, primary drying, and secondary drying. During the freezing step, most of the water is converted into ice at temperatures close to −40°C. Then, the pressure of the system is reduced using vacuum pumps, and the shelf temperature is raised to facilitate ice sublimation during primary drying. In the secondary drying stage, the shelf temperature is further raised to efficiently remove unfrozen water by desorption to provide a low residual water content, typically less than 1% [Patel *et al*., 2009].

Freeze-dried formulations have the advantage of higher stability, and easy handling (shipping and storage) [Pikal, 1998; Carpenter and Chang, 1996]; freeze-drying results are particularly useful to increase the shelf life of the products, such as live virus vaccines [Hansen *et al*., 2015], biologics [Rey and May, 2016] and other injectables. Furthermore, many bio-pharmaceutical products based on therapeutic proteins such as monoclonal antibodies require lyophilization to be stable.

Lyophilization is also a promising approach to ensure the long-term stability of nanocarriers based on liposomes because it increases the shelf-life of formulation providing a lyophilized cake to be reconstituted with water prior to administration. To maintain the same particle size distribution after the

lyophilization/rehydration cycle, a cryoprotectant needs to be added. Since the process of freeze-drying leads can destroy the phospholipid bilayer [Ghanbarzadeh *et al*., 2013] with formation of lipid aggregates.

For this reason, when formulations based on lipid nanovectors are lyophilized, the parameters such as the freezing rate and temperature, which influence the morphology of the products freeze-dried need to be carefully taken selected. Especially, the integrity of the membrane of liposomes during freeze-drying is essential. It is necessary protect the double lipid layers from damage caused by ice crystals during the freezing, inhibit the vesicle aggregation after dehydration, and avoid phase transition during rehydration; moreover, attention must be paid during the reconstitution of the lyophilized product when air is incorporated. [Chengiun *et al*., 2010]. Moreover, the formation of ice inside the membrane is fatal for the vesicle so it should be absolutely avoided [Crowe *et al*., 1987]. Furthermore, the formulation based on lipid nanovectors frozen without any cryoprotectants generally show a decrease in homogeneity with a considerable increase in the size and polydispersity index. This behaviour is typical of the destabilization of particles due to their aggregation. The average diameter of the particles increases, probably due to the breaking of the hydrogen bond between the water molecules and phospholipids [Mehnert *et al*., 2012].

To prevent these issues, the freeze-drying process of SANPs dispersion was carefully investigated. A preliminary thermodynamic study was carried out to select the most suitable additive for SANPs lyophilization among different cryoprotectants.

In general, when during the lyophilization process and, in particular, during the secondary drying, the lipid membrane reaches the temperature of the phase transition, the encapsulated drug is readily released from the liposomes on going from the gel phase to the liquid crystalline one. A cryoprotectant hampers the phase transition and protects liposomes from the damage due to ice aggregation, by preventing phase separation of the different lipids and preventing the encapsulated drug from leaking out [Chengiun *et al*., 2010]. Thus, a cryoprotectant is an additive, in general a sugar, able to provide a protective effect through two mechanisms. The first is related to replacement of water, due to sugar interaction with PLs head groups; this causes the decrease of phase transition temperature of the lipid membrane by incorporating sugar

molecule in place of water molecule. The second is related to matrix formation: during freeze-drying, the concentration of the sugar solution increases and, consequently, a sugar matrix is formed. The latter prevents the vesicles from coalescing and aggregating and also protects the lipid layer from the damage due to possible formation of ice crystals during freezing. Furthermore, the interaction between the liposome surface and the matrix reduces the surface tension, thereby stabilizing the dried nanovectors [Wolfe *et al*., 1999; Sun *et al*., 1996].

As described by G. Strauss and H. Hauser (1986) the extent of membrane disruption depends on the membrane mobility at the moment of freezing and the sucrose exerts its protective effect by binding to the membrane interface [Strauss and Hauser, 1986].

Furthermore, as explained by Crowe J. *et al*. (1987), freeze-dried unilamellar vesicles leak their entire load to the medium upon rehydration. Contrariwise, it was showed that similar vesicles freeze-dried in the presence of trehalose can be stabilized and, in this case, 100% of the trapped solute is retained [Crowe *et al*., 1987].

Finally, Alihosseini *et al*. reported that mannitol is used due to its capability to maintain the chemical-physical characteristics of drugs and avoid aggregation of nanoparticles [Alihosseini et. al, 2015].

Thus, in this study, sucrose, mannitol and trehalose have been analyzed as potential cryoprotectant.

The cryoprotectant properties of sugars strongly depend on the ability to form an amourphous/crystalline solid upon rapid freezing [Izutsu *et al*., 1993]. In this context, differential scanning calorimetry (DSC) is used as an analytical tool to evaluate the phenomena from both a qualitative and a quantitative point of view [Martini *et al*., 1997]. Thus, a thermodynamic study was carried out to select the most suitable cryoprotectant for SANPs lyophilization among trehalose, mannitol and sucrose. More in details, for each additive including into the SANPs, the thermodynamic cycle was studied and peak temperatures, along with variations of enthalpy (ΔH), were studied to evaluate the presence of crystallization peaks [Gill *et al*., 2010]. In this study, the DSC technique was used because of the possibility to evaluate the presence of thermal transitions in a sample when this is heated/cooled [Gill *et al*., 2010]. A good cryoprotectant

should not show any thermal transition of the formulation that including it [Chengiun *et al*., 2010]. From the result of this study was possible select the substances without crystallization peaks, which are no desiderable during the lyophilization process. Moreover, the “safe temperature” for the lyophilization process was determined in this study [Tang and Pikal, 2004].

The first part of the Ph.D. activity described in this chapter was focused on a DSC study, for monitoring the frozen state behaviour of three cryoprotectants, namely sucrose, mannitol and trehalose. From this first step, the cryoprotectant most suitable for preserving the product during the lyophilization process has been selected for the following phases of the study. Subsequently, the lyophilization parameters, such as the temperature, pressure and time as well as the freezing method, were evaluated. Once optimized the lyophilisation process, Zol-encapsulating SANPs have been freeze-dried, re-hydrated and analyzed in term of physical-chemical characteristics. Finally, preliminary *in vitro* and *in vivo* studies were carried out on GBM cell line, to evaluate if freeze-dried and reconstituted Zol-encapsulating SANPs maintained the ability to deliver Zol in tumor cell and in GBM tissues thus inhibiting cell/tumor proliferation.

3.3 Materials and methods

3.3.1 Materials

Zoledronic acid (Zol), trehalose, mannitol, sucrose were kindly provided by Lisapharma S.p.a. (Erba, Italy). 1,2-dioleoyl-3-trimethylammonium-propane chloride (DOTAP) was kindly provided by Lipoid GmbH (Ludwigshafen, Germany), cholesterol (CHOL), 1,2-distearoyl-sn-glycero-3-phosphoethanolamine-N-[amino(polyethylene glycol)-2000] (DSPE-PEG_{2000}) were purchased from Avanti Polar (Alabama, Usa). Sodium chloride, sodium hydroxide (NaOH), calcium chloride ($CaCl_2$), sodium phosphate dibasic (Na_2HPO_4), potassium chloride, human transferrin (Tf), were obtained from Sigma-Aldrich Co. (Milan, Italy).

3.3.2 Methods

3.3.2.1 Differential Scanning Calorimetric analysis (DSC)

Thermoanalytical tests were carried out by a TA Q20 differential scanning calorimeter (DSC, TA Instruments, USA). For each experiment, 15 µl of product were placed in a hermetic DSC pan. Single scans were performed under an inert nitrogen atmosphere in the -60 ÷ +60°C temperature range at a 2°C/min heating or cooling rate under an inert nitrogen atmosphere at constant 50 ml/min flow rate. The optimized thermal cycle is described in Table 3.3.2.1.1. Triplicate experiments were carried out.

1. Equilibrate at 40.00 °C
2. Ramp 2.0 °C/min to -60.00 °C
3. Isothermal for 10 minutes
4. Ramp 2.0 °C/min to +60.00 °C
5. Equilibrate at 40.00 °C

Table 3.3.2.1.1: Thermal cycle on formulation at Differential Scanning Calorimetry (DSC).

3.3.2.2 Lyophilization

The lyophilization method was performed by Martin Christ Freeze-dryer EPSILON 2-6 LSCplus in SIRTON Pharmaceuticals S.p.a. and by Laboratory Freeze Dryers LyoQuest-55/85 in laboratory scale. The volume of the formulation was around 20 ml in industrial scale and 1.7 ml in laboratory scale. Cryoprotectants were added after filtration of product in ratio 5% (w/w) with formulation. The parameters of the process were held constant in both lyophilizations: the value of the pressure was between 0.13 mbar and 0.2 mbar while the temperature was between -80 °C and -50 °C. The process of freezing in Sirton was longer (48h) compared to the instantaneous freezing by nitrogen in laboratory.

3.3.2.3 Preparation of freeze-dried SANPs

PEGylated cationic liposomes (2.5 mg/ml) (DOTAP/chol/DSPE-PEG_{2000} 1:1:0.5 weight ratio) were prepared by hydration of a thin lipid film, followed by extrusion. 1 ml of PLs was mixed with 5 mg of human Tf, at room temperature for 15 minutes, obtaining a colloidal dispersion here named PL-Tf.
CaP NPs were prepared and complexed with Zol. Briefly, an aqueous solution of dibasic hydrogen phosphate (10.8 mM) was added, dropwise and under magnetic stirring, to an aqueous solution of calcium chloride (18 mM) and, after 10 minutes of reaction, the resulted dispersion was filtered twice through a 0.22 µm filter. CaPZ were prepared mixing 500 µl of CaP with 91 µl (0.4 mg) of an aqueous solution of Zol (0.125 M) in phosphate buffer at pH 9.5 for 15 minutes.
Finally, SANPs were prepared by mixing PL-Tf complex with CaPZ, at room temperature for 15 min and then filtered through a 0.22 µm filter.
SANPs were prepared with or without cryoprotectants. When a cryoprotectant was included, mannitol, trehalose or sucrose were added at 5% w/w, taking into the account the theoretical solid component of SANPs.

3.3.2.4 Particle size

SANPs, before and after freeze-drying and reconstitution with water, were characterized in terms of mean diameter and polydispersity index (PI). In particular, mean diameter was determined at 20°C by photon correlation spectroscopy (PCS) (N5, Beckman Coulter, Miami, USA). For these measurements, each sample was analyzed with detector at 90° angle. Polydispersity index (PI) was used as measure of the particle size distribution. For each batch, mean diameter and size distribution were the average of three measures, while for each formulation; the mean diameter and PI were calculated as the values averaged over three different batches.

3.3.2.5 Zeta potential

The zeta-potential (ζ) of the SANPs before and after freeze-drying and reconstitution with water, was measured in water by means of a Zetasizer Nano

Z (Malvern, UK). For each batch, data of ζ were collected as the average of 20 measurements, while for each formulation the ζ was calculated as the average of ζ over three different batches.

3.3.2.6 Cell proliferation assay

Human GBM cell line T98G was provided by ATCC. Cells were grown in EMEM, supplemented with 10 % heat-inactivated fetal bovine serum, 20 mM HEPES, 100 U/ml penicillin, 100 mg/ml streptomycin, 1 % L-glutamine and 1 % sodium pyruvate. Cells were cultured at 37 °C in a 5 % CO_2 −95 % air environment in a humidified incubator.

Cells were seeded in serum-containing media in 96-well plates at the density of 2 × 103 cells/well. After 24 h incubation at 37 °C, cells were treated with increasing concentrations of the different formulations and reference compounds (1.5-200 μM) for 72 h. Cell viability was assessed by adding MTT [3-(4,5-dimethylthiaZol-2-yl)-2,5- diphenyl tetrazolium bromide] solution in phosphate- buffered saline (PBS) to a final concentration of 5 mg/ml. The plates were then incubated at 37 °C for an additional 4 h and the MTT-formazan crystals were solubilized in 1 N isopropanol/hydrochloric acid 10 % solution at 37 °C on a shaking table for 20 min. The absorbance values of the solution in each well were measured at 570 nm using a Bio-Rad 550 microplate reader (Bio-Rad Laboratories, Milan, Italy). Percentage of cell viability was calculated as the following formula (absorbance of the treated wells - absorbance of the blank control wells)/(absorbance of the negative control wells - absorbance of the blank control wells). All MTT experiments were performed in quadruplicate.

3.3.2.7 *In vivo* study

All animal experimentation procedures were approved by the Italian Ministry of Health and were in compliance with the national and international directives (D.L. March 4, 2014, no. 26; directive 2010/63/EU of the European Parliament and European Council; Guide for the Care and Use of Laboratory Animals, United States National Research Council, 2011). Male nude (nu/nu) mice, 6–8

weeks old and weighing 22–24 g were purchased from Envigo S. Pietro al Natisone, (Udine).

Mice were anesthetized and injected intracranially with 5 x 10^4 U87MG LUC glioblastoma cells /mouse, through the center-middle area of the frontal bone to a 2-mm depth, using a 0.1-ml glass micro-syringe and a 27-gauge disposable needle. One hour prior to intracranial implantation, the mice were weighed and pre-medicated with a subcutaneous injection of 0.5 mg/ kg of Metacam (meloxicam) in saline to control for post-operative pain and inflammation. The medication was carried out until the end of the experiment.

After 5 days mice were randomized, divided in four groups and treatment started. The following groups were evaluated: untreated; SANPs 1, SANPs 4 freeze-dried. Mice were treated intravenously (*i.v.*) at 20 µg Zol/mouse/d for three times a week for 3 consecutive weeks.

Mice were imaged using the IVIS imaging system 200 series (Caliper Life Sciences, Hopkinton, MA, USA). Briefly, mice were anesthetized with a combination of tiletamine–Zolazepam (TelaZol, Virbac, Carros, France) and xylazine (xylazine/ Rompun BAYER) given intramuscularly at 2 mg/kg. Then mice were injected intraperitoneally with 150 mg/kg D-luciferin (Caliper Life Sciences), and imaged in the supine position 10 min after luciferin injection. Imaging was performed at baseline (day of tumor cell injection) and several times during the experiment. Data were acquired and analyzed using the living image software version 4.3 (Caliper Life Sciences). Tumor growth was monitored by photons analysis. Complete tumor regression was defined as an undetectable bioluminescent signal in the brain of mice, lasting for at least five weeks.

Animals were closely monitored by visual inspection and weighed daily from start of treatment and sacrificed when evident signs of tumor burden (especially weight loss >20% and severe neurological dysfunction).

3.4 Results and discussion

3.4.1 Selection of the cryoprotectants by differential scanning calorimetric (DSC) study

In this study, DSC was used to analyze the frozen-state behaviour of different cryoprotectants in order to select the most suitable candidate for SANPs cryoprotection; deionized water was used as a reference. Thus, sucrose, trehalose and mannitol were added as cryoprotectants to the formulation at a 5% w/w taking into account the theoretical solid component of SANPs and the analysis were effectuated on final products (SANPs + cryo) by DSC. Onset and peak temperatures, along with variations of enthalpy (ΔH), were observed. The obtained thermograms displayed an exothermic peak of crystallization and an endothermic peak of fusion related to water. In the first thermogram is reported the thermal cycle of the depurated water used as reference.

The DSC thermogram of water, displayed in Figure 3.4.1.1, shows an endothermic peak with an onset at (-0.57 ± 1.55)°C, peak at (2.58 ± 0.01)°C, and a heat of fusion was (338 ± 13) J/g, which is consistent with literature data (334 J/g) [Kirsh *et al*., 1999].

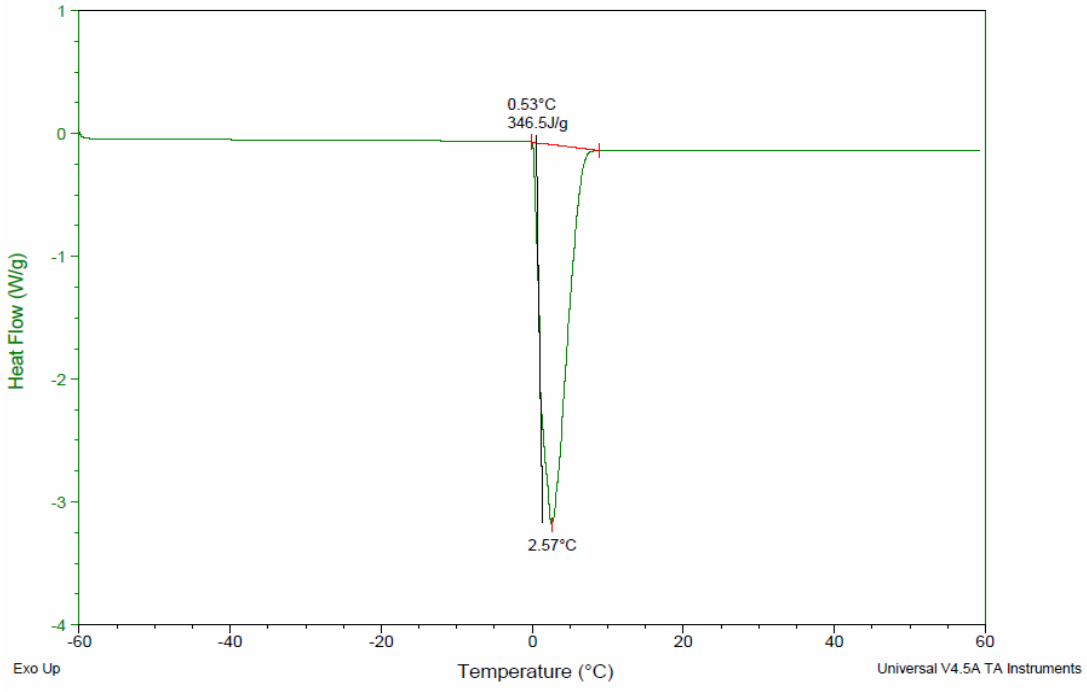

Figure 3.4.1.1: Thermal cycle of reference depurated water.

Fig. 3.4.1.2 displays the thermogram of the formulation containing mannitol. A small exothermic peak was detected at (-20.4 ± 2.2) °C, with a heat of (3.21 ± 0.37) J/g. This peak can be reasonably attributed to a partial crystallization of mannitol during the heating phase. An endothermic peak associated to water melting appears at (-1.60 ± 0.10)°C, with a melting heat of (297 ± 13) J/g. In this thermogram, the endothermic peak is broader than the peak of water because of the presence of solutes. It is noticeable that the extrapolated onset temperature is slightly lower compared to the onset temperature of water.

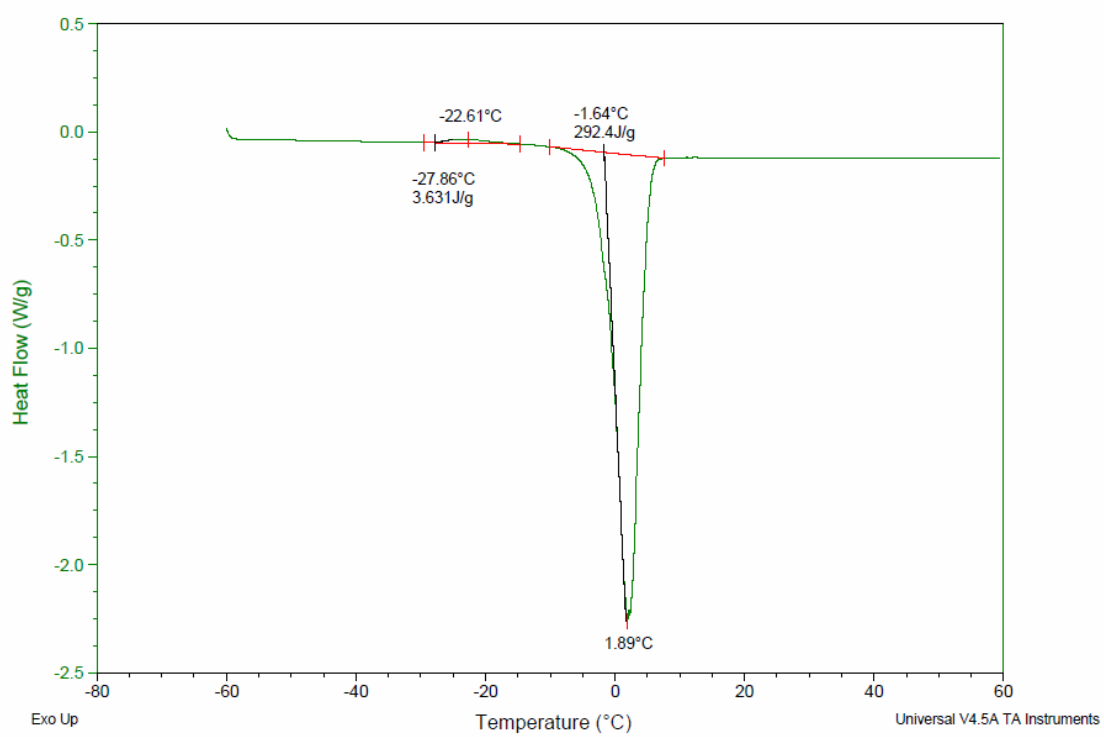

Figure 3.4.1.2: Thermal cycle of formulation added with mannitol.

Figure 3.4.1.3 reports the DSC thermogram of the formulation containing trehalose. An endothermic peak was detected, with an extrapolated onset temperature of (-1.24 ± 0.03) °C and a fusion heat of (296 ± 17 J/g). Again, the peak is broader than the peak of water because of the presence of solutes.

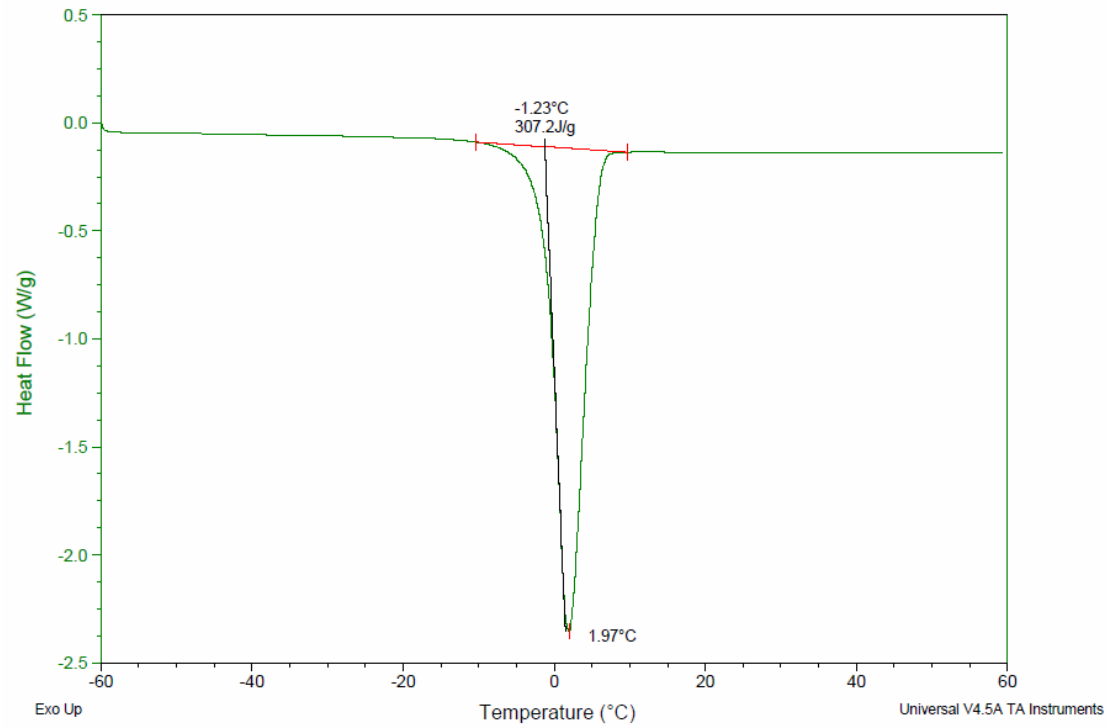

Figure 3.4.1.3: Thermal cycle of formulation added with trehalose.

Likewise, in presence of sucrose, an extrapolated onset temperature of (-1.65 ± 0.09) °C was found out, and a fusion heat (283 ± 9 J/g) determined (Figure 3.4.1.4). Again, a broader endothermic peak has been found due to the presence of solutes.

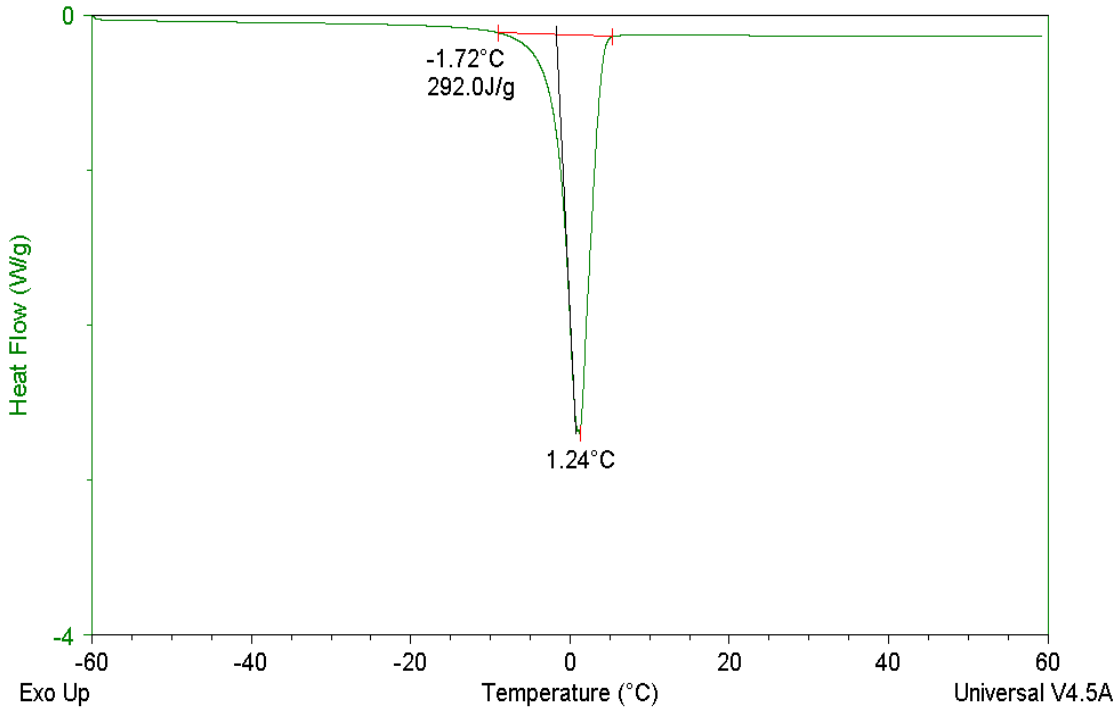

Figure 3.4.1.4: Thermal cycle of formulation added with sucrose.

A summary of the parameters acquired in the DSC analyses is reported in Table 3.4.1.1.

Phase	Parameter	Water	Mannitol	Sucrose	Trehalose
Heating	Left limit (°C) ± sd*	-	-27.8 ± 1.6*	-	-
	Peak (°C) ± sd*	-	-20.4 ± 2.2*	-	-
	Right limit (°C) ± sd*	-	-14.3 ± 2.0*	-	-
	Onset (°C) ± sd*	-	-26.2 ± 2.1*	-	-
	ΔH (J/g) ± sd*	-	3.21 ± 0.38*	-	-
Heating	Left limit (°C) ± sd*	-0.23 ± 0.10*	-9.24 ± 1.14*	-9.67 ± 0.6*	-10.0 ± 0.4*
	Peak (°C) ± sd*	2.58 ± 0.01*	1.99 ± 0.38*	1.35 ± 0.30*	1.73 ± 0.22*
	Right limit (°C) ± sd*	8.26 ± 0.83*	7.52 ± 0.40*	7.57 ± 1.10*	8.14 ± 1.72*
	Onset (°C) ± sd*	-0.57 ± 1.55*	-1.60 ± 0.10*	-1.65 ± 0.09*	-1.24 ± 0.03*
	ΔH (J/g) ± sd*	338 ± 13*	297 ± 13*	283 ± 9*	296 ± 17*

*standard deviation on almost three different batches

Table 3.4.1.1: Thermal cycle of water as reference and of formulations added with mannitol, trehalose and sucrose.

The result of these analyses showed that sucrose and trehalose possess similar thermodynamic features, while in the case of mannitol a peculiar thermodynamic behaviour was found. In particular, a small crystallization peak was detected. The peak was associated to the transition between crystal and amorphous form of this sugar, which is generally unwanted in the perspective of obtaining an optimized lyophilized product. Mannitol was thus excluded in the following step of the study.

3.4.2 Lyophilization study

The study of SANPs lyophilization was carried out at the Sirton Pharmaceutical (Villa Guardia (CO), Italy) in agreement with Lisapharma s.p.a. Freeze-drying of SANPs dispersion was tested in presence of sucrose or trehalose as cryoprotectants to preserve the product during the lyophilization process.

Firstly, in order to design an optimized freeze-drying process, not only the properties of the excipients used (investigated by DSC in paragraph 2.4.1) but also the collapse temperature of the formulation, should be known (Scutellà and Bourlès, 2020). More in details, the macroscopic collapse temperature of the formulation (Tc) is the temperature above which the freeze-dried product loses macroscopic structure and collapses during freeze drying [Tang and Pikal, 2004]. Tc is usually about 2°C higher than transition glass temperature (Tg), which is often associated with the glass transition temperature in the frozen state [Pikal and Shah, 1990], or equals the eutectic temperature (Teu) if solutes are crystallized in the frozen solution. In order to produce an acceptable freeze-dried product, it is always required to lyophilize a formulation at the temperature lower than Tc [Pikal (I), 1990, Pikal (II), 1990]. For this reason we decided to set up the “safe temperature” of the formulation 10 degrees under the temperature of the beginning of the endothermic curve. Therefore, in the case of formulation with trehalose or sucrose, the endothermic curve of fusion started around -10 °C in the DSC study, suggesting that the temperature of the preparation should to be set up to ≤ -20 °C during the sublimation phase.

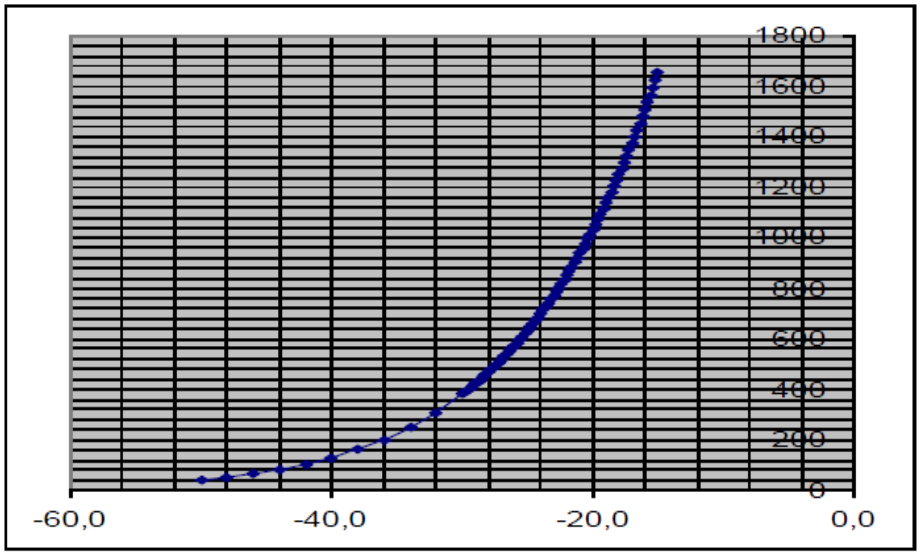

Figure 3.4.2.1: Relationship between Temperature - Vapour pressure of water (ppH_2O).

Once that the value of the “safe temperature” during the sublimation phase was fixed at ≤ -20 °C, the second parameter to establish for a lyophilization method is the pressure into the chamber of freeze-dryer. As evident from the Figure 3.4.2.1, considering that the water at 25°C has a ppH_20 = 760 Torr, therefore a temperature of -20°C has a ppH_20 = 776 mTorr, this ppH_2O at -20°C corresponding at 1.034 mbar (776 mTorr x K, where K is the constant factor mmHg/microbar= 1.333322) at sublimation front. Therefore, taking into account the resistances that vapour comes across when it reach from the vial, therefore from the chamber, the freeze-drier condenser, the chamber pressure should be set to at least 1/5 of this value and therefore ≤ 0.2 mbar.

Thus, the lyophilization was carried out at Sirton Pharmaceuticals s.p.a. by Martin Christ Freeze-dryer EPSILON 2-6 LSCplus, starting from these first observations and considerations. Indeed, the lyophilization process was set up for the SANPs following the addition of cryoprotectants trehalose and sucrose. The lyophilization cycle, divided in freezing, primary drying or sublimation, and secondary drying is represented and summarized in Figure 3.4.2.2.

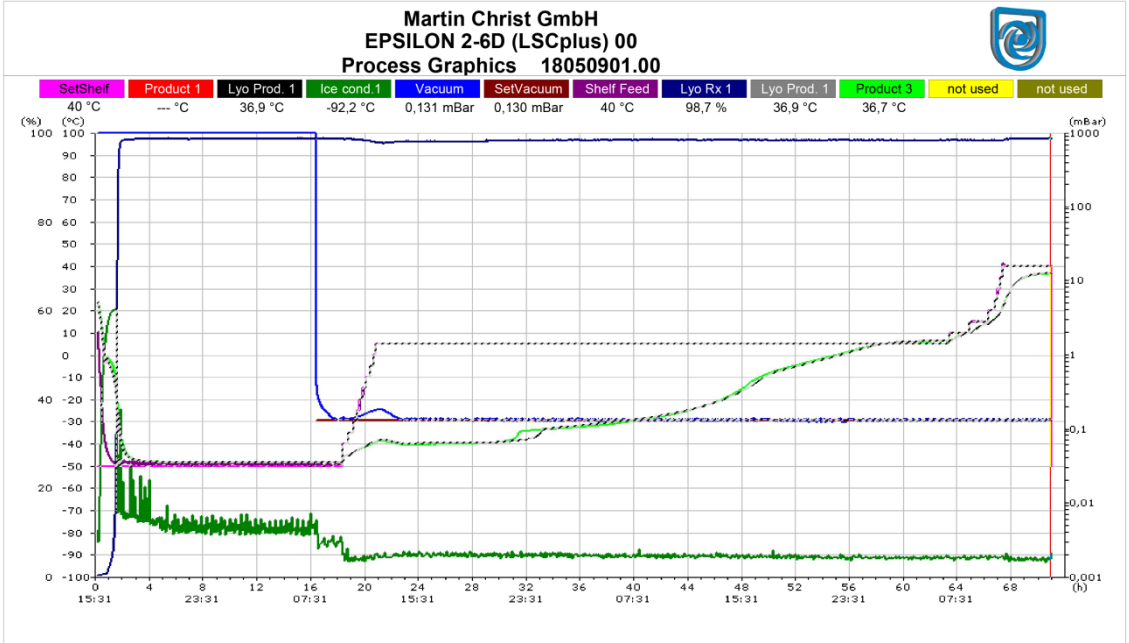

Phase	Pressure	Temperature of plates	Speed	Conductibility Resistance	Time
Freezing	max 0.2 mbar	from T_{amb} to -50°C	1 °C/min	> 90%	18h
Sublimation	0.13 mbar	from -50°C to 5°C	0.15 °C/min	> 90%	22h
Secondary drying	0.13 mbar	from 5°C to 40°C	0.15 °C/min	> 90%	6h

Figure 3.4.2.2: Lyophilization cycle.

During the freezing step, most of the water is converted into ice at temperatures about −50°C. Then, the pressure of the system is reduced using vacuum pumps, and the shelf temperature is raised to facilitate ice sublimation during primary drying. In the secondary drying stage, the shelf temperature is further raised to efficiently remove unfrozen water by desorption to provide a low residual water content [Patel *et al*., 2009].

Before starting the lyophilization process, all the vials were hermetically closed with the exception of two in which it was put the probes to check the temperature. More in details, during the “freezing phase” the temperature of the plates was decremented until -50°C with a speed of approximately 1°C/min and maintained for around 18 h. A cooling rate of this magnitude yields moderate

supercooling with moderate ice surface area and a reasonably fast freezing rate; it also (usually) produces uniform ice structure [Crowe *et al*., 1987]. When the temperature of -50°C was reached, the conductibility resistance of the dried cake was >90%, an optimum value to guarantee the rigidity and avoid softening that could cause collapse and fusion of the dried structure of the cake [Franks and Auffret, 2007]. Thereafter, during the “Sublimation phase”, the pressure of the chamber has been reduced and maintained at 0.13 mbar and the temperature of the plates was incremented until 5 °C with a speed approximately of 0.15°C/min. Due to the risk of collapse, especially in secondary drying, the shelf temperature should be increased slowly in this phase because a fast temperature ramp might cause collapse of dried cake of the product [Tang and Pikal, 2004]. The probes, placed into the vials, have allowed quantifying the time that the vials have used to reach the same temperature of the plates. This time was around 20 h and other 2 h were used to allow reaching the same value for all the vials. In fact, the vials with the probes generally use less time to reach the temperature compared to the vials without the probes, which are hermetically closed. During this time the conductibility resistance of the preparation was >90% [Franks and Auffret, 2007]. To calculate this time, the height of the cake need to calculated as follows [Jennings, 1980]:

$$tsubl = k \times h1.5$$

$$h = V/((((R - s \times 2)/2)2) \times \pi) \times 100$$

Where:

tsubl = time for sublimation phase

k = constant (22.58)

h = height of the cake

V = volume of formulation (16.6 ml)

R = vial volume (50 ml)

s = glass thickness (1.2 mm)

Finally, the temperature of the plates was incremented until 40 °C, with a speed of approximately 0.15°C/min, and maintained at this value for around 6 h to obtain the “Secondary drying” [Tang and Pikal, 2004]. During this time the

conductibility resistance of the preparation was >90% [Franks and Auffret, 2007]. All the process has been conducted manually.

In the first phase of sublimation, a peak of pressure at 0.18 mbar was detected, but this event did not influenced the process because the conductibility resistance of the preparation was always >90% and the temperature of the product was always under the safe temperature of -20°C (around -40°C).

The value of the speed was chosen based on the necessity to maintain the conductibility resistance of the preparation >90% [Franks and Auffret, 2007].

The formulations freeze-dried in these conditions are reported in Figure 3.4.2.3.

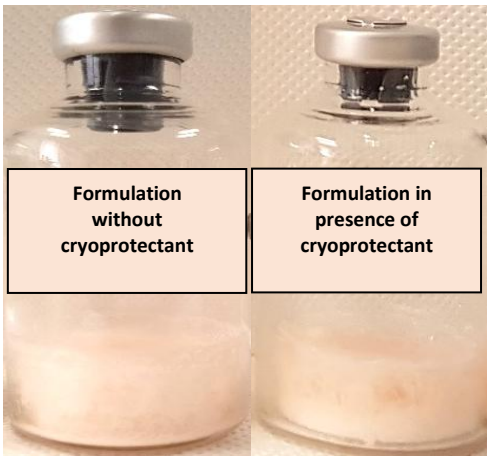

Figure 3.4.2.3: Formulation lyophilized in presence of sucrose as cryoprotectant (on the right) or without (on the left).

The formulation freeze-dried without cryoprotectants as well as the formulation freeze-dried in presence of trehalose have been re-hydrated and analyzed. The results showed a significant increase in nanoparticle size and PI following lyophilization (Table 3.4.2.1). For this reason, these formulations were discarded for the following studies on cells and *in vivo*.

Cryoprotectant	Lyophilization	Mean (nm) ± sd*	PI± sd*	PZ (mV) ± sd*
-	Before	131.0±10.7*	0.143±0.020*	+5.9±0.7*
	After	244.2±14.0*	0.466±0.030*	+6.4±0.9*
Sucrose	Before	162.4±6.8*	0.216±0.020*	+8.1±2.0*
	After	159.6±15.4*	0.245±0.030*	+7.4±0.7*
Trehalose	Before	123.3±4.2*	0.149±0.010*	+5.4±0.6*
	After	380.0±7.7*	0.514±0.30*	+6.5±1.5*

*standard deviation on almost three different batches

Table 3.4.2.1: Mean diameter, polydispersity index, zeta potential of formulations without or with different kind of cryoprotectants.

Although the characteristics of the product lyophilized using sucrose as cryoprotectant showed good technological characteristics, the cake resulted separated in two phases (the formulation and the sucrose as shown in Figure 3.4.2.3 on the right) probably for the low freezing rate. Further changes in the lyophilization process, e.g. the freezing time, were investigated to improve the aspect of the freeze-dried product. In particular, a new lyophilization set up with a rapid freezing in nitrogen liquid (reported in Table 3.4.2.2 as SANPs 1) was tested to avoid the separation of the product in two phases.

Furthermore, formulations characterized by some changes, as described in Chapter 2 (paragraph 2.5.1), in particular SANPs performed with the lyophilized transferrin (SANPs 2), SANPs performed with zoledronic acid incremented in volume (SANPs 3) and SANPs 4 performed with both changes, were also lyophilized. Sucrose was added to all the formulations before lyophilization.

The results of the characteristics after re-hydration of SANPs 1, SANPs 2, SANPs 3 and SANPs 4, are reported in Table 3.4.2.2.

Formulation	Lyophilization	Mean (nm) ± sd*	PI± sd*	PZ (mV) ± sd*
SANPs 1	Before	134.4±3.3*	0.126±5.3*	+5.3±0.1*
	After	145.6±15.4*	0.245±0.03*	+8.9±3.3*
SANPs 2	Before	140.7±11.6*	0.155±0.020*	+7.1±1.4*
	After	151.5±2.6*	0.232±0.030*	+13.4±0.4*
SANPs 3	Before	121.1±1.5*	0.124±0.040*	+6.2±0.3*
	After	184.0±3.2*	0.299±0.040*	+6.2±1.0*
SANPs 4	Before	110.8±6.5*	0.165±0.040*	+8.2±3.2*
	After	91.3±6.3*	0.220±0.030*	+12±2.3*

*standard deviation on almost three different batches

Table 3.4.2.2: Mean diameter, polydispersity index, zeta potential of formulations without or with some changes before and after lyophilization.

As is possible see in Table 3.4.2.2 all the products showed good mean diameter, polydispersity index and zeta potential, but the formulation SANPs 4 showed the lower mean diameter and PI. Furthermore, the product prepared as described above showed a cake with homogeneous appearance (Figure 3.4.2.4) and was selected as lead product of our study for further *in vitro* and *in vivo* studies.

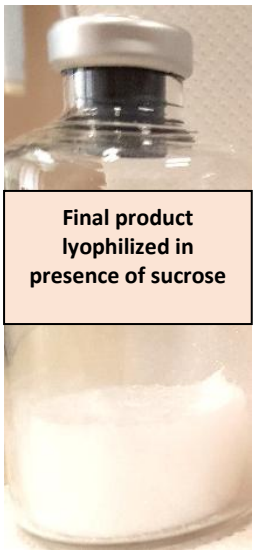

Figure 3.4.2.4: Final product lyophilized in presence of sucrose with both changes on human transferrin and zoledronic acid.

3.5 Cell proliferation assay

Although the SANPs showed physical-chemical characteristics suitable for i.v. use, the ability to deliver Zol following the freeze-drying step was also investigated on a GBM cell line, by measuring the ability of the bisphosphonate to inhibit cell proliferation. In particular, the ability of SANPs 4 and SANPs 4 freeze-dried after reconstitution was studied on T98G GBM cell line after 72 hours of incubation with the formulations. Briefly, cells were seeded in serum-containing media in 96-well plates. After 24 h incubation at 37 °C, cells were treated with increasing concentrations of the different formulations and plain SANPs (used as reference compounds) (1.5-200 μM) for 72 h. Finally, MTT assay was performed.

As reported in Figure 3.5.1, a preliminary result showed that the dried formulation is characterized by a high efficacy because it manages to inhibit the cell viability at very low concentration. More in details, both plain SANPs resulted no toxic on the cells showing a percentage of cell viability between 72% and 100%, respectively. SANPs 4 had an IC50 corresponding to 12.5 μM, while SANPs 4 freeze-dried had an IC50 = <1.56 μM. These results suggest that SANPs 4 freeze-dried is much more powerful in delivering Zol, requiring a lower concentration for inhibiting 50% of cell viability compared to SANPs 4.

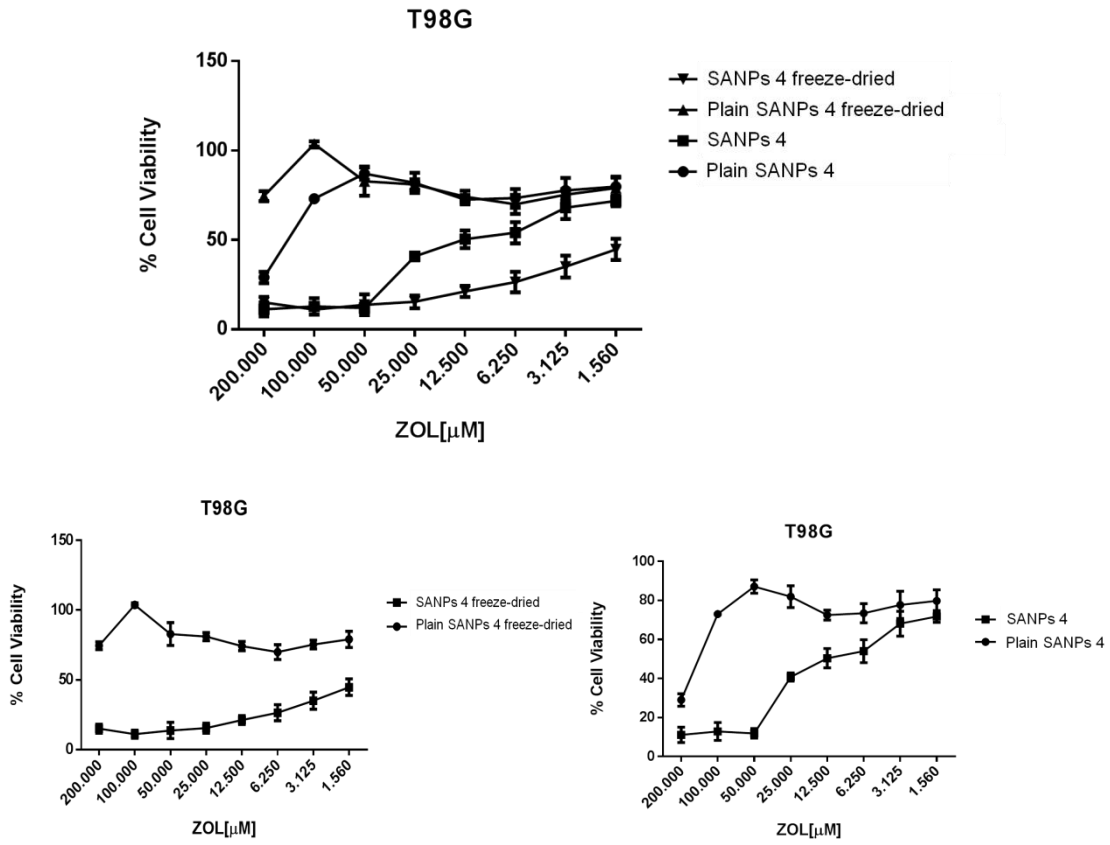

Figure 3.5.1: Cell viability assay on SANPs 4 and SANPs 4 freeze-dried.

3.6 *In vivo* study

The therapeutic efficacy of the different SANPs formulations *in vivo* was evaluated in an orthotopic GBM. To this purpose $5x10^4$ U87MG LUC cells were inoculated intra-brain into immuno-compromised mice. This tumor model closely recapitulates histological phenotype consistent with of human GBM. After 5 days, when the tumor mass became visible by bioluminescence analysis, the mice were divided into four groups: untreated mice, mice treated with SANPs 1 (SANPs prepared with previously developed protocol) and with SANPs 4 freeze-dried (SANPs prepared according to the protocol developed in this Ph.D. activity). Interestingly, in all cases, SANPs formulations were well tolerated as no toxic deaths or body weight loss was reported in animals. As reported in Table 3.6.1, in mice treated with both SANPs 1 and 4 freeze-dried we observed the complete disappearance of the tumor, showed by an undetectable

bioluminescent signal, in the brain of 1 out of six mice, lasting for at least five weeks.

These *in vivo* preliminary results support the potential use of SANPs formulations for the treatment of GBM, for which no effective therapies are at this moment available. Furthermore, the results reported for the freeze-dried product are similar compared to the results obtain analyzing the formulation prepared following the previous protocol.

Treatment groups	Complete Tumor regression
SANPs 1	1/6
SANPs 4 freeze-dried	1/6

Table 3.6.1: Antitumor efficacy of SANPs formulations against orthotopic GBM. SANPs 1 (SANPs prepared following previously protocol), SANPs 4 freeze-dried.

3.7 Conclusions

This phase of the study explored a further evolution of SANPs technology, reducing the complexity of the preparation protocol. In particular, the aim of the study was to provide a formulation ready-for-use starting from a freeze-dried powder to be reconstituted by addition of the solvent.

Firstly, a DSC study was performed on different kind of cryoprotectants to evaluate the excipient suitable to protect the formulation during the lyophilization process. This study was useful also to understand the parameters to set up during the lyophilization process. Thereafter, a lyophilization process was carried out by deep investigation of all the phases of the process. Thus, SANPs, as modified in Chapter 2 (paragraph 2.5.1), were lyophilized. Finally, all the products were characterized after re-hydration in terms of mean diameter, polydispersity index and zeta potential. The analysis showed that sucrose used as cryoprotectant, more than trehalose, allowed to maintain colloidal characteristics of the SANPs suitable for intravenous administration. Further controls on cell culture and *in vivo* were carried out. In particular, SANPs freeze-dried and reconstituted with water maintained the ability to deliver Zol in cells, as suggested by the inhibition of the cell proliferation found on T98G cell lines. In addition, in preliminary experiments in an orthotopic model of GBM, the newly developed SANPs formulation maintains the same ability to induce tumor regression (complete tumor regression in one animal/6 animals).

REFERENCES

Alihosseini F. , Ghaffari S., Reza Dabirsiaghi A., Haghighat S. Freeze-drying of ampicillin solid lipid nanoparticles using mannitol as cryoprotectant, Brazilian Journal of Pharmaceutical Sciences vol. 51, n. 4 (2015). doi.org/10.1590/S1984-82502015000400005.

Carpenter J.F. and Chang B.S. Lyophilization of protein pharmaceuticals. In K. Avisand and V. Wu (eds.), Biotechnology and Biopharmaceutical Manufacturing, Processing and Preservation, Intepharm Press, Buffalo Grove, IL, pp. 199–263 (1996).

Chengiun C., Dandan H., Cuifang C., An overview of liposome lyophilization and its future potential, Journal of controlled release, 142(3), pp.299-311, (2010).

Crowe J.H., Crowe L.M., Carpenter J.F., Stabilization of dry phospholipid-bilayers and proteins by sugars, Biochemical Journal, 242(1), pp.1-10, (1987).

Franks F. and Auffret T. RSC publishing. Freeze-drying of Pharmaceuticals and Biopharmaceuticals. Principle and practice. Chapter 8, 111 (2007).

Ghanbarzadeh S., Valizadeh H. and Zakeri-Milani P. The Effects of Lyophilization on the Physico-Chemical Stability of Sirolimus Liposomes. Adv Pharm Bull. 3(1): 25–29 (2013). doi: 10.5681/apb.2013.005.

Gill P., Moghadam T.T., Ranjbar B. Differential Scanning Calorimetry Techniques: Applications in Biology and Nanoscience, J. Biomol. Tech., 21, 167-193 (2010).

Goldspiel B., Hoffman J.M., Griffith N.L. ASHP guidelines on preventing medication errors with chemotherapy and biotherapy. Am J Health Syst Pharm.; 72:e6–35 (2015).

Hansen L.J.J., Daoussi R., Vervaet C., Remon J.P.,.De Beer T.R.M. Freeze-drying of live virus vaccines: A review. Vaccine. 33 (42): 5507–5519 (2015). doi:10.1016/j.vaccine.2015.08.085.

Hua S., De Matos M.B.C., Metselaar J.M. and Storm G. Current Trends and Challenges in the Clinical Translation of Nanoparticulate Nanomedicines: Pathways for Translational Development and Commercialization. Frontiers in Pharmacology. Volume 9,Article 790 (2018). doi: 10.3389/fphar.2018.00790

Izutsu K, Yoshioka S, Terao T. Decreased protein-stabilizing effects of cryoprotectants due to crystallization. Pharm Res. 10(8):1232-7 (1993).

Jennings T. Optimisation of the Lyophilisation Schedule. Advanced Lyophilization (1980).

Kirsh Yu.E., Yanul N.A., Kalninsh K.K. Structural transformations and water associate interactions in poly-N-vinylcaprolactam–water system. European Polymer Journal. Volume 35, Issue 2, Pages 305-316 (1999).

Martini A., Kume S., Crivellente M., Artico R. Use of subambient differential scanning calorimetry to monitor the frozen-state behavior of blends of excipients for freeze-drying. PDA J Pharm Sci Technol.51(2):62-7 (1997).

Patel S.M., Bhugra C., and Pikal M. J. Reduced Pressure Ice Fog Technique for Controlled Ice Nucleation during Freeze-Drying. AAPS PharmSciTech. Vol. 10, No. 4 (2009).

Pikal M.J. and Shah S. The collapse temperature in freeze drying: dependence on measurement methodology and rate of water removal from the glassy phase. Int. J. Pharm. 62:165–186 (1990).

Pikal M.J. Freeze-drying of proteins part II: formulation selection.BioPharm 3:26–30 (1990).

Pikal M.J. Freeze-Drying of Proteins. In V. H. L. Lee (ed.), Peptide and Proteins Delivery, Marcel Dekker, New York (1998).

Pikal M.J. Freeze-drying of proteins. Part I: process design. BioPharm 3:18–28 (1990).

Rey L.; May J. Freeze-Drying/Lyophilization of Pharmaceutical and Biological Products (Third ed.). Informa healthcare. (2016).

Salzano G., Marra M., Porru M., Zappavigna S., Abbruzzese A., La Rotonda M.I., Leonetti C., Caraglia M., De Rosa G.. Self-assembly nanoparticles for the delivery of bisphosphonates into tumors. Int J Pharm. Jan 17;403(1-2):292-7 (2011).

Salzano G., Zappavigna S., Luce A., D'Onofrio N., Balestrieri M.L., Grimaldi A., Lusa S., Ingrosso D., Artuso S., Porru M., Leonetti C., Caraglia M., DeRosa G. Transferrin-Targeted Nanoparticles containing Zoledronic Acid as a potential tool to inhibit Glioblastoma growth. J. Biomed. Nanotechnol. 12:1–20 (2016).

Scutellà B, Bourlès E. Development of freeze-drying cycle via design space approach: a case study on vaccines. Pharm Dev Technol. 25(10):1302-1313 (2020). doi: 10.1080/10837450.2020.1806298

Strauss, G. and Hauser H., Stabilization of lipid bilayer vesicles by sucrose during freezing, H. Proc. Natl. Acad. Sci. U.S.A. 83, 2422-2426, https://doi.org/10.1073/pnas.83.8.2422 (1986).

Sun W.Q., Leopold A.C., Crowe L.M. and Crowe J.H., Stability of dry liposomes in sugar glasses. Biophys. J., 70, 1769-1776, doi: 10.1016/S0006-3495(96)79740-0 (1996).

Tang X. C. and Pikal M. J. Pharmaceutical research. Design of Freeze-Drying Processes for Pharmaceuticals: Practical Advice. 21,2 (2004).

Wolfe J. and Bryant G., Freezing, drying, and/or vitrification of membrane-solute-water systems, Cryobiology, 391 03-129 (1999).

Wolfgang M., Karsten M., Solid lipid nanoparticles Production, characterization and applications, Advanced Drug Delivery Reviews, pp.83-101 (2012).

CHAPTER 4

Self-assembling nanoparticles for delivery of microRNA to the brain to revert chemoresistance in therapy against glioblastoma

4.1 microRNA

Non-coding RNAs (nc-RNA) such as microRNAs (miRNAs) have emerged as new regulators of gene expression across various biological processes, including cell cycle regulation, differentiation, metabolism and aging [Bayraktar *et al*., 2017]. miRNAs are involved in many diseases such as cardiovascular and neurodegenerative diseases and but they also play a vital role in the pathogenesis of human cancers and in clinical applications as therapeutics [Bartel, 2004]. miRNAs can be used to classify a wide variety of human cancers and to define the molecular architecture of human cancers [Calin and Croce, 2006; Volinia *et al*., 2006]. miRNAs are characterized by 18-25 nucleotides in length and regulate the expression of target genes at the posttranscriptional level through interaction with complementary sequences usually found in the 3'-UTRs of target mRNAs, resulting in inhibition of translation and/or in mRNA degradation [Bartel, 2004].

Several oncogenic and tumor suppressor miRNAs have been identified as the promoters of tumor formation and growth when they are expressed in various cancers [Esquela-Kerscher and Slack, 2006]. Over the years, growing evidences have shown that miRNAs have an important role in breast cancer progression, invasion, angiogenesis and metastasis. Apparently, some miRNAs functionally take part in several important cell proliferation pathways and their expression is responsible for evading growth suppressors and sustaining proliferative signalling in breast cancer cells [Hwang *et al*., 2013; Tanic *et al*., 2012]. miRNA 603 (miR-603) was recently identified through genome-wide analysis in glioblastoma [Kushwaha *et al*., 1974] and thyroid cancer with a potential role in cell transformation [Mussnich *et al*., 2013]. In fact, miRNA-603, has been identified as powerful suppressor of O^6-methylguanine methyl transferase (MGMT) expression in GBM [Kushwaha *et al*., 2014].

4.2 SANPs encapsulating miRNA

Nanocarriers based on cationic lipids have been largely investigated to overcome biopharmaceutical issues associated with therapeutic use of drugs and potential agents in the treatment of several disease and, especially cancer Campani *et al*., 2016].

The development of therapeutics based on miRNAs, and in general on nucleic acids, is hampered by their rapid degradation in biological fluids, their poor uptake into the target cells and their not specific biodistribution [Baumann and Winkler, 2015]. The use of lipid nanocarriers has been largely proposed to overcome the biopharmaceutical issues associated with the therapeutic use of nc-RNA [Campani *et al*., 2016]. The efficacy of this strategy is confirmed by current ongoing clinical trials using lipid nanoparticles (NPs) to deliver nc-RNAs in different forms of cancer [Kanasty *et al*., 2013; Xu *et al*., 2015], such as GBM that is currently treated with radiotherapy in combination with chemotherapy.

Generally, the development of safe and efficient miRNA carriers is a prerequisite for the success of combination therapy. Currently, the combination of gene and chemical drugs can be classified into three categories: 1) chemotherapy combined with gene carrying nanoparticles [Bai *et al*., 2015], 2) co-delivery [Yao *et al*., 2015] and 3) use of multiple nanocarriers [Yoon *et al*., 2014]. Using separate delivery systems has the advantage of controlling timing and dosage regimen for the chemotherapy and for the gene drugs [Young *et al*., 2015].

Lipid nanoparticles possess many advantages, including biocompatibility, rapid cellular uptake, and potential for large-scale production [Yoon *et al*., 2013].

For this reason, SANPs encapsulating miRNA could be an efficient tool in the treatment of GBM.

GBM is currently treated with radiotherapy in combination with chemotherapy, namely with temozolomide (TMZ) [Pegg *et al*., 1990]. However, TMZ, especially after prolonged treatments, has only a very limited activity mainly due to the occurrence of chemoresistance mainly attributed to the activity of the O^6-methylguanine methyl transferase (MGMT) [Perazzoli *et al*., 2015; Ochs and Kaina, 2000; Kanasty *et al*., 2013].

For this part of the study, miRNA-603, that has been identified as powerful suppressor of O^6-methylguanine methyl transferase (MGMT) expression in GBM [Kushwaha *et al*., 2014], will be taken into account. SANPs encapsulating miR603 could be a powerful tool to enhance the efficacy on DNA alkylating agent, e.g. TMZ, in the treatment of GBM.

4.3 Aim of the work

SANPs are core-shell nanoparticles obtained by a self-assembling process and designed for an easy scale-up and set up to facilitate the technology transfer [Campani *et al*., 2018]. However, while for bisphosphonates the usefulness of this technology has been largely demonstrated [Salzano *et al*., 2010; Marra *et al*., 2011; Salzano *et al*., 2016], the possibility to use SANPs for the delivery of other chemical species, e.g. nucleic acids, remain to be demonstrated. Thus, in this study, the potential of SANPs for the delivery of nucleic acids was investigated. In particular, a specific miRNA, e.g. miR603, wild type or methylated, was used as model miRNA, also for its potential to revert chemoresistance in the treatment of GBM [Kushwaha *et al*., 2014].

To this aim, lipid composition, namely the type of cationic lipid, the presence of a neutral lipid and the type of PEGylated lipid, was optimized.

More in details, three different cationic lipids, namely 1,2-dioleoyl-3-trimethylammonium-propane chloride (DOTAP), N-[1-(2,3-dioleyloxy)propyl]-N,N,N-trimethylammonium chloride (DOTMA) or 3ß-[N-(N',N'-dimethylaminoethane)-carbamoyl]cholesterol hydrochloride (DC-chol), two neutral lipids, namely cholesterol (CHOL) and dioleoylphosphatidylethanolamine (DOPE), and two PEGylated lipids, namely N-palmitoyl-sphingosine-1 {succinyl[methoxy(polyethylene glycol)$_{2000}$]} (PEG_{2000}-Cer^{16}) (cer-PEG) and 1,2-distearoyl-sn-glycero-3-phosphoethanolamine-N-[amino(polyethylene glycol)-$_{2000}$] ($DSPE\text{-}PEG_{2000}$) were tested in this study.

All the prepared SANPs were characterized in terms of size, zeta potential and encapsulation efficiency of miRNAs.

Stability of SANPs have been tested in bovine serum albumin (BSA) or plasma; moreover, hemolytic activity of the formulations on red blood cells was

investigated. Cytotoxicity of the different prepared SANPs was also tested on two different GBM cell lines. Then, formulations selected in the previous studies were tested for the delivery of the miR603 in two GBM cells. Finally, the biodistribution of the miRNA, when administered with SANPs, was studied in different organs in an orthotopic model of GBM.

4.4 Materials and methods

4.4.1 Materials

MicroRNA (miRNA), namely microRNA-603 (miR603) (5'-CACACACUGCAAUUACUUUUGC-3'), was synthesized wild type or with chemically modified 5'-O-methyl nucleotides (miR603 O-Met) by Tema Ricerca s.r.l. (Bologna, Italy). 1,2-dioleoyl-3-trimethylammonium-propane chloride (LIPOID DOTAP-CL or DOTAP), N-[1-(2,3-dioleyloxy)propyl]-N,N,N-trimethylammonium chloride (DOTMA) or 3ß-[N-(N',N'-dimethylaminoethane)-carbamoyl]cholesterol hydrochloride (DC-chol), cholesterol (CHOL), dioleoylphosphatidylethanolamine (DOPE), N-palmitoyl-sphingosine-1 {succinyl[methoxy(polyethylene glycol)$_{2000}$]} (cer-PEG$_{2000}$) (cer-PEG) and 1,2-distearoyl-sn-glycero-3-phosphoethanolamine-N-[amino(polyethylene glycol)-$_{2000}$] (DSPE-PEG$_{2000}$) were purchased from Spectra2000 s.r.l. (Rome, Italy). Sodium chloride, calcium chloride, sodium phosphate dibasic, potassium chloride and bovine serum albumin (BSA), were obtained from Sigma-Aldrich Co. (Milan, Italy). Human plasma was obtained from healthy volunteers.

4.4.2 Methods

4.4.2.1 Preparation of hybrid self-assembling nanoparticles encapsulating miRNA (SANPs-miRNA)

Hybrid self-assembling nanoparticles (SANPs) were prepared as previously reported [Salzano *et al*., 2011] with some modifications. The SANPs preparation was schematically represented in Figure 4.4.2.1.1. In a first step, PEGylated cationic liposomes (PLs) consisting of DOTAP/chol/DSPE-PEG$_{2000}$ (mM ratio

1:1.8:0.125), DOTAP/DSPE-PEG_{2000} (mM ratio 1:0.125), DOTAP/DOPE/DSPE-PEG_{2000} (mM ratio 1:1:0.125), DOTMA/chol/DSPE-PEG_{2000} (mM ratio 1:1.8:0.125), DOTMA/DSPE-PEG_{2000} (mM ratio 1:0.125), DOTMA/DOPE/DSPE-PEG_{2000} (mM ratio 1:1:0.125), DC-chol/chol/DSPE-PEG_{2000} (mM ratio 1:1.8:0.125), DC-chol/DSPE-PEG_{2000} (mM ratio 1:0.125), DC-chol/DOPE/DSPE-PEG_{2000} (mM ratio 1:1:0.125), DOTAP/chol/cer-PEG (mM ratio 1:1.8:0.125), DOTAP/cer-PEG (mM ratio 1:0.125), DOTAP/DOPE/cer-PEG (mM ratio 1:1:0.125), DOTMA/chol/cer-PEG (mM ratio 1:1.8:0.125), DOTMA/cer-PEG (mM ratio 1:0.125), DOTMA/DOPE/cer-PEG (mM ratio 1:1:0.125), DC-chol/chol/cer-PEG (mM ratio 1:1.8:0.125), DC-chol/cer-PEG (mM ratio 1:0.125), DC-chol/DOPE/cer-PEG (mM ratio 1:1:0.125) were prepared by hydration of a thin lipid film followed by extrusion. Briefly, the thin film was obtained by a rotary evaporator (Laborota 4010 digital, Heidolph, Schwabach, Germany). Then, the lipid film was hydrated with RNAse free water for still 2 hours. The liposome suspension was then extruded using a thermobarrel extruder system (Northern Lipids Inc., Vancouver, BC, Canada) passing repeatedly the suspension under nitrogen through polycarbonate membranes with decreasing pore sizes from 400 to 100 nm (Nucleopore Track Membrane 25 mm, Whatman, Brentford, UK). After preparation, liposomes were stored at 4°C. Separately, calcium-phosphate colloidal dispersion (CaP NPs) were prepared. Briefly, an aqueous solution of dibasic hydrogen phosphate (10.8 mM) at pH 9.5 was added 1:1 v/v, dropwise and under magnetic stirring at about 1500 rpm, to an aqueous solution of calcium chloride (18mM) at pH 9.5 for 10 minutes and filtered with cellulose filter (0.22 µm filter membranes of regenerate cellulose). CaP NPs were prepared before the use. The colloidal dispersion was then mixed with an aqueous solution of miRNAs (0.2 mM of miRNA in RNAse free water corresponding to 1.4mg/ml of miR603 and 1.2mg/ml of miR603-OMet) by vortex for 10 seconds in a ratio of 50:1 v/v and allowed to react for 10 minutes, resulting in CaP/miRNAs NPs. Finally, SANPs-miRNA, were prepared by mixing, in equal volume, CaP/miRNAs NPs and different PLs by vortex for 10 seconds and allowed to react for 25 minutes. The concentration of miR603 in the final formulations was 35 µg/ml or 30µg/ml for miR603 O-Met. Plain SANPs, without miRNAs, were prepared similarly. Each formulation was prepared in triplicate.

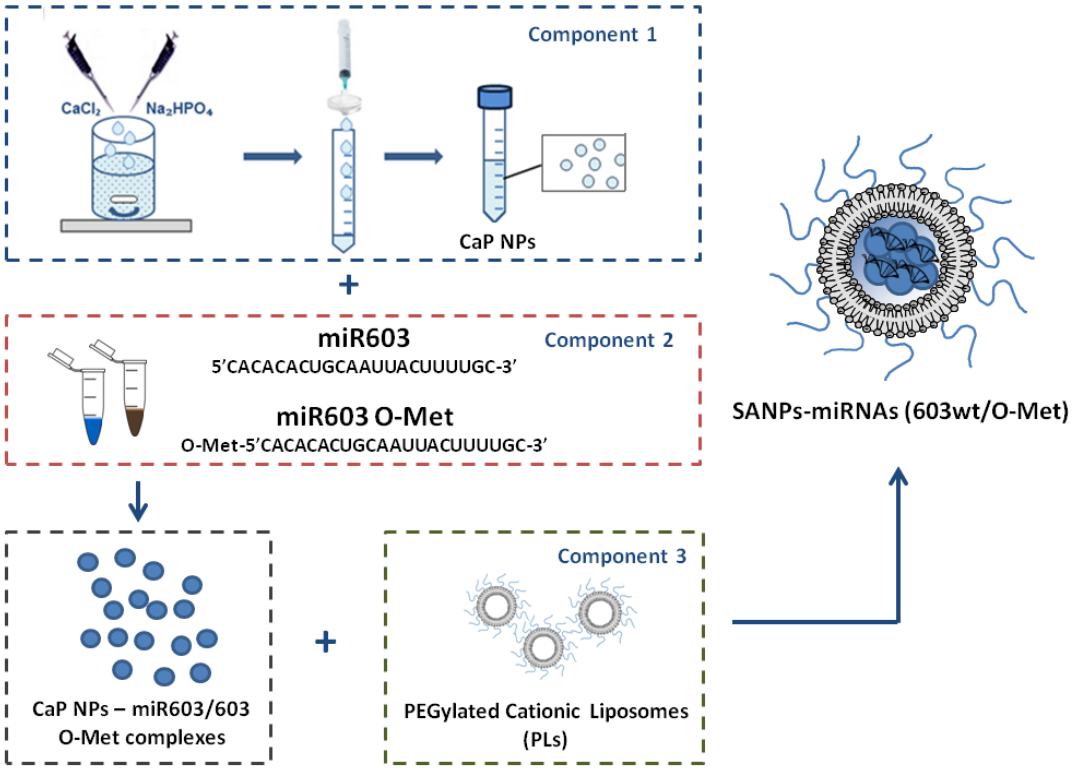

Figure 4.4.2.1.1: Preparation of hybrid self-assembling NPs encapsulating miRNAs (SANPs-miRNAs).

4.4.2.2 Physical-chemical characterization of self-assembling nanoparticles encapsulating miRNA (SANPs-miRNA) and plain SANPs

PLs, plain SANPs (without miRNA) and SANPs-miRNA were characterized in terms of mean diameter, polydispersity index (PI), and zeta potential (ζ). In particular, mean diameter was determined at 20°C by photon correlation spectroscopy (PCS) (N5, Beckman Coulter, Miami, USA) while zeta potential (ζ) was measured in deionized and filtered water by the Zetasizer Nano Z (Malvern, UK). For each formulation, the mean diameter, the PI and the ζ were calculated as the mean of measures carried out on at least three different batches.

4.4.2.3 miRNA encapsulation into SANPs

The amount of miR603/miR603 O-Met encapsulated in the final SANPs-miRNA was determined by indirect measure of unencapsulated miRNA, separated by ultracentrifugation (Optima Max E, Beckman Coulter, USA) at 80000 rpm, 4 °C, for 40 minutes. The supernatants were analyzed by UV (UV-1800, UV Spectrophotometer) at the wavelengths of 260 nm and the concentration of miRNAs was calculated by a calibration curve of miR603 or miR603 O-Met (R^2=0,999) in H_2O. Each analysis was carried out in duplicate.

4.4.2.4 Stability of SANPs-miRNA in biological fluids

The stability of SANPs and SANPs-miRNA were tested in bovine serum albumin (BSA), (1% w/v in 20 mM phosphate buffer saline, isosmotic with NaCl 0,9% w/v physiological solution)) and human plasma. To recover human plasma, human blood was centrifuged at 2000 rpm for 15 minutes to separate the erythrocytes from the plasma. Human plasma was withdrawn and diluted at 1% v/v in 20 mM phosphate buffer pH 7.4 and NPs were added (1% w/v). The interactions with SANPs or SANPs-miRNAs with serum proteins as well as the NPs aggregation were evaluated by monitoring the mean size of the both SANPs and SANP-miRNAs formulations in BSA and human plasma up to 4 hours at 37°C. Each analysis was prepared in duplicate.

Hemolysis assay on SANPs and SANPs-miRNAs have been performed on fresh human blood as previously reported by Mahmoud *et al*. (2014), with slight modifications. Briefly, the erythrocytes were collected from the plasma by centrifugation at 2000 rpm for 15 min, and then reconstituted in aqueous solution of NaCl 0.9% w/v. This step was repeated three times. The erythrocytes were diluted 1:10 with the solution of NaCl 0.9% (w/v) and then 0.2% (w/v) of formulations were added, mixed at 600 rpm for 30 second by vortex and incubated in a shaker bath at 37°C for 4 hours. The negative control (0% hemolysis) was obtained by diluting 1:10 human blood in NaCl 0.9% (w/v), whereas the positive control (100% hemolysis) was prepared by adding an

excess of water to human erythrocytes, to induce lysis. Afterwards, the samples were withdrawn, placed on ice for 2 minutes to quench erythrocyte lysis and centrifuged (3000 rpm for 5 minutes) to separate the supernatant from the pellet, consisting of intact red blood cells. The obtained supernatant was centrifuged another time (3000 rpm for 5 minutes) and the content of hemoglobin was determined by spectrophotometer Thermo Fisher Scientific 1510 Multiskan Go measuring the absorbance (ABS) at λ=540 nm. The percentage of hemolysis was calculated using the formula:

$$\text{Hemolysis } \% = ((ABS_{sample} - ABS_0)/(ABS_{100} - ABS_0))*100$$

Where ABS_0 was the absorbance of the negative control and ABS_{100} was the absorbance of the positive one.

4.4.2.5 Real-time quantitative PCR

Cell transfection efficiency was evaluated by Real-time quantitative PCR using ViiA 7 System (Applied Biosystems, California, USA). Cells were transfected or not with miRNAs or treated with different formulations of nanoparticles containing miRNAs at a concentration of 50 nM. After 24, 48, 72 hours, total RNA from suspension cell line LN229 and U87MG (5×105 cells) was obtained by mirVana miRNA Isolation Kits (Ambion, Life Technologies, California, USA) according to manufacturer's instructions. The integrity, quality and quantity of RNA were assessed by the NanoDrop ND-1000 Spectrophotometer (Thermo Fisher Scientific, Wilmington, DE, USA). Oligo-dT-primed cDNA was obtained using the High Capacity cDNA Reverse Transcription Kit (Applied Biosystems). The single-*vial* TaqMan miRNA assays (Ambion, Life Technologies, California, USA) was used to detect and quantify mature miRNAs according to the manufacturer's instructions by the use of the Real-time PCR ViiA7 (Applied Biosystems, California, USA). MiRNAs expression was normalized on U-6 (Ambion, Life Technologies, California, USA). Comparative real-time PCR (RT-PCR) was performed in triplicate, including no template controls, and relative expression was calculated using the comparative cross-threshold (Ct) method.

4.4.2.6 Cell viability assay

We assessed the viability of the cell lines using a microplate colorimetric assay that measures the ability of viable cells to transform a soluble tetrazolium salt (MTT) to an insoluble purple formazan precipitate. Cells were plated at the appropriate density in 96-well microtitre plates. After 24 h, cells were exposed to various concentrations of different formulations of nanoparticles or the conventional anticancer drug temozolomide to test their cytotoxicity. After 72 h, 50 µl of MTT (1 mg · ml^{-1}) and 200 µl of medium were added to the cells in each well. After 4 h incubation at 37°C, the medium was removed, then the formazan crystals were solubilised by adding 100 µl of DMSO and by mixing it in an orbital shaker for 20 min. Absorbance at 570 nm was measured using a plate reader. Experiments were performed in triplicate. As a control, 0.5% DMSO was added to untreated cells. Data were expressed as mean ± sd.

4.4.2.7 RNA extraction on mouse biopsies and Real-time quantitative PCR

SCID male mice (5-6 weeks old) purchased from Charles River (Calco, Italy) were injected intracranially with U87MG human GBM line at 2.5 x 105 cells/mouse and after two weeks mice were treated intravenously with 6.8 µg miR603/mouse of two different SANPs-miRNA that are, PL-CaP-603-DOTAP-C1, composed of CaP and PLs consisting of DOTAP/CHOL/DSPE-PEG mM ratio 1:1.8:0.125), and PL-CaP-603-DOTAP-2, composed CaP and PLs of DOTAP/cer-PEG (mM ratio 1:0.125) formulations. Mice were euthanized 6 h and 18 h after the treatment and plasma and organs collected and maintained at -80 °C until analysis. All animal experiments comply with the ARRIVE guidelines and have been be carried out in accordance with EU Directive 2010/63/EU for animal experiments.

Total RNA was extracted from mouse biopsies by mirVana miRNA Isolation Kits (Ambion, Life Technologies, California, USA) according to manufacturer's instructions as follows. In details, tissues were homogenized in 300 µl of Disruption Buffer. Successively, an equal volume of Denaturing Buffer

(previously set at 37 °C) was added to the tissues homogenate and they were incubated in ice for 5–10 min. Then, Phenol-chloroform was added in the *vial* in a volume equal to the total volume and centrifugated at 10000 rcf for 5 min. After centrifugation, the aqueous phase was collected and a volume of absolute ethanol equal to 1.25 times that of the collected volume was added. Then 700 µl at a time were collected, applied in Filter Cartridge and centrifuged at 10000 rcf for 5 min. 700 µl of Wash Solution 1 were added on each Filter Cartridge, followed by centrifugation at 10000 rcf for 40 s, later two washings with 500 µl of Wash Solution 2 were performed. Finally, 50 µl of Eluition Buffer (preheated at 95 °C) were added to the Filter Cartridge, previously placed on new *vial*s. Then, the samples were quantized to Nanodrop (Technologies Inc., Wilmington, DE). cDNA was obtained by using the TaqMan® Small RNA Assays Kit (Applied Biosystems) according to the manufacturer's instructions. The single-*vial* TaqMan miRNA assays (Ambion, Life Technologies, California, USA) was used to detect and quantify mature miR603 according to the manufacturer's instructions by the use of the Real-time PCR ViiA7 (Applied Biosystems, California, USA). MiR603 expression was normalized on U-6 (Ambion, Life Technologies, California, USA). Comparative real-time PCR (RT-PCR) was performed in triplicate, including no template controls, and relative expression was calculated using the comparative cross-threshold (Ct) method.

4.5 Results and discussion

4.5.1 Composition of different formulations based on SANPs and complexed with miR603

The aim of this study was to propose and optimize SANPs for the delivery of miR603 (wild type or O-methylated in 5') in brain tumor. To this aim, SANPs with different lipid composition, i.e. different cationic lipids, neutral lipids, and type of PEGylated lipids, have been tested.

Three different cationic lipids largely used for transfection purposes, namely DOTAP, DOTMA and DC-chol, were tested in this study. Cationic lipids were used to "anchor" the lipid shell to the inorganic core of the SANPs, but also as transfection agent for the nucleic acid. Each cationic lipid was used alone or

associated to two different neutral lipids, namely CHOL and DOPE. CHOL has been used to improve the transfection efficiency of cationic liposomes [De Rosa *et al*., 2008; Hosseini *et al*., 2019]. Similarly, the addition of the fusogenic lipid DOPE to the formulation is considered a well-established strategy to promote the escape of nucleic acids from endosomes [Litzinger and Huang, 1992; Khatri *et al*., 2014]. Moreover, it has been demonstrated that the introduction of "helper lipids", such as DOPE or CHOL, can stabilize the carrier membrane, reducing vesicle aggregation in the presence of serum proteins [Xiong *et al*., 2011]. Finally, in all the formulations, a PEGylated lipid, namely DSPE-PEG_{2000} or cer-PEG_{2000}, (reported into figures and tables as 1 and 2 respectively) was included. The inclusion of a PEGylated shell on the liposome surface has been used to increase the stability of SANPs-miRNA in biological fluids [Jiang *et al*., 2010].

In table 4.5.1.1 the composition of all the SANP formulations prepared in this study is summarized.

Lipid composition of the formulation (mM ratio)							Formulation legend			
DOTAP	DOTMA	Dc-Chol	CHOL	DOPE	DSPE-PEG	Cer-PEG	Cationic liposome	SANPs	SANPs encapsulating wild type miR603	SANPs encapsulating O-methylated miR603
1	-	-	1.8	-	0.125	-	PL-DOTAP C1	SANPs-DOTAP C1	SANPs-603-DOTAP C1	SANPs-603Omet-DOTAP C1
1	-	-	-	-	0.125	-	PL-DOTAP 1	SANPs- DOTAP 1	SANPs-603-DOTAP 1	SANPs-603Omet-DOTAP 1
1	-	-	-	1	0.125	-	PL-DOTAP D1	SANPs-DOTAP D1	SANPs-603-DOTAP D1	SANPs-603Omet-DOTAP D1
-	1	-	1.8	-	0.125	-	PL-DOTMA C1	SANPs-Dotma C1	SANPs-603-Dotma C1	SANPs-603Omet-Dotma C1
-	1	-	-	-	0.125	-	PL-DOTMA 1	SANPs-Dotma 1	SANPs-603-Dotma 1	SANPs-603Omet-Dotma 1
-	1	-	-	1	0.125	-	PL- DOTMA D1	SANPs-Dotma D1	SANPs-603-Dotma D1	SANPs-603Omet-Dotma D1
-	-	1	1.8	-	0.125	-	PL-DCchol C1	SANPs-Dcchol C1	SANPs-603-Dcchol C1	SANPs-603Omet-Dcchol C1
-	-	1	-	-	0.125	-	PL-DCchol 1	SANPs-Dcchol 1	SANPs-603-Dcchol 1	SANPs-603Omet-Dcchol 1
-	-	1	-	1	0.125	-	PL-DCchol D1	SANPs-Dcchol D1	SANPs-603-Dcchol D1	SANPs-603Omet-Dcchol D1
1	-	-	1.8	-	-	0.125	PL-DOTAP C2	SANPs-DOTAP C2	SANPs-603-DOTAP C2	SANPs-603Omet-DOTAP C2
1	-	-	-	-	-	0.125	PL- DOTAP 2	SANPs-DOTAP 2	SANPs-603-DOTAP 2	SANPs-603Omet-DOTAP 2
1	-	-	-	1	-	0.125	PL-DOTAP D2	SANPs-DOTAP D2	SANPs-603-DOTAP D2	SANPs-603Omet-DOTAP D2
-	1	-	1.8	-	-	0.125	PL-DOTMA C2	SANPs- DOTMA C2	SANPs-603-DOTMA C2	SANPs-603Omet-DOTMA C2
-	1	-	-	-	-	0.125	PL-DOTMA 2	SANPs-DOTMA 2	SANPs-603-DOTMA 2	SANPs-603Omet-DOTMA 2
-	1	-	-	1	-	0.125	PL-DOTMA D2	SANPs-DOTMA D2	SANPs-603-DOTMA D2	SANPs-603Omet-DOTMA D2
-	-	1	1.8	-	-	0.125	PL-DCchol C2	SANPs-DCchol C2	SANPs-603-DCchol C2	SANPs-603Omet-DCchol C2
-	-	1	-	-	-	0.125	PL-DCchol 2	SANPs-DCchol 2	SANPs-603-DCchol 2	SANPs-603Omet-DCchol 2
-	-	1	-	1	-	0.125	PL-DCchol D2	SANPs-DCchol D2	SANPs-603-DCchol D2	SANPs-603Omet-DCchol D2

Table 4.5.1.1: Composition of the different formulations of hybrid self-assembling nanoparticles (SANPs) prepared plain or complexed with miR603 and miR603 O-Met.

4.5.2 Physical-chemical characterization of SANPs

Mean diameter, polydispersity index and surface charge of PLs, plain SANPs and SANPs-miRNAs (also called PL-CaP, PL-CaP-603 and PL-CaP-603-OMet respectively into the charts and tables) are reported in figure 4.5.2.1, 4.5.2.2 and 4.5.2.3, respectively.

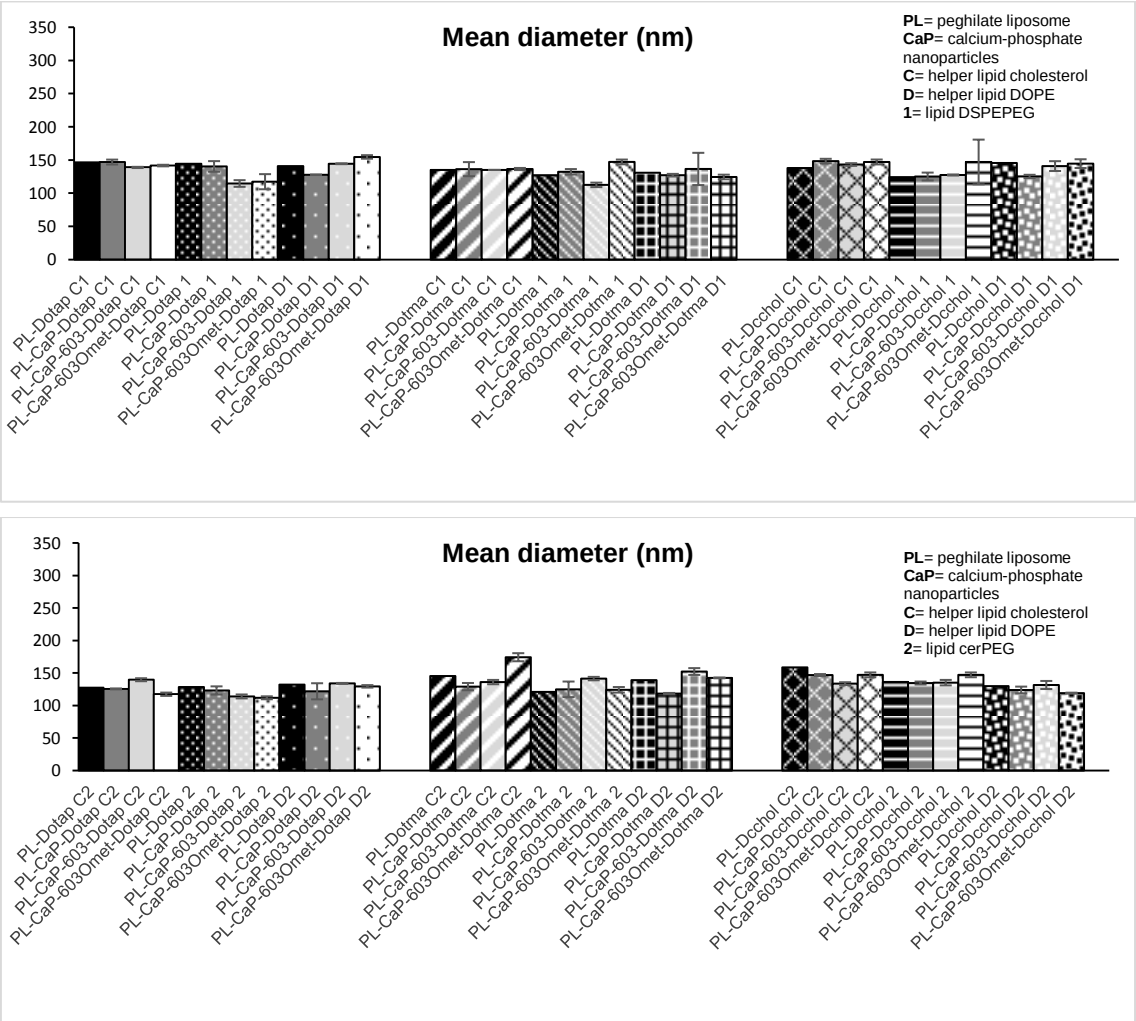

*standard deviation calculated on average of three batches

Figure 4.5.2.1: Mean diameter (nm) of the PEGylated liposomes and SANPs before and following complexation with miR603 and miR603 O-Met.

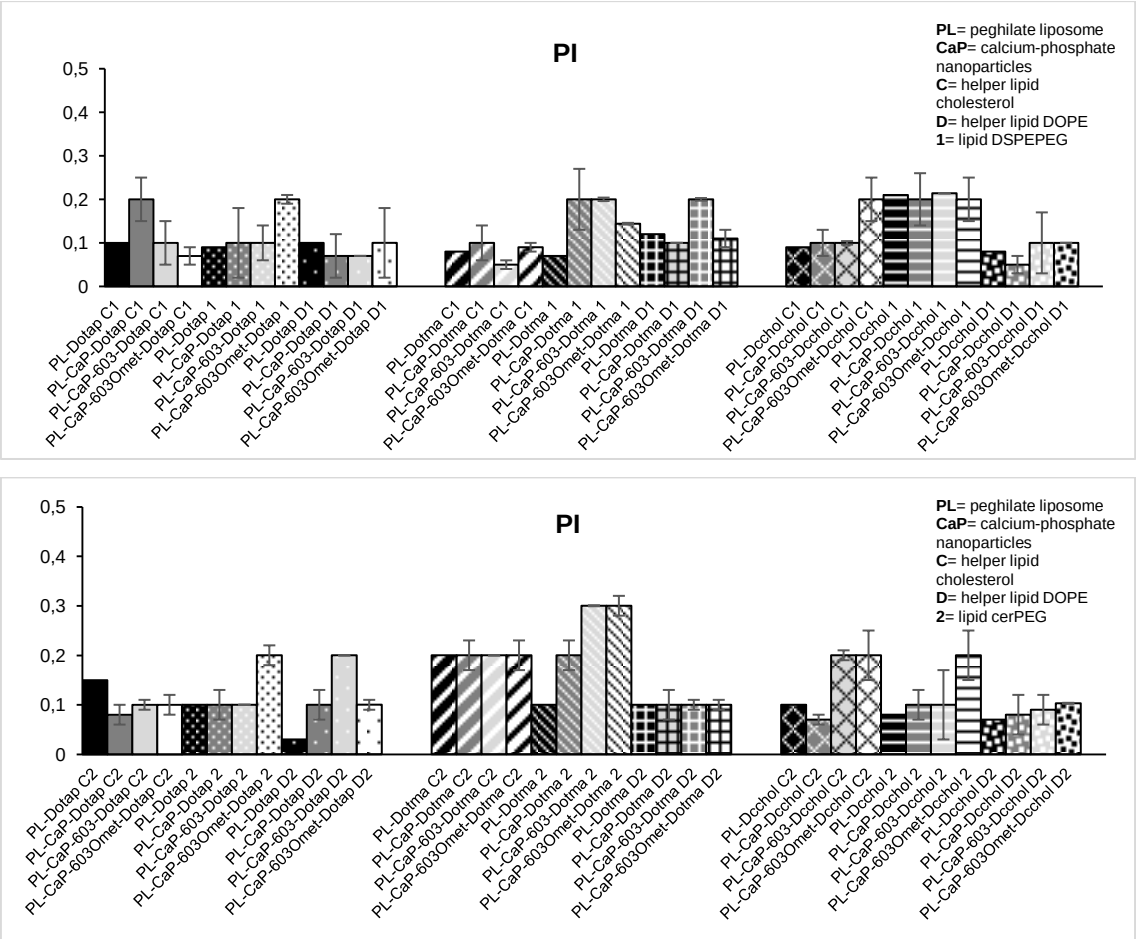

*standard deviation calculated on average of three batches

Figure 4.5.2.2: Polydispersity index (PI) of the PEGylated liposomes and SANPs before and following complexation with miR603 and miR603 O-Met.

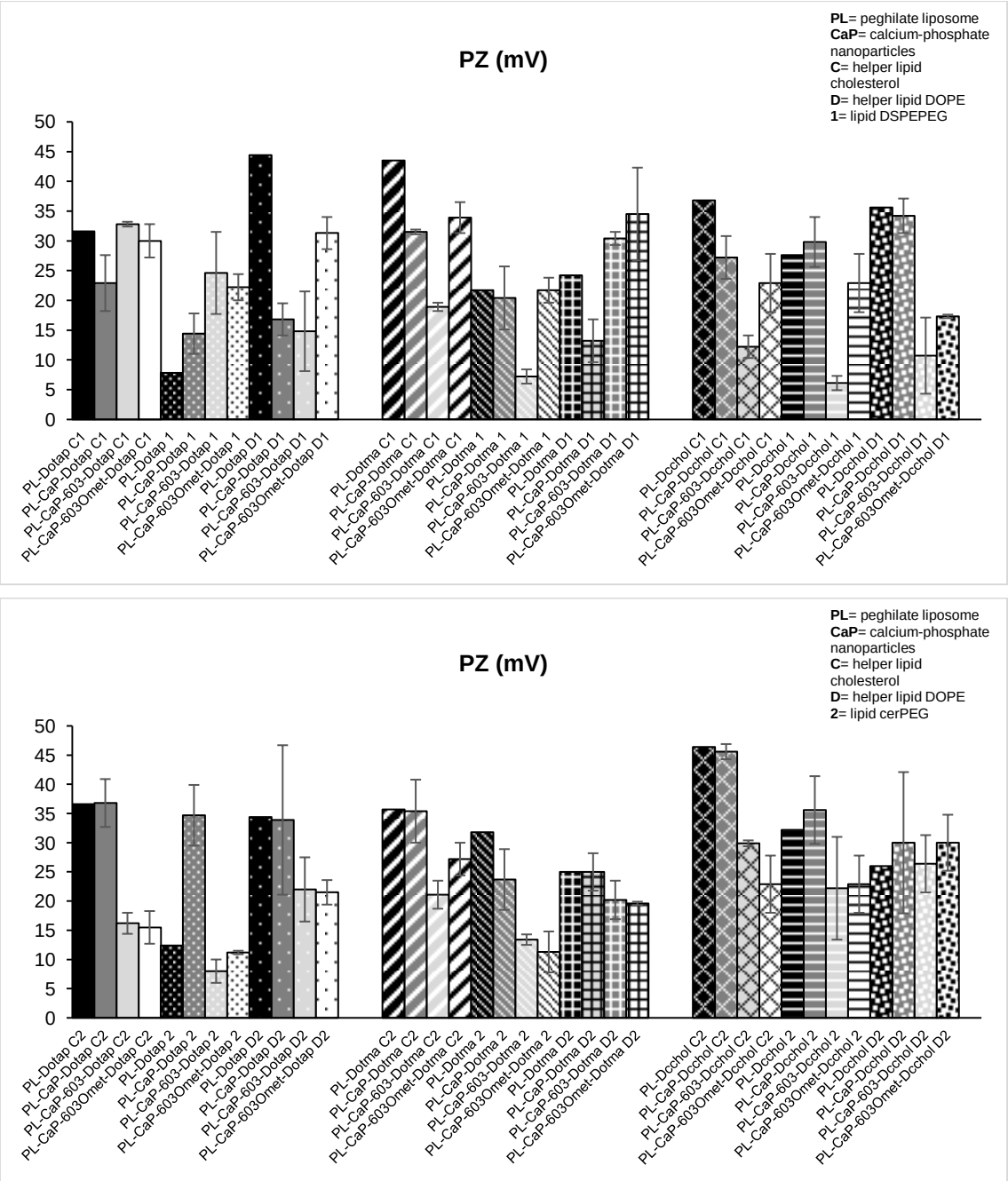

*standard deviation calculated on average of three batches

Figure 4.5.2.3: Zeta potential (ζ) of the PEGylated liposomes and SANPs before and following complexation with miR603 and miR603 O-Met.

PLs had a mean diameter ranging between about 120 and 160 nm. The complexation of PLs with the CaP dispersion resulted in plain SANPs with a mean diameter generally around 140 nm and a PI between about 0.05 and 0.2, suggesting that the lipid composition has no a significant effect on the SANPs

size. On the case of liposomes based on the cationic lipid and PEGylated lipid, the size and the consequent high curvature of the bilayer could lead to the localization of PEGylated lipids on the outer layer of the membrane, thus shielding the positive charge of the cationic lipid. On the other hand, the inclusion of neutral lipids could contribute to the reorganization of the bilayer shifting toward a more homogeneous distribution of PEGylated lipid between the outer and the inner layers of the membrane, and consequent increase of the ζ value.

The addition of the miRNAs to plain SANPs did not significantly affect the mean size, with a weak effect on the PI that remains under 0.2, with the exception of the formulation containing DOTMA and cer-PEG_{2000} (PI ~ 0.3), (Figure 4.5.2.2*)*. Moreover, the encapsulation of miRNA influenced the ζ, being this effect strictly depending on the formulation (Figure 4.5.2.3). In particular, in the majority of the formulations, a reduced ζ was found, suggesting that the anionic charged miRNA interact with the cationic lipid, also at the level of the external lipid shell. In the formulations PL-CaP-603-Dotap1 and PL-CaP-603 DotmaD1, and also in formulations PL-CaP-603OMet-Dotap 1, PL-CaP-603OMet-Dotap D1 and PL-CaP-603OMet Dotma D1 the inclusion of miRNAs lead to increase of zeta potential; this could be ascribed to the lipid rearrangement inducing the shielding of the cationic charges by the PEGylated lipids.

In table 4.5.2.1, the amount of miRNAs encapsulated, expressed as miRNA actual loading (mmol of miRNAs/mmol of cationic lipid), and miRNA encapsulation efficiency (EE) (expressed as percentage respect to the miRNA initially used in the formulations) in the SANPs-miRNAs, are reported.

Formulation	EE (%) miRNA ± sd	mmol miRNA/ mmol cationic lipid± sd*	Formulation	EE (%) miRNA ± sd*	mmol miRNA/ mmol cationic lipid± sd*
PL-CaP-603-DOTAP C1	100±0.0*	1.52±0.0*	PL-CaP-603 O-Met-DOTAP C1	89±14.7	1.13±0.2*
PL-CaP-603-DOTAP 1	100±0.0*	1.42±0.0*	PL-CaP-603 O-Met-DOTAP 1	98±2.5	1.23±0.0*
PL-CaP-603-DOTAP D1	100±0.0*	1.53±0.0*	PL-CaP-603 O-Met-DOTAP D1	100±0.0	1.26±0.0*
PL-CaP-603-Dotma C1	100±0.0*	1.53±0.0*	PL-CaP-603 O-Met-Dotma C1	100±0.0	1.26±0.0*
PL-CaP-603-Dotma 1	100±0.0*	1.53±0.0*	PL-CaP-603 O-Met-Dotma 1	100±0.0	1.26±0.0*
PL-CaP-603-Dotma D1	100±0.0*	1.53±0.0*	PL-CaP-603 O-Met-Dotma D1	100±0.0	1.26±0.0*
PL-CaP-603-Dcchol C1	99±0.2*	1.53±0.0*	PL-CaP-603 O-Met-Dcchol C1	100±0.0	1.26±0.0*
PL-CaP-603-Dcchol 1	81±0.0*	1.24±0.0*	PL-CaP-603 O-Met-Dcchol 1	100±0.0	1.26±0.0*
PL-CaP-603-Dcchol D1	99±0.4*	1.52±0.0*	PL-CaP-603 O-Met-Dcchol D1	100±0.0	1.26±0.0*
PL-CaP-603-DOTAP C2	100±0.4*	1.53±0.0*	PL-CaP-603 O-Met-DOTAP C2	100±0.0	1.26±0.0*
PL-CaP-603-DOTAP 2	82±6.4*	1.26±0.1*	PL-CaP-603 O-Met-DOTAP 2	94±1.71	1.10±0.0*
PL-CaP-603-DOTAP D2	75±19.8*	1.16±0.3*	PL-CaP-603 O-Met-DOTAP D2	72±21.4	0.91±0.3*
PL-CaP-603-DOTMA C2	100±0.0*	1.53±0.0*	PL-CaP-603 O-Met-DOTMA C2	100±0.0	1.26±0.0*
PL-CaP-603-DOTMA 2	100±0.0*	1.53±0.0*	PL-CaP-603 O-Met-DOTMA 2	100±0.0	1.26±0.0*
PL-CaP-603-DOTMA D2	100±0.0*	1.53±0.0*	PL-CaP-603 O-Met-DOTMA D2	100±0.0	1.26±0.0*
PL-CaP-603-DCchol C2	100±0.0*	1.31±0.0*	PL-CaP-603 O-Met-DCchol C2	92±0.0	1.07±0.0*
PL-CaP-603-DCchol 2	96±0.0*	1.47±0.0*	PL-CaP-603 O-Met-DCchol 2	77±4.9	1.10±0.1*
PL-CaP-603-DCchol D2	96±0.6*	1.48±0.0*	PL-CaP-603 O-Met-DCchol D2	85±13.7	1.10±0.2*

*standard deviation on almost three different batches

Table 4.5.2.1: Encapsulation of miRNA into the different SANP formulations (expressed as amount of mmol of miRNAs/mmol of cationic lipid) and encapsulation efficiency (EE) (expressed as percentage respect to the miRNA initially used in the formulations).

All the formulations were characterized by very high miRNA encapsulation efficiency, ranging from about 72 to 100%, the lowest encapsulation being observed in the case of the formulation based on DOTAP, DOPE and cer-PEG. The comprehension of the lipid rearrangement and SANPs architecture affecting the efficiency of the miRNAs complexation are very complex and cannot be clarified in this study. However, we can hypothesize that SANPs with the lowest encapsulation efficiency are characterized by a more compact

structure that limits the complexation and encapsulation of large amount of miRNAs.

4.5.3 Stability of SANPs-miRNAs formulation

In a second phase of the study, considering that the SANPs-miRNAs are designed for an intravenous administration, the SANPs physical stability was tested firstly in a BSA solution at 1% w/v (for a first screening) and then in human plasma up to 4 hours at 37 °C. The aggregation of SANPs-miRNAs in presence of serum proteins was evaluated by monitoring the mean size of the formulations (1% w/v) in both media. SANPs mean diameters in BSA and in plasma are reported in the Figure 4.5.3.1 and Figure 4.5.3.2, respectively.

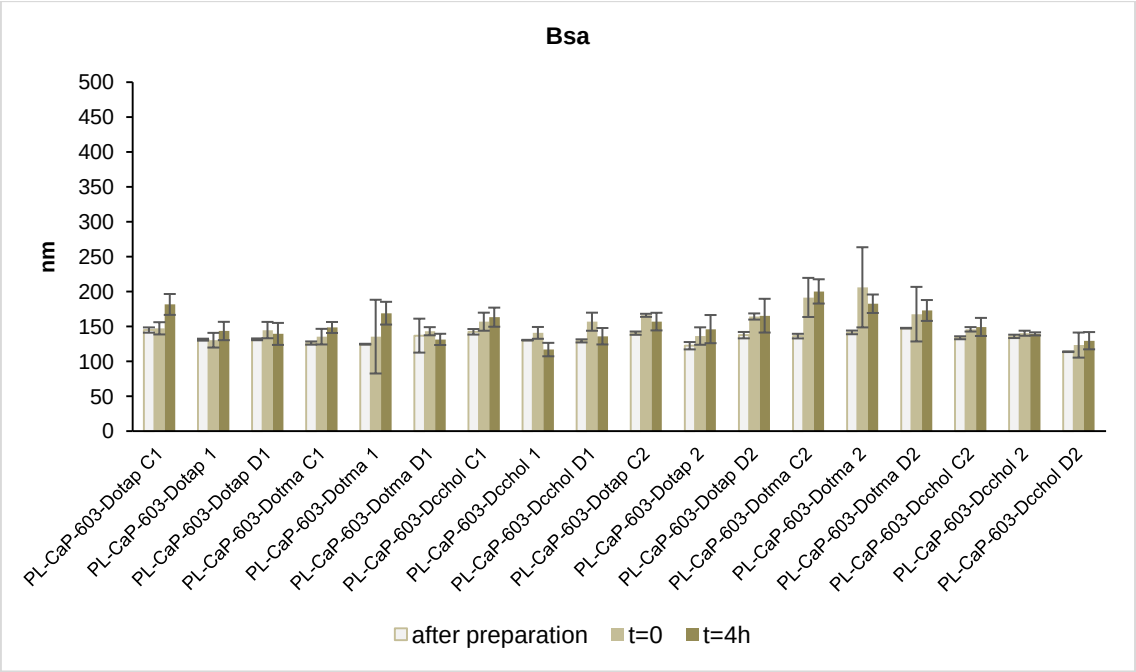

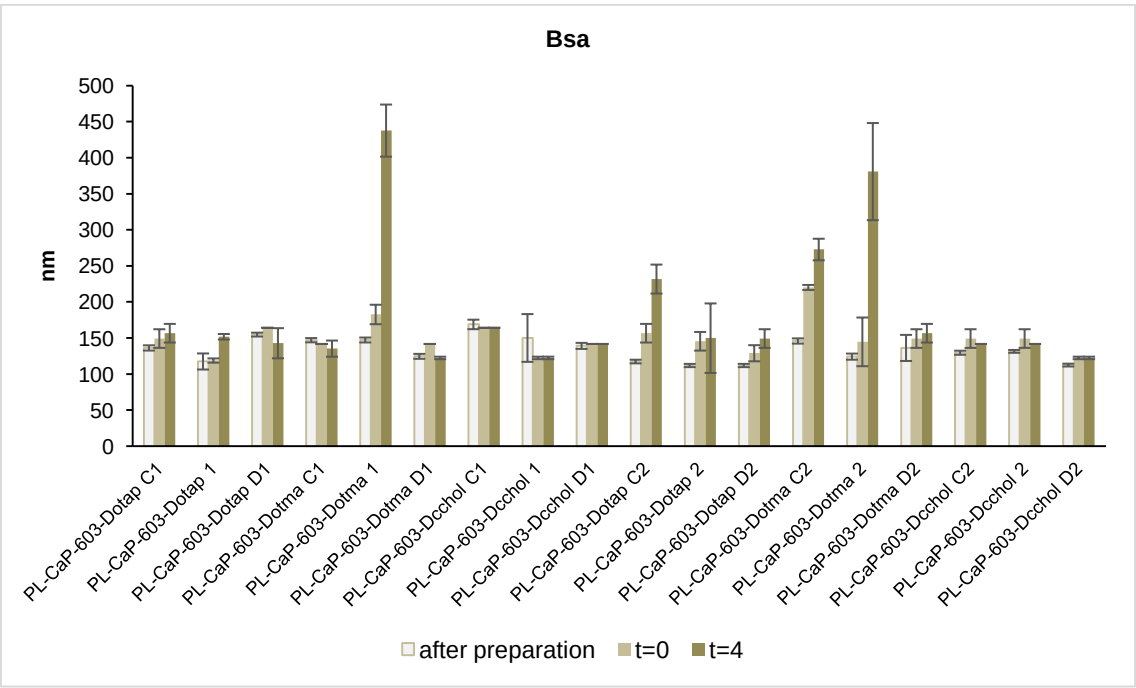

*standard deviation calculated on average of three batches

Figure 4.5.3.1: Stability of SANPs-miR603 (up) and SANPs-miR603 O-Met (down) in bovine serum albumin (BSA) after incubation (t=0) and after four hours (t=4).

All the formulations complexed with miR603 did not significantly change their mean size following incubation in BSA for 4 h (Figure 4.5.3.1). However, significant increase in size, presumably aggregation, was found in formulations combining DOTMA and both $DSPEPEG_{2000}$ and cer-PEG complexed with miR603 O-Met following incubation in BSA for 4 h.

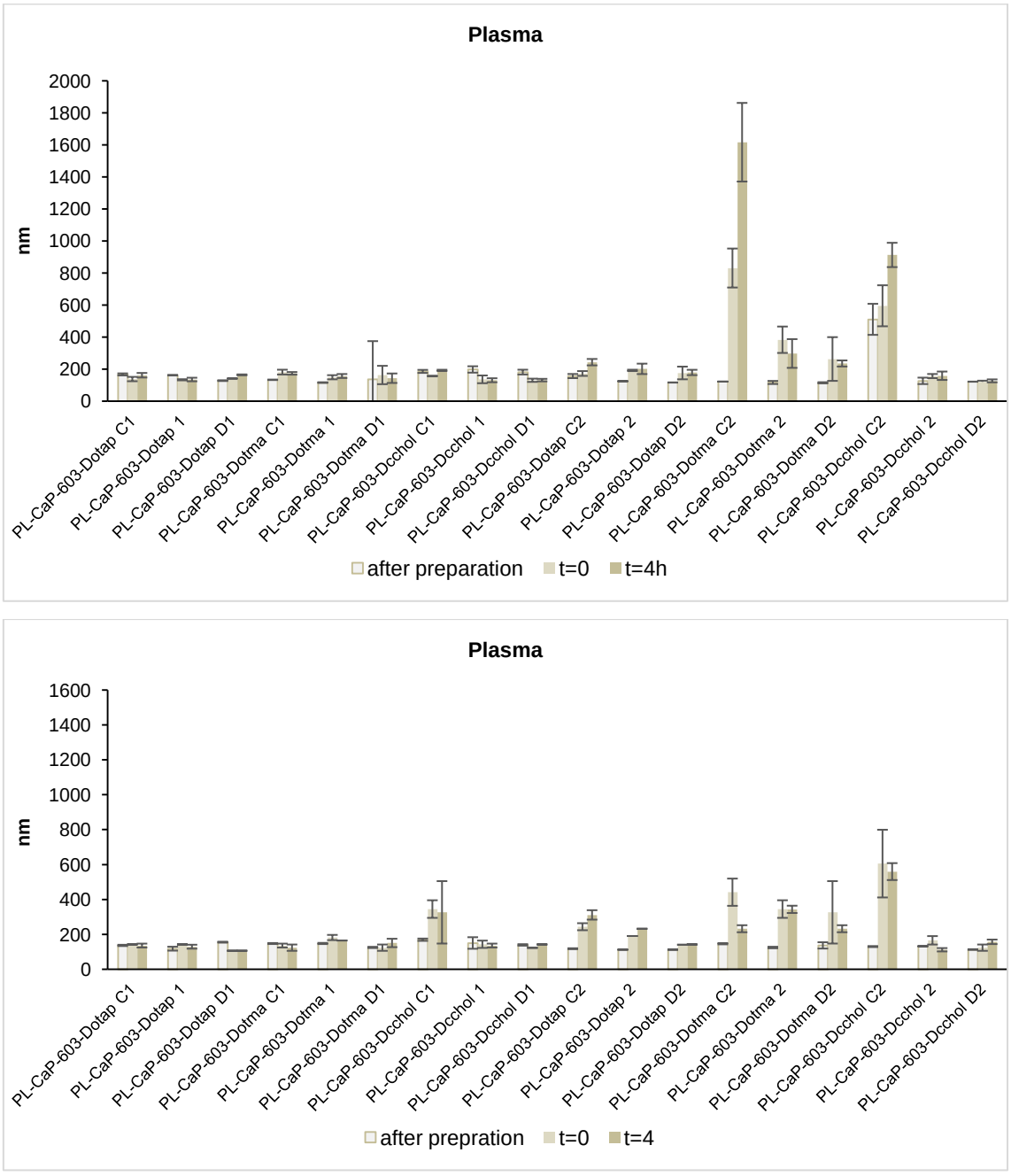

*standard deviation calculated on average of three batches

Figure 4.5.3.2: Stability of SANPs-miR603 (up) and SANPs-miR603 O-Met (down) in plasma after incubation (t=0) and after four hours (t=4).

On the contrary, the stability of SANPs-miRNAs in human plasma (Figure 4.5.3.2) strictly depended on the formulation. Significant increase in size, presumably aggregation, was found in formulations combining DOTMA and cer-PEG. Moreover, the formulations with DC-chol associated to cholesterol and both $DSPEPEG_{2000}$ and cer-PEG were found to aggregate in plasma. It is well known that ceramide can interact with the hydrophobic portion of proteins [Krönke, 1999]. Particle aggregation found in some formulations should be due to the reorganization of the different components; in these formulations, the characteristics of nanoparticle surface should allow interaction with plasma proteins, different than BSA, with consequent aggregation.

4.5.4 Hemolytic activity of SANPs-miRNAs

The hemolytic activity of SANPs-miRNAs was then evaluated in human blood. In particular, according to ASTM F 756-17, a hemolytic activity less than 2% was considered non-toxic, while at levels between 2 and 5% only slightly toxic. As reported in table 4.5.4.1, SANPs-miRNAs showed a different hemolytic effect depending on the composition. In particular, the combination of DOTMA and cer-PEG_{2000} led always to a hemolytic activity from light to important (from 3% to 16%). For all the other formulations, hemolytic values close or lower than 2% were observed, suggesting no toxicity on the red blood cells.

Previous studies underlined the relationship between physical stability of nanoparticles and their hemocompatibility [Vuddanda *et al*., 2014; Jansook *et al*., 2018]. In this study, also formulations, e.g. SANPs-miR603-DOTMA 2 and SANPs-miR603-DOTMA D2, that were stable in presence of proteins, showed significant hemolytic activity. Thus, in this case, a direct interaction of the SANPs with the membrane of red blood cells should be hypothesized. Once more, this interaction could be enhanced by the presence of cer-PEG that can enhance membrane propensity to form a hexagonal II phase, thus changing the membrane fluidity, which may impinge on fusion processes with cell membrane [Krönke, 1999], e.g. membrane of red blood cells.

Formulations	Haemolysis % ± sd*	Formulations	Haemolysis % ± sd*
PL-CaP-miR603-DOTAP C1	1.11 ± 0.003*	PL-CaP-miR603-OMet-DOTAP C1	1.05 ± 0.010*
PL-CaP-miR603-DOTAP 1	0.08 ± 0.004*	PL-CaP-miR603-OMet-DOTAP 1	1.48 ± 0.017*
PL-CaP-miR603-DOTAP D1	0.19 ± 0.005*	PL-CaP-miR603-OMet-DOTAP D1	0.96 ±0.014*
PL-CaP-miR603-DOTMA C1	2.45 ± 0.006*	PL-CaP-miR603-OMet-DOTMA C1	2.46 ± 0.010*
PL-CaP-miR603-DOTMA 1	1.46 ± 0.002*	PL-CaP-miR603-OMet-DOTMA 1	1.52 ± 0.012*
PL-CaP-miR603-DOTMA D1	1.12 ± 0.004*	PL-CaP-miR603-OMet-DOTMA D1	0.49 ± 0.004*
PL-CaP-miR603-DCchol C1	0.73 ± 0.011*	PL-CaP-miR603-OMet-DCchol C1	1.06 ± 0.004*
PL-CaP-miR603-DCchol 1	0.21 ± 0.001*	PL-CaP-miR603-OMet-DCchol 1	0.99 ± 0.005*
PL-CaP-miR603-DCchol D1	0.07 ± 0.002*	PL-CaP-miR603-OMet-DCchol D1	1.24 ± 0.014*
PL-CaP-miR603-DOTAP C2	0.09 ± 0.003*	PL-CaP-miR603-OMet-DOTAP C2	2.19 ± 0.007*
PL-CaP-miR603-DOTAP 2	1.00 ± 0.013*	PL-CaP-miR603-OMet-DOTAP 2	2.86 ± 0.013*
PL-CaP-miR603-DOTAP D2	1.72 ± 0.008*	PL-CaP-miR603-OMet-DOTAP D2	2.17 ± 0.010*
PL-CaP-miR603-DOTMA C2	6.13 ± 0.019*	PL-CaP-miR603-OMet-DOTMA C2	2.97 ± 0.010*
PL-CaP-miR603-DOTMA 2	16.74 ± 0.033*	PL-CaP-miR603-OMet-DOTMA 2	5.08 ± 0.010*
PL-CaP-miR603-DOTMA D2	5.23 ± 0.060*	PL-CaP-miR603-OMet-DOTMA D2	4.45 ± 0.100*
PL-CaP-miR603-DCchol C2	2.38 ± 0.030*	PL-CaP-miR603-OMet-DCchol C2	2.28 ± 0.026*
PL-CaP-miR603-DCchol 2	1.98 ± 0.014*	PL-CaP-miR603-OMet-DCchol 2	0.94 ± 0.022*
PL-CaP-miR603-DCchol D2	1.97 ± 0.012*	PL-CaP-miR603-OMet-DCchol D2	1.00 ± 0.009*

*standard deviation on almost three different batches

Table 4.5.4.1: Hemolytic activity of SANPs-miRNAs.

4.5.5 Cytotoxicity of SANPs-miRNAs

The cytotoxicity of the SANP formulations at different concentrations, namely from 20 to 200 nM, were tested, in collaboration with Prof. M. Caraglia and his research group in University of Campania Luigi Vanvitelli (Napoli), on two glioblastoma cell lines, e.g. LN229 and U87MG. The formulations showing cell viability lower than 80% at 100 nM were considered “highly toxic”. Formulations showing cell viability lower than 80% of at the 200 nM, but higher than 80% at 100 nM, were considered “slightly toxic”. Formulations showing on both cell lines 80% of cell viability at the highest concentration (200 nM) were considered not toxic in our experimental conditions. The non-toxic SANPs were used for the following phase of the study. The results are summarized in table 4.5.5.1. When considering the different cationic lipid used in this study, DOTMA and DC-chol based formulations were generally found from slightly to very toxic. Other authors found a higher cytotoxicity *in vitro* when using lipoplexes based on DC-

chol [Lechanteur *et al*., 2018], compared to DOTAP. Similarly, the higher cytotoxicity of DOTMA compared to the DOTAP has previously been reported and reasonably attributed to the biodegradable ester bond present only in the latter [Obika *et al*., 1999]. DOTAP-based SANPs were found not toxic on both the cell lines, when prepared with DSPE-PEG. The use of cer-PEG, only in the formulation containing DOPE, led to a slight toxicity (IC50 of 86 nM) found on LN229 cells.

Formulation	Cytotoxicity - IC50 (nM)	
	U87MG	LN229
PL-CaP-DOTAP C1	No toxic	No toxic
PL-CaP- DOTAP 1	No toxic	No toxic
PL-CaP-DOTAP D1	No toxic	No toxic
PL-CaP-Dotma C1	176.9	171.0
PL-CaP-Dotma 1	No toxic	No toxic
PL-CaP-Dotma D1	Highly toxic	Highly toxic
PL-CaP-Dcchol C1	Highly toxic	Highly toxic
PL-CaP-Dcchol 1	Highly toxic	Highly toxic
PL-CaP-Dcchol D1	Highly toxic	Highly toxic
PL-CaP-DOTAP C2	No toxic	No toxic
PL-CaP-DOTAP 2	No toxic	No toxic
PL-CaP-DOTAP D2	No toxic	85.6
PL-CaP- DOTMA C2	142.1	159.3
PL-CaP-DOTMA 2	156.0	182.5
PL-CaP-DOTMA D2	Highly toxic	Highly toxic
PL-CaP-DCchol C2	Highly toxic	Highly toxic
PL-CaP-DCchol 2	Highly toxic	Highly toxic
PL-CaP-DCchol D2	Highly toxic	Highly toxic

Table 4.5.5.1: Cytotoxicity of SANPs-miRNAs.

Taking into account these data, we considered that the formulations based on DOTAP, alone or associated with CHOL, were stable in serum, have no hemolytic, and were not cytotoxic; these formulations were used in the following step of the study.

4.5.6 Delivery of miRNAs in GBM cell lines

The selected formulations were used to deliver miRNAs in LN229 and U87MG. This study was performed in collaboration with Prof. M. Caraglia and his research group in University of Campania Luigi Vanvitelli (Napoli).

The uptake of miRNAs was measured by RT-PCR after 24 and 48 h of cell incubation with the formulations. As positive control, the commercial transfection agent lipofectamine was used.

Transfection with lipofectamine leads to a significant miR603 uptake in both LN229 and U87MG, only in the case of w.t. miR603. In fact, as showed in Figure 3.10.1, the uptake of O-Met miR603 was found negligible suggesting a lack of the delivery of the miR603 O-Met in both cell lines either 24h or 48h of incubation. Thus, the formulations characterized by the inclusion of the miR603 O-Met, despite the good results obtained from the study performed, was not considered for the following step of the study.

In the case of w.t. miR603 delivered with lipofectamine, the highest miRNA uptake was found after incubation for 24 h, while miR603 levels progressively reduced after 48 and 72 h of incubation, respectively. This suggests a very poor miR603 stability into the cells following transfection, although this point should be further investigated. The cell incubation with SANPs encapsulating the miR603 led to a strong increase of the miR603 uptake into the cells (Figure 4.5.6.1). In particular, in LN229 cells the formulation DOTAP/cer-PEG lead to a significant improvement of the miR603 uptake after 24 and 48 h of incubation. Interestingly, a higher level of miRNA was found following 48 h of incubation with DOTAP/chol/DSPE-PEG and DOTAP/DSPE-PEG, suggesting that the release of naked miR603 into the cells could be delayed with this formulation (Figure 4.5.6.1, left panel). In the case of U87MG (Figure 4.5.6.1, right panel), the miR603 uptake into the cells increased from 1.2 to 12.5 times depending on the SANP formulations used. As in the case of LN229, the highest miRNA delivery was observed with the formulation DOTAP/cer-PEG. However, in the case of U87MG, the intracellular level of miR603 was found very low following 48 h of incubation. Thus, it could be hypothesized that a “sustained release” of miRNA into LN229 occurs, while in the case of U87MG a faster and higher

delivery takes place, with consequent faster intracellular degradation of the miR603 into the cells.

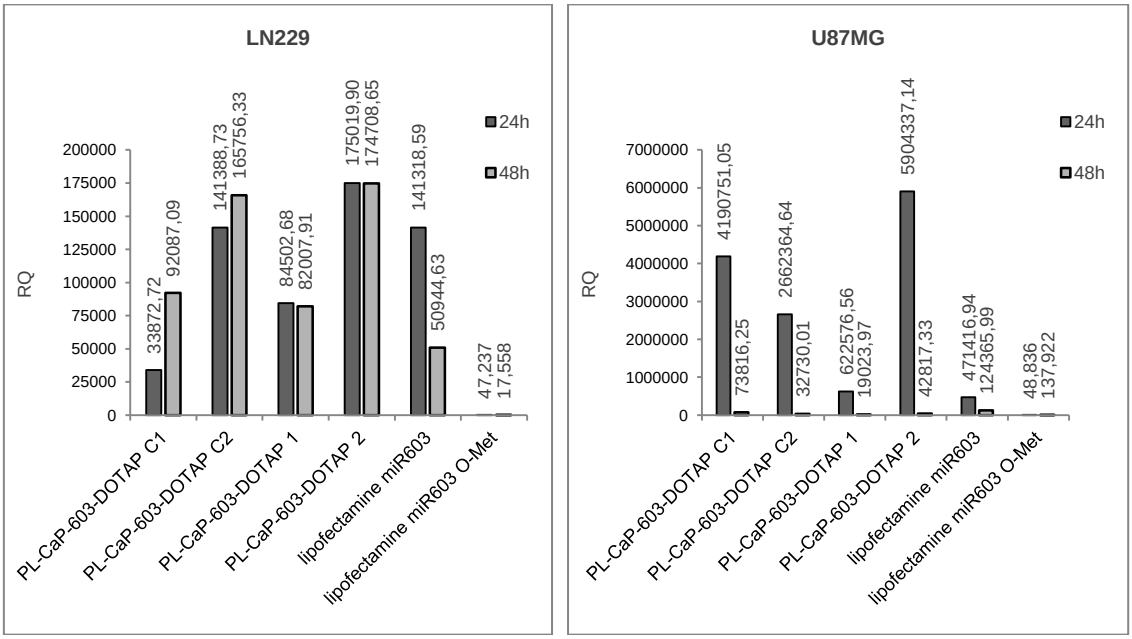

Figure 4.5.6.1: Intracellular uptake of miRNAs, measured by RT-PCR, after 24 and 48 h of LN229 (left panel) and U87MG (right panel) incubation with the formulations. Lipofectamine was used for comparison purpose.

The higher delivery of miRNA found in the case of SANPs based on DOTAP/cer-PEG could be ascribed to the role of cer-PEG. Previously, other authors compared the use of cer-PEG and DSPE-PEG in lipoplexes encapsulating siRNA, demonstrating superior transfection in the case former [Lechanteur *et al*., 2016]. In the case of lipoplexes, it has been reported that cationic lipids and RNA can adopt a lamellar or a hexagonal phase [Smisterová *et al*., 2001], being the latter the most favourable to the transfection and in particular to the endosomal escape of RNA [Rädler *et al*., 1997; Koltover *et al*., 1998; Dan and Danino, 2014]. Shi *et* co-workers demonstrated that DSPE-PEG stabilize the lipoplexes in lamellar phase whereas cer-PEG_{2000} favour the hexagonal organization [Shi *et al*., 2002]. Finally, it has been suggested that cer-PEG provide a steric hindrance of PEG chain lower than DSPE-PEG, thus promoting endosomal escape of siRNA [Lechanteur *et al*., 2016]. It is worthy of note that lipofectamine, used in this study for comparison purpose, consists on

non-PEGylated liposomes that should provide higher transfection compared to PEGylated lipid nanoparticles. SANPs used in this study are PEGylated lipid nanoparticles and provided transfection efficiency up to about 400 times higher than lipofectamine. To explain the high delivery efficiency of SANPs, we could hypothesize that also the CaP components could play a role. The potential of calcium phosphate nanoparticles as transfection agents has been largely reported [Mostaghaci *et al*., 2016; Xu *et al*., 2016]. Colloidal calcium phosphate particles have also endosomal escape properties that could be beneficial in the miRNA delivery by SANPs [Ma, 2014] in combination with the cationic lipid.

4.5.7 Biodistribution of miR603 encapsulated in SANPs

The ability of the selected SANP formulations to deliver *in vivo* miR603 was also investigated, in collaboration with Prof. Leonetti and his research group in Regina Elena National Cancer Institute (Roma). In particular, the biodistribution of miRNA encapsulated in SANPs with different lipid compositions, namely SANPs-603-DOTAP C1 and SANPs-603-DOTAP 2, has been studied in an orthotopic model of GBM. RNA distribution in brain, lungs, kidneys, heart, and liver have been studied before (time zero) and following 6 and 18 h from the SANPs administration. The results are reported in figure 4.5.7.1. Independently on the formulation, the highest levels of miR603 were found at 6 h from the administration. Different levels of miR603 were observed in the different organs with the highest levels found in the lungs. Interestingly, miR603 levels were significantly affected by the formulation, with the highest accumulation always in the case of the formulation SANP-603-DOTAP 2. In particular, when compared with the formulation DOTAP/CHOL/DSPE-PEG, the use of the formulation based on DOTAP/cer-PEG allowed achieving more than two times higher miR603 accumulation into the brain. This difference was also larger in the case of the other organs, especially in the case of lung where one order of magnitude of miR603 accumulation was found.

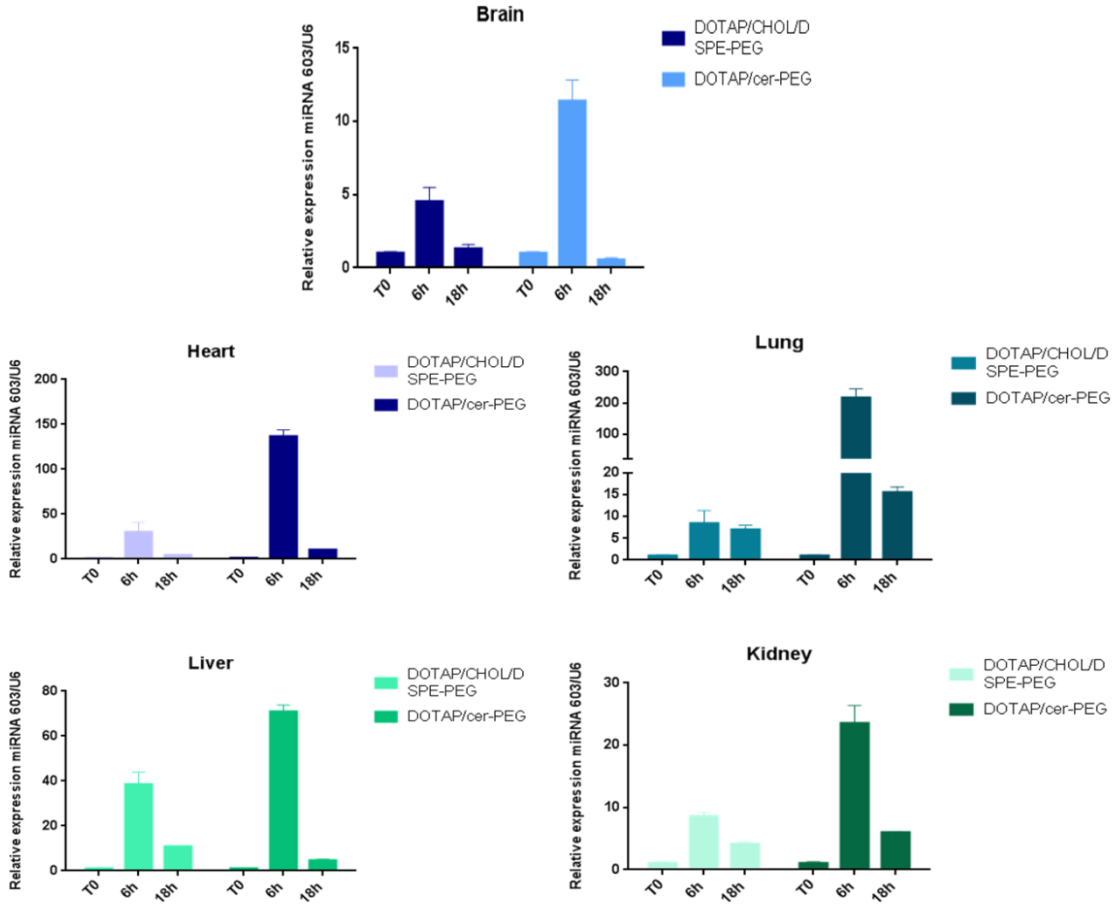

Figure 4.5.7.1: Levels of miR603 accumulated in brain, lungs, kidneys, heart, and liver before or following 6 and 18 h from the administration of PL-CaP-603-DOTAP-C1 and PL-CaP-603-DOTAP-2 formulations.

All together these results suggest that SANPs technology can be successfully proposed as delivery system for non-coding RNA (e.g. siRNA or miRNA). In particular this study provides insights for the optimization of lipid composition combining small size, high RNA encapsulation, stability in presence of plasma protein, hemocompatibility, low cytotoxicity, high transfection efficiency and *in vivo* delivery in different organs, including into the brain in a relevant orthotopic model of GBM.

4.6 Conclusions

This study provides the proof-of-principle to further boost the study of the SANPs as promising delivery tool for nucleic acids, e.g. miRNA. The finding underlines that the use of the cationic lipid into SANPs is not only mandatory for anchoring the lipid shell to the core, but also able to influence SANPs architecture, physical and biological stability, and the delivery process.

Among the neutral lipid used here, the DOPE provided a slight toxicity in some formulations, thus only SANPs based on DOTAP and DOTAP/chol were selected. Finally, the use of cer-PEG_{2000} provided the highest delivery efficiency, compared to the DSPE-PEG. Biodistribution study underlined that such SANPs are able to deliver miRNA 603 in different organs but allow also an accumulation of significant levels of the nucleic acid in the brain in an orthotopic model of GBM.

Further studies will clarify if the amounts of miRNA 603 delivered in the different organs, e.g. into the brain, will allow to achieve a pharmacological effect.

REFERENCES

Bai M., Shen M., Teng Y. Enhanced therapeutic effect of Adriamycin on multidrug resistant breast cancer by the ABCG2-siRNA loaded polymeric nanoparticles assisted with Ultrasound. Oncotarget. 6(41):43779–43790 (2015).

Bayraktar R., Pichler M., Kanlikilicer P., Ivan C., Bayraktar E., Kahraman N., Aslan B., Oguztuzun S., Ulasli M., Arslan A., Calin G., Lopez-Berestein G., Ozpolat B. MicroRNA 603 acts as a tumor suppressor and inhibits triplenegative breast cancer tumorigenesis by targeting elongation factor 2 kinase. Oncotarget, Vol. 8, No. 7, pp: 11641-11658 (2017). doi: 10.18632/oncotarget.14264.

Bartel D.P. MicroRNAs: genomics, biogenesis, mechanism, and function. Cell. 116:281-297 (2004).

Baumann V. and Winkler J. MiRNA-based therapies: Strategies and delivery platforms for oligonucleotide and non-oligonucleotide agents. Future Med Chem. 6(17): 1967–1984 (2014). doi: 10.4155/fmc.14.116.

Calin G.A., Croce C.M. MicroRNA signatures in human cancers. Nature reviews Cancer. 6:857-866 (2006).

Campani V., Giarra S., De Rosa G. Lipid-based core-shell nanoparticles: Evolution and potentialities in drug delivery. OpenNano. Vol.3, p.5-17 (2018).

Campani V., De Rosa G., Misso G., Zarone M.R., Grimaldi A.. Lipid Nanoparticles to Deliver miRNA in Cancer. Curr Pharm Biotechnol.17(8):741-9 (2016).

Dan N., Danino D. Structure and kinetics of lipid-nucleic acid complexes. Adv. Colloid Interface Sci. 205:230-9. doi: 10.1016/j.cis.2014.01.013 (2014).

De Rosa G., De Stefano D., Laguardia V., Arpicco S., Simeon V., Carnuccio R., Fattal E. Novel cationic liposome formulation for the delivery of an oligonucleotide decoy to NF-kappaB into activated macrophages. Eur J Pharm Biopharm. 70(1):7-18. doi: 10.1016/j.ejpb.2008.03.012 (2008).

Esquela-Kerscher A, Slack FJ. Oncomirs - microRNAs with a role in cancer. Nature reviews Cancer. 6:259-269 (2006).

Hosseini E.S., Hosseinkhani S. Cholesterol-rich lipid-mediated nanoparticles boost of transfection efficiency, utilized for gene editing by CRISPR-Cas9. 14:4353-4366 (2019). doi: 10.2147/IJN.S199104.

Hwang M.S., Yu N., Stinson S.Y., Yue P., Newman R.J., Allan B.B., Dornan D. miR-221/222 targets adiponectin receptor 1 to promote the epithelial-to-mesenchymal transition in breast cancer. PloS one. 8:e66502 (2013).

Jansook P., Pichayakorn W., Ritthidej G.C. Drug Amphotericin B-loaded solid lipid nanoparticles (SLNs) and nanostructured lipid carrier (NLCs): effect of drug loading and biopharmaceutical characterizations. Dev Ind Pharm. 44(10):1693-1700 (2018). doi: 10.1080/03639045.2018.1492606.

Jiang J., Yang S.J., Wang J.C., Yang L.J., Xu Z.Z., Yang T., Liu X.Y., Zhang Q. Sequential treatment of drug-resistant tumors with RGD-modified liposomes0 containing siRNA or doxorubicin. Eur J Pharm Biopharm. 76(2):170-8 (2010). doi: 10.1016/j.ejpb.2010.06.011.

Kanasty R., Dorkin J.R. , Vegas A., Anderson D. Delivery materials for siRNA therapeutics. Nat Mater. 12(11):967-77 (2013).

Khatri N., Baradia D., Vhora I., Rathi M., Misra A. Development and characterization of siRNA lipoplexes: Effect of different lipids, *in vitro* evaluation in cancerous cell lines and in vivo toxicity study. AAPS PharmSciTech. 15, 1630–1643 (2014). doi: 10.1208/s12249-014-0193-9.

Koltover I., Salditt T., Rädler J.O. An inverted hexagonal phase of cationic liposome-DNA complexes related to DNA release and delivery. Safinya C.R. Science. 3;281(5373):78-81 (1998). doi: 10.1126/science.281.5373.78.

Krönke M. Biophysics of ceramide signaling: interaction with proteins and phase transition of membranes. Chem Phys Lipids 101(1):109-21 (1999).

Kushwaha D., Ramakrishnan V., Ng K., Steed T., Nguyen T., Futalan D., Akers J.C., Sarkaria J., Jiang T., Chowdhury D., Carter B.S., Chen C.C.. A genome-wide miRNA screen revealed miR-603 as a MGMT-regulating miRNA in glioblastomas. Oncotarget. 2014; 5:4026-4039 (1974). doi: 10.18632/oncotarget

Kushwaha D., Ramakrishnan V., Ng K., Steed T., Nguyen T., Futalan D., Akers J.C., Sarkaria J., Jiang T., Chowdhury D., Carter BS., Chen CC. A genome-wide miRNA screen revealed miR-603 as a MGMT-regulating miRNA in glioblastomas. Oncotarget. 5(12):4026-39. (2014) doi: 10.18632/oncotarget.1974.

Lechanteur A., Sanna V., Duchemin A., Evrard B., Mottet D, Piel G. Cationic Liposomes Carrying siRNA: Impact of Lipid Composition on Physicochemical Properties, Cytotoxicity and Endosomal Escape. 8(5), 270. Nanomaterials. (2018). doi: 10.3390/nano8050270.

Lechanteur A., Furst T., Evrard B., Delvenne P., Hubert P., Piel G. PEGylation of lipoplexes: The right balance between cytotoxicity and siRNA effectiveness. 10;93:493-503. Eur J Pharma Sci (2016). doi: 10.1016/j.ejps.2016.08.058. E.

Litzinger D.C., Huang L. Biochim Biophys Acta. Biodistribution and immunotargetability of ganglioside-stabilized dioleoylphosphatidylethanolamine liposomes. 1104(1):179-87 (1992). doi: 10.1016/0005-2736(92)90148-f.

Ma D. Enhancing endosomal escape for nanoparticle mediated siRNA delivery. Nanoscale. 6(12):6415-25 (2014). doi: 10.1039/c4nr00018h.

Mahmoud D.B., Shukr M.H., Bendas E.R. In vitro and in vivo evaluation of self-nanoemulsifying drug delivery systems of cilostaZol for oral and parenteral administration. Int J Pharm. 476 (1-2), 60-69. (2014). doi: 10.1016/j.ijpharm.2014.09.045.

Marra M., Salzano G., Leonetti C., Porru M., Franco R., Zappavigna S ., Liguori G., Botti G., Chieffi P., Lamberti M., Vitale G., Abbruzzese A. , La Rotonda M.I., De Rosa G., Caraglia M. New self-assembly nanoparticles and stealth liposomes for the delivery of Zoledronic acid: a comparative study. Biotechnol Adv; 30,302-9 (2012). doi: 10.1016/j.biotechadv.2011.06.018.

Mostaghaci B., Loretz B., Lehr C.M. Calcium Phosphate System for Gene Delivery: Historical Background and Emerging Opportunities. Curr Pharm Des. 22(11):1529-33 (2016). doi: 10.2174/1381612822666151210123859.

Mussnich P., D'Angelo D., Leone V., Croce C.M., Fusco A. The High Mobility Group A proteins contribute to thyroid cell transformation by regulating miR-603 and miR-10b expression. Molecular oncology. 7:531-542 (2013).

Obika S., Yu W., Shimoyama A., Uneda T., Minami T., Miyashita K., Doi T., Imanishi T. Properties of cationic liposomes composed of cationic lipid YKS-220 having an ester linkage: adequate stability, high transfection efficiency, and low cytotoxicity. Biol Pharm Bull. 22(2):187-90 (1999).

Ochs K, Kaina B. Apoptosis induced by DNA damage O6-methylguanine is Bcl-2 and caspase-9/3 regulated and Fas/caspase-8 independent. Cancer Res. 60(20):5815-24 (2000).

Pegg A.E. Mammalian O6-alkylguanine-DNA alkyltransferase: regulation and importance in response to alkylating carcinogenic and therapeutic agents. Cancer Res. 1;50(19):6119-29 (1990).

Perazzoli G. , Prados J. ,Ortiz R. , Caba O., Cabeza L., Berdasco M., Gónzalez B., Melguizo C. Temozolomide Resistance in Glioblastoma Cell Lines: Implication of MGMT, MMR, P-Glycoprotein and CD133 Expression. PLOS ONE. 10(10): e0140131 (2015). doi: 10.1371/journal.pone.0140131.

Rädler J.O., Koltover I., Salditt T., Structure of DNA-cationic liposome complexes: DNA intercalation in multilamellar membranes in distinct interhelical packing regimes. Safinya C.R. Science. 275(5301):810-4 (1997). doi: 10.1126/science.275.5301.810.

Salzano G., Marra M., Porru M., Zappavigna S., Abbruzzese A., La Rotonda M. I., Leonetti C., Caraglia M., De Rosa G. Self-assembly nanoparticles for the delivery of bisphosphonates into tumors. Int. J. Pharm. 403, 292 (2011). doi: 10.1016/j.ijpharm.2010.10.046.

Salzano G., Zappavigna S., Luce A., D'Onofrio N., Balestrieri M.L., Grimaldi A., Lusa S., Ingrosso D., Artuso S ., Porru M., Leonetti C., Caraglia M., De Rosa G. Transferrin-Targeted Nanoparticles Containing Zoledronic Acid as a Potential Tool to Inhibit Glioblastoma Growth. J Biomed Nanotechnol. 12, 811-30 (2016).

Shi F., Wasungu L., Nomden A., Stuart M.C.A., Polushkin E., Engberts J. B., Hoekstra D. Interference of poly(ethylene glycol)–lipid analogues with cationic-lipid-mediated delivery of oligonucleotides; role of lipid exchangeability and non-lamellar transitions. Biochem. J. 366, 333–341 (2002). doi: 10.1042/BJ20020590.

Smisterová J., Wagenaar A., Stuart M.C., Polushkin E., ten Brinke G., Hulst R., Engberts J.B., Hoekstra D. Molecular shape of the cationic lipid controls the structure of cationic lipid/dioleylphosphatidylethanolamine-DNA complexes and the efficiency of gene delivery. J Biol Chem. 276(50):47615-22 (2001). doi: 10.1074/jbc.M106199200.

Tanic M., Yanowsky K., Rodriguez-Antona C., Andres R., Marquez-Rodas I., Osorio A., Benitez J., Martinez-Delgado B. Deregulated miRNAs in hereditary breast cancer revealed a role for miR-30c in regulating KRAS oncogene. PloS one. 7:e38847 (2012).

Volinia S., Calin G.A., Liu C.G., Ambs S., Cimmino A., Petrocca F., Visone R., Iorio M., Roldo C., Ferracin M., Prueitt R.L., Yanaihara N., Lanza G., Scarpa A., Vecchione A., Negrini M. A microRNA expression signature of human solid tumors defines cancer gene targets. Proceedings of the National Academy of Sciences of the United States of America. 103:2257-2261 (2006).

Vuddanda P.R., Rajamanickam V.M., Yaspal M., Singh S. Investigations on agglomeration and haemocompatibility of vitamin E TPGS surface modified berberine chloride nanoparticles. Biomed Res Int. 2014:951942. doi: 10.1155/2014/951942 (2014). doi: 10.1016/s0009-3084(99)00059-6.

Xiong F., Mi Z., Gu N. Cationic liposomes as gene delivery systems: Transfection efficiency and new application. Pharmazie. 66, 158–164 (2011).

Xu C., Wang J. Delivery systems for siRNA drug development in cancer therapy. Asian Journal of Pharmaceutical Sciences. 10, 1, 1-12 (2015).

Xu X., Li Z., Zhao X., Keen L., Kong X. Calcium phosphate nanoparticles-based systems for siRNA delivery. Regen Biomater. 3(3):187-95 (2016). doi: 10.1093/rb/rbw010.

Yao Y., Su Z., Liang Y., Zhang N. pH-Sensitive carboxymethyl chitosan-modified cationic liposomes for sorafenib and siRNA co-delivery. Int J Nanomedicine. 10:6185–6197 (2015).

Yoon G., Park J.W., Yoon I.S. Solid lipid nanoparticles (SLNs) and nanostructured lipid carriers (NLCs): recent advances in drug delivery. J Pharm Invest. 43(5):353–362 (2013).

Yoon H.Y., Son S., Lee S.J. Glycol chitosan nanoparticles as specialized cancer therapeutic vehicles: sequential delivery of doxorubicin and Bcl-2 siRNA. Sci Rep. 4:6878 (2014).

Young Yhee J., Son S., Lee H. Nanoparticle-based combination therapy for cancer treatment. Curr Pharm Des. 21(22):3158–3166 (2015).

CHAPTER 5

SANPs modification with hyaluronic acid for targeting of CD44-overexpressing cells

5.1. Hyaluronic acid modified systems for targeted drug delivery.

New cancer therapies based on NPs have attracted great deal of interest due to their ability to encapsulate anticancer drugs and to control their release at tumor target site [Brigger *et al*., 2002; Cho *et al*., 2008]. Furthermore, NPs can increase the drug concentration in cancer cells and help overcoming the limitations of conventional chemotherapy, which lacks specificity and elicits severe toxic effects toward healthy cells [Ricci and Zong, 2006]. Functionalized NPs can recognize and bind tumor cells, and can also be internalized by receptor-mediated endocytosis [Byrne *et al*., 2008; Peer *et al*., 2007; Torchilin, 2006]. In this frame, the polysaccharide hyaluronic acid (HA) has attracted significant research attention for tumor-targeted delivery [Ossipov, 2010; Choi *et al*., 2010; Toole, 2004].

Hyaluronic acid is a linear macromolecular mucopolysaccharide that is composed by alternately repeating disaccharide units of D-glucuronic acid and N-acetyl-D-glucosamine [Alaniz *et al*., 2016]. HA plays a significant role in cell growth and in maintaining the structural stability of tissue [Robert, 2015; Reed *et al*., 1988; Schaefer, 2010]. It has good biocompatibility, biodegradability, high viscoelasticity, [Widjaja *et al*., 2014]. Moreover, HA interacts with specific receptors on the surface of cells. Hyaluronic acid receptors are abundant in some specific tissues such as liver, kidney, and most tumor tissues [Rosso *et al*., 2013]. Following binding to the receptors on the cell surface, HA is uptaken into the cell through the endocytosis mediated by the HA receptor [Huang, 2018]. For these reasons, HA has attracted considerable interest from researchers for biomedical applications, including drug delivery systems [Saravanakumar *et al*., 2013; Arpicco *et al.* 2013]. In particular, three main groups of cell receptors binding HA have been identified: cluster of differentiation 44 (CD44), receptor for HA-mediated motility (RHAMM) and intercellular adhesion molecule-1 (ICAM-1) [Wayne, 1996]. These receptors can

be used for selective tumor targeting. CD44 receptor is involved in tumor invasion and metastasis in cancer cells and has been associated with the cellular adhesion process, including aggregation and migration in normal biological systems [Sironen *et al*., 2011; Sneath and Mangham, 1998]. RHAMM shows increased expression in tumor cells related to metastases [Telmer *et al*., 2011; Gust *et al*., 2009].

The HA-binding receptors, especially CD44, are characterized by domains hardly accessible [Nagano and Saya, 2004] for that small size and long-circulating HA-modified nanovectors are needed for targeted delivery to CD44-overxpressing cells [Yerushalmi *et al*., 1994; Margalit *et al*., 1996, Gabizon *et al*., 2001; Tardi *et al*., 2000]. The use of CD44-targeted nanovectors can provide multiple advantages. Indeed, when HA-nanovectors interact with CD44 receptors, the endogen substrate can't activate the receptor with consequent inhibition of cell proliferation dependent on the CD44 receptor. On the other hand, the HA-modified nanosystem linked to the binding site of the CD44 receptor should be uptaken by endocytosis mediated by the receptor, thus increasing the drug release into the CD44-overexpressing cells [Peer and Margalit, 2004]. Thus, since CD44 and RHAMM are ubiquitous in tumoral tissues, and also in neuronal tissues [Nagano and Saya, 2004], the combination between HA and nanovectors loaded by antitumoral drug, could be an valid strategy to improve the efficacy of chemotherapy of several kind of tumors [Peer *et al.*, 2007], such as epithelial, ovarian, colon, stomach and acute leukemia [Toole *et al*., 2002; Arpicco *et al*., 2013; Zoller, 1995; Sneath and Mangham, 1998], including brain tumors. For these reasons, several works reports the use of nanovectors for active targeting of CD44-overxpressing cells, especially in tumour initiating cells [Misra *et al*., 2011; Hertweck *et al*., 2011, Nishiyama, 2007, Arpicco *et al*. 2013; Han *et al*., 2015; Kim *et al*., 2013; Chen *et al.,* 2013]. Cationic HA-modified liposomes have been developed by Taetz *et al.* for treating of lung cancer [Taetz *et al.*, 2009]. Arpicco *et al.,* who modified liposomes containing gemcitabine by HA for the treatment of pancreatic adenocarcinoma [Arpicco *et al*., 2013]. An evidence of efficient drug delivery by these systems on brain tumors has been provided by Hayward *et al*. who modified liposomes by HA chemical conjugated (HALNPs) for U87-GBM

targeting [Hayward *et al*., 2016], by Cohen *et al*. that devised an in situ strategy to deliver RNAi directly to U87-GBM site using HA-grafted lipid-based nanoparticles (LNPs) [Cohen *et al*., 2015]. Then, Yang *et al* modified ion-pairing liposomal nanoparticles with HA for the treatment of glioma [Yang *et al*., 2018].

5.2. Aim of the work

In this part of the Ph.D. thesis, the modification of self-assembling nanoparticles surface with HA (SANPs-HA) for targeting of CD44-overexpressing cells has been investigated. In particular, two different self-assembling protocol have been proposed to prepare SANPs-HA. Moreover, HA with different molecular weight as well as presence of DSPE-PEG on SANPs-HA, have been tested in this study. In the first step of the study, SANPs-HA have been fully characterized in terms of size, zeta potential, and degree of HA associated to the SANPs. In the second step of the study, SANPs-HA encapsulating zoledronic acid (SANPs-HA-Zol) were prepared and characterized in terms of size, zeta potential, HA association to the nanoparticles, Zol encapsulation. Moreover, the stability of SANPs-HA and SANPs-HA-Zol was also investigated. Finally, cytotoxicity of the different prepared HA-modified SANPs was also tested on cell lines overexpressing the CD44 receptor.

5.3 Materials and methods

5.3.1 Materials

Zoledronic acid (Zol) has been kindly provided by Lisapharma S.p.a. (Erba, Italy). 1,2-dioleoyl-3-trimethylammonium-propane chloride (DOTAP) was kindly provided by Lipoid GmbH (Ludwigshafen, Germany). 1,2-distearoyl-sn-glycero-3-phosphoethanolamine-N-[amino(polyethylene glycol)-2000] (DSPE-PEG_{2000}) and cholesterol (CHOL) were purchased from Avanti Polar (Alabama, Usa). Sodium chloride (NaCl), sodium hydroxide (NaOH), calcium chloride ($CaCl_2$), sodium phosphate dibasic (Na_2HPO_4), potassium phosphate dibasic (K_2HPO_4), potassium chloride (KCl), Tetra-N-Butyl Ammonium Solfate Hydroxide, absolute ethanol HPLC grade, acetonitrile HPLC grade, sulfuric acid, carbazole, sodium

tetraborate decahydrate were obtained from Sigma-Aldrich Co. (Milan, Italy). Hyaluronic acid (HA), molecular weight: 1600 kDa, was obtained from DSM Nutritional Products (Aesch, Switzerland). Hyaluronic acid (HA), molecular weights: 1437 kDa, 803 kDa, 200 kDa and 180 kDa, were obtained from Altergon italia (Avellino, Italy).

5.3.2 Methods

5.3.2.1 Liposomes preparation

PEGylated cationic liposomes (PLs) (DOTAP/chol/DSPE-PEG_{2000} 1:1:0.5 weight ratio and DOTAP/chol 1:1 weight ratio) were prepared by hydration of a thin lipid film, followed by extrusion. Briefly, the lipid mixture was dissolved in 1 ml of a mixture chloroform/methanol (2:1 v/v). The organic solution was removed by rotavapor. Then the lipid film was hydrated with 1 mL of water, and the resulting dispersion was extruded using a thermobarrel extruder system, through polycarbonate membranes with progressively lower porosity from 0.4 to 0.1 μm. The liposomes were stored at 4 °C before use.

5.3.2.2 Calcium-phosphate nanoparticles (CaP NPs)

An aqueous solution of dibasic hydrogen phosphate (10.8 mM) was added, dropwise and under magnetic stirring, to an aqueous solution of calcium chloride (18 mM). The pH of both solutions was adjusted beforehand to 9.5 with NaOH 0.1 M. The resulting dispersion (CaP NPs) was filtered through a 0.22 μm filter and stored at 4 °C before use.

5.3.2.3 HA stock preparation

HA with different molecular weights were weighted and dissolved in deionized filtered water at the following concentration 2%, 1%, 0.5%, 0.2%, 0.1%, 0.05% and 0.0125% (w/v). At the highest concentrations, the HA was keep in ice bath under magnetic stirring overnight to achieve complete solubilization.

5.3.2.4 Preparation of SANPs-HA

SANPs-HA were prepared with two different methods, summarized as follows:

A) in the case of method A, PLs were complexed with CaP NPs (1:1 v/v), stirred by vortex and leave to react for 15 minutes. Then, the HA solution stock was added to PL-CaP 1:1 (v/v), stirred by vortex and leave to react for 15 minutes.

B) in the case of method B, HA solution stock was complexed with PLs (1:1 v/v), stirred by vortex and leave to react for 15 minutes. Then, the CaP NPs were added to PL-HA 1:1 (v/v), stirred by vortex and leave to react for 15 minutes.

The SANPs-HA prepared following methods A and B were characterized in terms of size, polydispersity index and zeta potential.

5.3.2.5 Preparation of SANPs-HA encapsulating zoledronic acid (SANPs-HA-Zol)

Zol were weighted and dissolved in a PBS buffer solution at pH 9.5 (Na_2HPO_4 10 mM (1.42 mg), KCl 2.7 mM (0.2 mg), NaCl 120 mM (7 mg) *per* ml) at concentration of 40 mg/ml.

Briefly, HA solution stock was complexed with PLs (1:1 v/v), stirred by vortex and leave to react for 15 minutes. Then, Zol was added at CaP NPs (1:50 v/v), stirred by vortex and leave to react for 15 minutes. Finally, the CaP-Z were added to PL-HA 1:1 (v/v), stirred by vortex and leave to react for 15 minutes.

5.3.2.6 Particle size

PLs, SANPs-HA and SANPs-HA-Zol were characterized in terms of mean diameter and polydispersity index (PI). In particular, mean diameter was determined at 20°C by Zetasizer Nano Ultra Pro (Malvern, UK). For these measurements, each sample was analyzed with detector at 90° angle. Polydispersity index (PI) was used as measure of the particle size distribution. For each batch, mean diameter and size distribution were the average of three

measures, while for each formulation, the mean diameter and PI were calculated as the values averaged over three different batches.

5.3.2.7 Zeta potential

The zeta-potential (ζ) of PLs, SANPs-HA and SANPs-HA-Zol was measured in water by means of a Zetasizer Nano Ultra Pro (Malvern, UK). For each batch, data of ζ were collected as the average of 20 measurements, while for each formulation the ζ was calculated as the average of ζ over three different batches.

5.3.2.8 Zol encapsulation efficiency

Encapsulation efficiency of Zol was determined by ultra high performance liquid chromatography (UHPLC). A UHPLC system consisting of an isocratic pump UHPLC LC-10AD (Shimadzu, Milano, Italia), equipped with injection valve 7725i (Rheodyne) and detector at λ= 220 nm, was used. The chromatograms were collected and analyzed by PC with Lab Solution software. The analysis was carried out by Gemini 5 µm C18 (250 X 4.60 mm, 110 Å Phenomenex, Klwid, USA) column with guard column. A mobile phase consisting of a mixture of acetonitrile and an aqueous solution 20:80 v/v (8 mM K_2HPO_4, 2 mM Na_2HPO_4 e 7 mM tetra-N-Butyl ammonium sulphate hydroxide, pH 7.0) was used. Previously, Zol-containing formulations were alkalized to pH 14 by the addition of NaOH (51.69 mg/ml). Analyses were carried out on supernatants under isocratic conditions, with a mobile phase flow of 1 ml/min at room temperature. The supernatants were obtained by ultracentrifugation (Optima Max E, Beckman Coulter, USA) at 80000 rpm, at 4 °C, for 40 minutes. The results obtained from the chromatogram analysis were expressed as encapsulation efficiency (EE), calculated as the ratio of the amount of Zol present in supernatants to the amount of Zol theoretically charged.

5.3.2.9 Carbazole assay for HA determination

For photometric determination of HA, the modified uronic acid carbazole reaction of Bitter *et al*. [Bitter 1962] based on Dische's carbazole reaction [Dische, 1947] was used. Briefly, in the first step, the samples containing the HA were centrifugated (by ultracentrifugation (Optima Max E, Beckman Coulter, USA) at 80000 rpm, at 4 °C, for 40 minutes and analyzed by Zetasizer Nano Ultra Pro (Malvern, UK) several times until the disappear of the peak related to other colloidal particles, which interfered with the assay. Supernatants were then used to perform an indirect test to calculate the degree of association (DA) of HA in SANPs-HA and SANPs-HA-Zol.

In the second step, 3 ml of 0.025 M sodium tetraborate decahydrate in sulphuric acid were cooled at 4°C for 30 minutes. Then 0.5 ml of HA stock solution or of the SANPs-HA/SANPs-HA-Zol were carefully added to the acid solution. Then, the resulting mix was sealed in vial and shaken by vortex for 30 seconds, followed by cooling for 20 seconds in ice bath under magnetic stirring; then the solution was heated for 10 min in boiling water bath and cooled down at room temperature. In the last step 0.1 ml of 0.125% (w/v) carbazole ethanolic solution was added to mix and shaken again. Finally, the resulting solution was heated for 15 min in a boiling water bath, cooled down at room temperature and the absorbance of samples was measured by spectrophotometric analysis (using the Thermo Fisher Scientific 1510 Multiskan Go spectrophotometer) at λ=530 nm.

5.3.2.10 Cytotoxicity of SANPs-HA and SANPs-HA-Zol

The cell lines used were MDA-MB-231 (human breast adenocarcinoma) and A2780 (human ovarian carcinoma). MDA-MB-231 cells were grown in DMEM supplemented with 10% FBS, 0.03% L-glutamine, 2% penicillin and streptomycin. A2780 cells were maintained in RPMI 1640 containing 10% FBS, 0.03% of L-glutamine, 2% penicillin and streptomycin, and 50 µg/ml of gentamicin sulfate. Cells were maintained in a humidified incubator at 37°C in 5% CO_2. The effect on cell growth inhibition was evaluated by the sulforhodamine B colorimetric proliferation assay (SRB) modified by Vichai and

Kirtikara [Vichai and Kirtikara, 2006]. MDA-MB-231 and A2780 cells, maintained in culture as described above, were seeded at 3×10^{-4} cells/well in 96 wells microtiter plates and incubated overnight to allow cellular adhesion. Various dilutions of SANPs-HA-Zol and SANPs-HA were added in triplicate and incubated for 24, 48 and 72 h.

5.4 Results and discussion

5.4.1 Preparation protocol set up

In a preliminary phase of the study, HA with different molecular weights (1600 kDa, 1437 kDa, 803 kDa, 200 kDa, 180 kDa) was used to prepare solution at different HA concentrations, namely 2%, 1%, 0.5%, 0.2%, 0.1%, 0.05% and 0.0125% (w/v). At the concentrations of 2%, 1%, 0.5% and 0.2% (w/v) the HA solubilisation resulted in highly viscous solution that were discarded for the following phases of the study.

Then, HA with several molecular weights (1600 kDa, 1437 kDa, 803 kDa, 200 kDa, 180 kDa) at concentrations of 0.1%, 0.05% and 0.0125% (w/v) were complexed with plain SANPs following two different methods (A or B). Moreover, to investigate the effect of the PEGylation on the interaction of HA with SANPs, two different compositions of liposomes, namely DOTAP/chol/DSPE-PEG_{2000} 1:1:0.5 weight ratio and DOTAP/chol 1:1 weight ratio, were investigated for this part of the experiment. All SANPs-HA formulations prepared with HA at 0.1% (w/v) rapidly aggregated after preparation; on the other hand, the majority of SANPs-HA formulations prepared with HA at 0.05% (w/v) showed flocculation after preparation. For these reasons, HA 0.0125% (w/v) stock solution was selected to go on the study.

Figure 5.4.1.1 showed the characteristics of SANPs-HA formulations prepared with HA 0.0125% (w/v) by methods A and B and obtained by complexation of DOTAP/chol PLs.

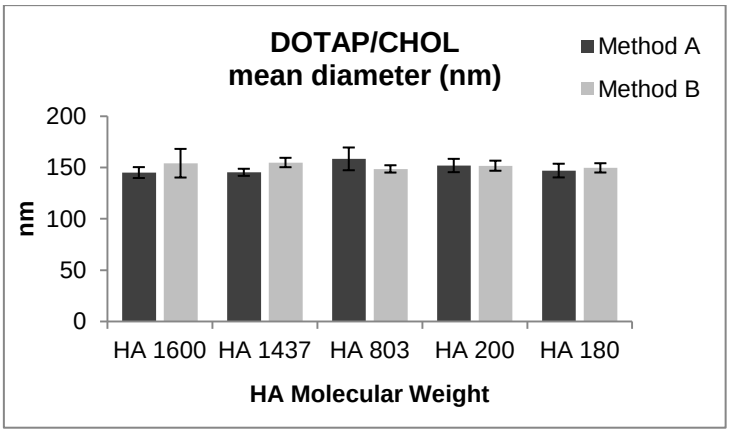

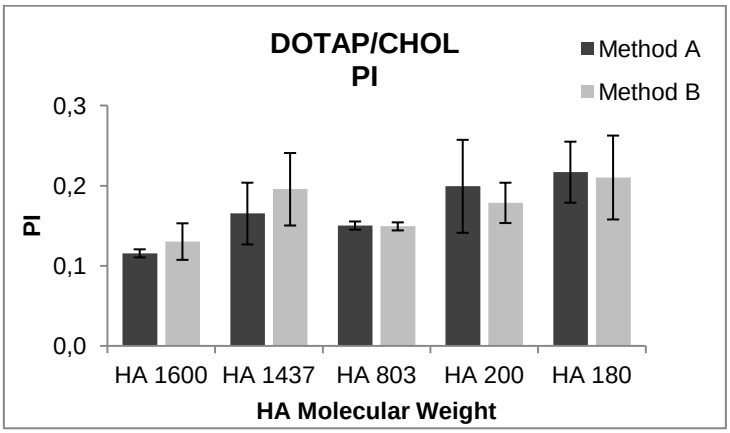

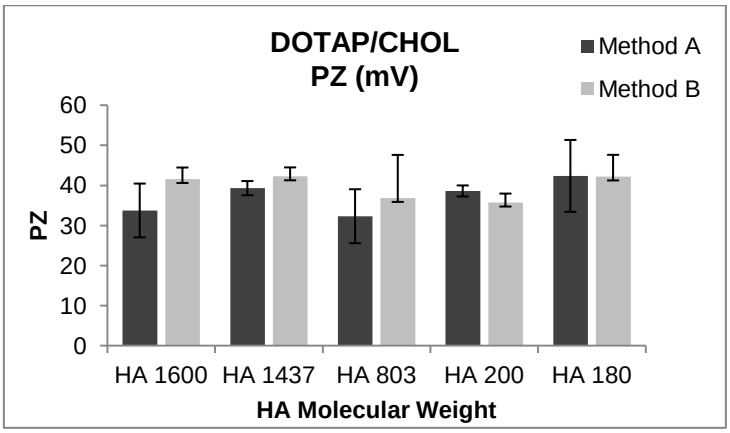

*standard deviation calculated on average of three batches

Figure 5.4.1.1: Characterization of SANPs-HA formulations prepared with HA 0.0125% (w/v) and DOTAP/chol PLs.

Figure 5.4.1.2 showed the characterization of SANPs-HA formulations prepared with HA 0.0125% (w/v) following methods A and B and obtained by complexation of DOTAP/chol/DSPE-PEG_{2000} PLs.

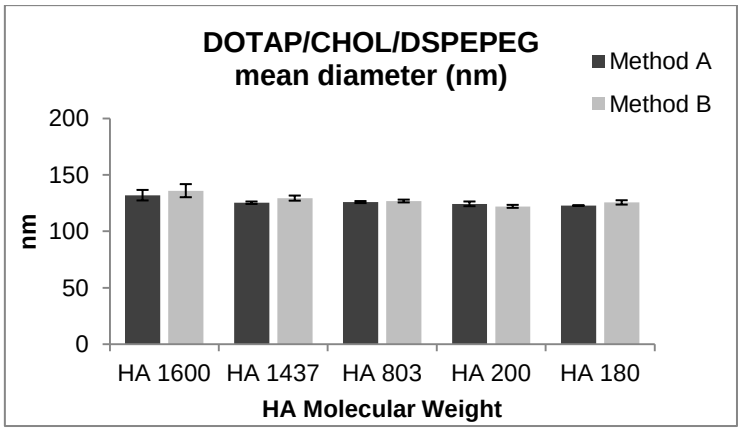

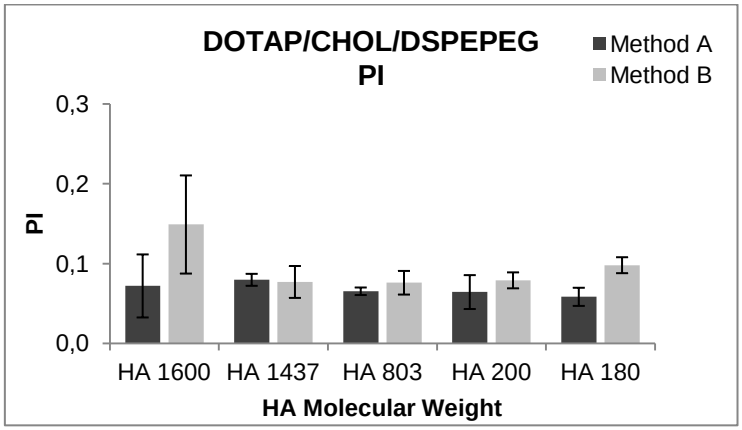

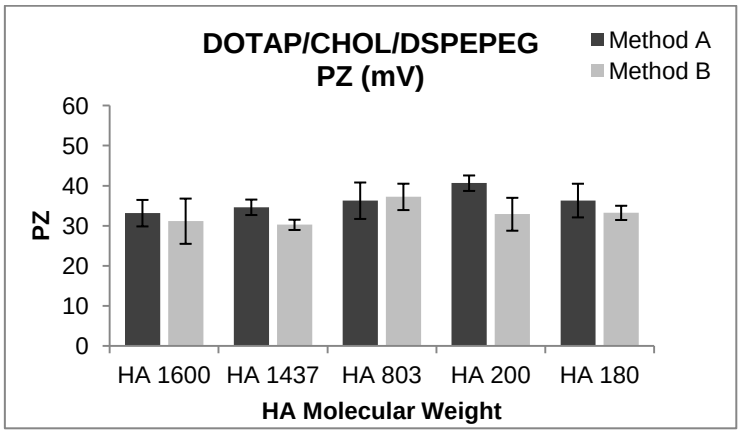

*standard deviation calculated on average of three batches

Figure 5.4.1.2: Characterization of SANPs-HA formulations prepared with HA 0.0125% (w/v) and DOTAP/chol/DSPEPEG PLs.

More in details, SANPs-HA prepared with DOTAP/chol PLs showed in both cases (Method A or B) mean diameter around 150 nm, PI < 0.2 and PZ around +40 mV; also in the case of SANPs-HA based on the inclusion of PEGylated PLs both methods were comparable showing mean diameter around 125 nm, PI < 0.15 and zeta potential around +35 mV (Figures 5.4.1.1 and 5.4.1.2). The

characterization of these formulations, showed that the use of PEGylated liposomes, compared to complexes characterized by non-PEGylated liposomes, resulted in smaller mean diameters and polydispersity index. No significant differences in terms of size were found between methods A and B, independently on the HA molecular weight. However, SANP-HA prepared with method A showed a zeta potential significantly higher suggesting a lower interaction between HA and SANPs. Thus, only the method B was used in the following phase of the study.

5.4.2 SANPs-HA-Zol preparation

In this part of the study, all SANPs-HA encapsulating Zoledronic acid (SANPs-HA-Zol) were prepared by method B. The use of PLs based on DOTAP/CHOL liposomes resulted in an SANPs flocculation. This was not observed in complexes containing PEGylated liposomes, for which a mean diameter around 150 nm, PI around 0.2 and PZ around +25 mV were found, independently on the HA molecular weights (Figure 5.4.2.1). SANPs-HA-Zol compared to SANPs-HA (both prepared with HA 0.0125% (w/v) at different molecular weight and DOTAP/chol/DSPEPEG$_{2000}$ PLs) have higher mean diameter, higher index of polydispersity, but lower surface charges. More in details, the Zol addition incremented the mean diameter from around 125 nm to around 150 nm. Also the PI was incremented in all SANPs-HA-Zol with the exception of the formulation based on the inclusion of HA 1600 that resulted in a decrease. Finally, the zeta potential decreased when including Zol in the formulation.

Thus, Zol encapsulation affects the SANPs interaction with HA, leading to flocculation, as suggested also by the lower zeta potential. Previous finding demonstrated that Zol is mainly located in the core of the SANPs [Ristori *et al.*, 2018]. However, it is possible to hypothesize that a small amount of Zol could be located at the interface, reducing the interaction among SANPs and HA, and favouring the formation of HA-based bridges between the particles, and leading to the observed flocculation. On the contrary, the presence of DSPE-PEG on the SANPs surface could hamper the flocculation for steric protection of the nanoparticles.

Thus, only SANPs-HA-Zol based on the inclusion of PEGylated liposomes were used for the following studies.

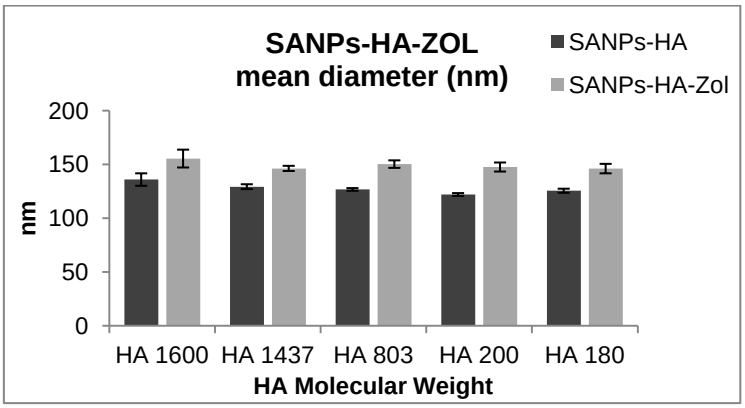

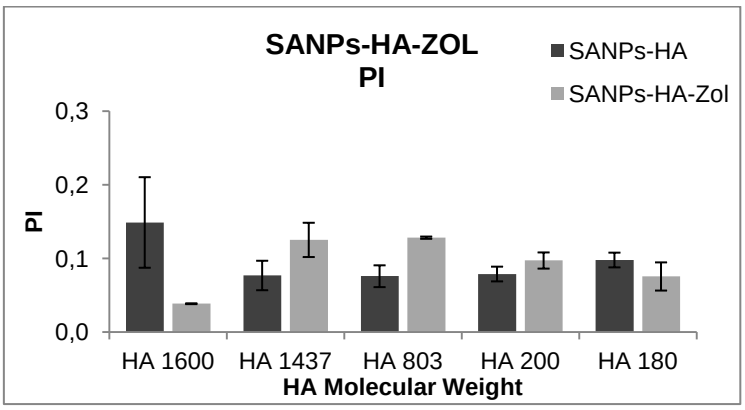

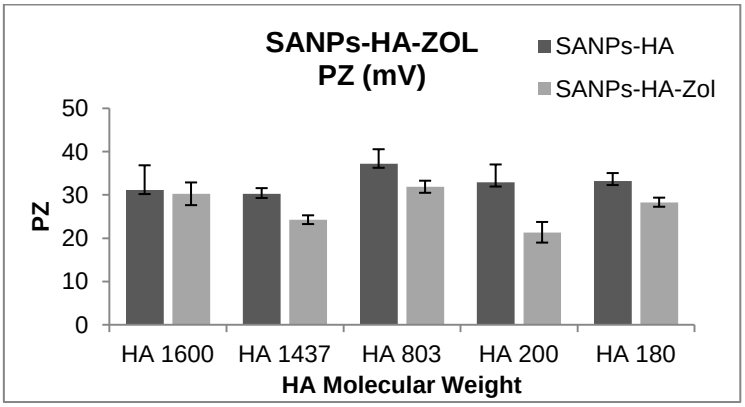

*standard deviation calculated on average of three batches

Figure 5.4.2.1: Characterization of SANPs-HA-Zol formulations prepared with HA 0.0125% (w/v) and DOTAP/chol/DSPEPEG$_{2000}$ PLs compared with SANPs-HA (Method B).

5.4.3 Physical stability of SANPs-HA and SANPs-HA-Zol

The stability of all the formulations selected in the phases of the study was investigated at 4°C until 1 month. The result of this study is reported in the Figure 5.4.3.1 for SANPs-HA and in Figure 5.4.3.2 for SANPs-HA-Zol.

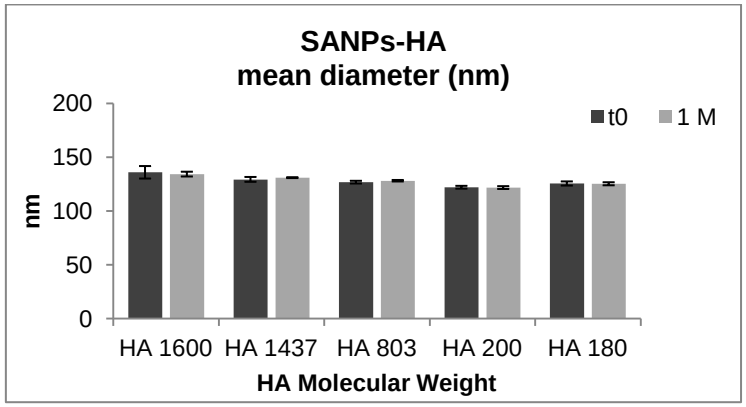

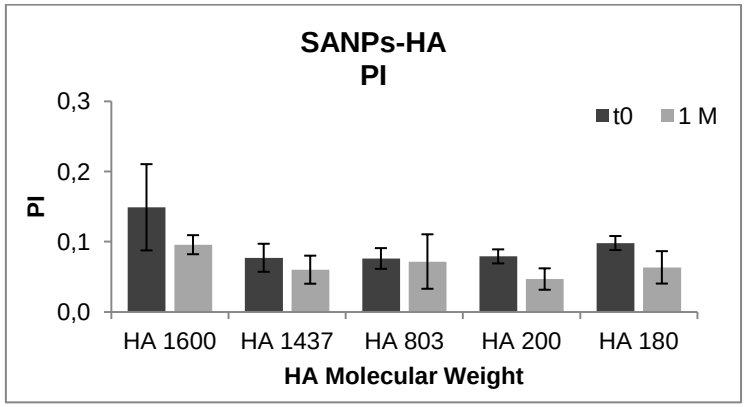

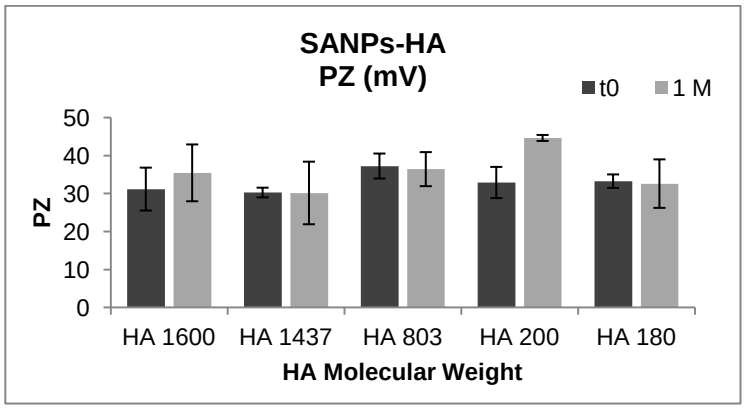

*standard deviation calculated on average of three batches

Figure 5.4.3.1: Characterization of SANPs-HA formulations after preparation (t0) and after 1 month (1M).

Analyzing the results reported in Figures 5.4.3.1, SANPs-HA showed no significant difference in the mean diameter following 1 month of storage at 4°C. with a decrease of the polydispersity index (PI < 0.1). Finally, the zeta potential resulted in a moderated increase with HA 1600 and HA 200.

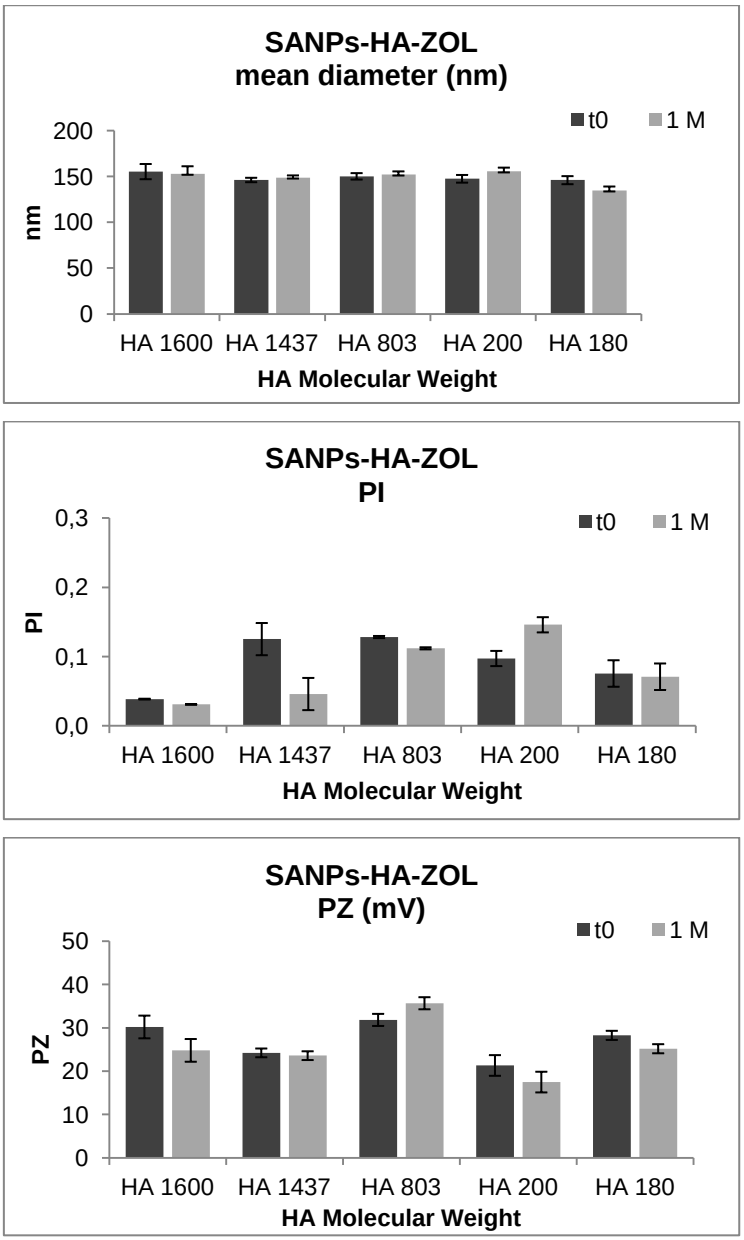

*standard deviation calculated on average of three batches

Figure 5.4.3.2: Characterization of SANPs-HA-Zol formulations after preparation (t0) and after 1 month (1M).

In the Figure 5.4.3.2 the characterization of SANPs-HA-Zol formulations after preparation and after 1 month is reported. Briefly, in term of mean diameter no significant differences were found. On the other hand, the PI decreased for all formulations with the exception of the formulation based on the inclusion of HA 200 that had a moderate increase, but always < 0.2. Finally, the zeta potential decreased for all formulations except for the formulation based on the inclusion of HA 803 that resulted in a moderate increase.

SANPs have been designed to be used few minutes following preparation. Here, stability studies showed that SANPs-HA/SANPs-HA-Zol did not change their size following 1 month of storage at 4°C, with some changes in IP and zeta potential; these changes could be attributed to a further maturation of the SANPs few days after preparation suggesting their use also following long term storage.

5.4.4 Zol encapsulation efficiency

The amount of Zol encapsulated in SANPs-HA-Zol was determined by indirect measure on unencapsulated Zol, by means of a calibration curve (R^2=0.9995) in H_2O (Figure 5.4.4.1).

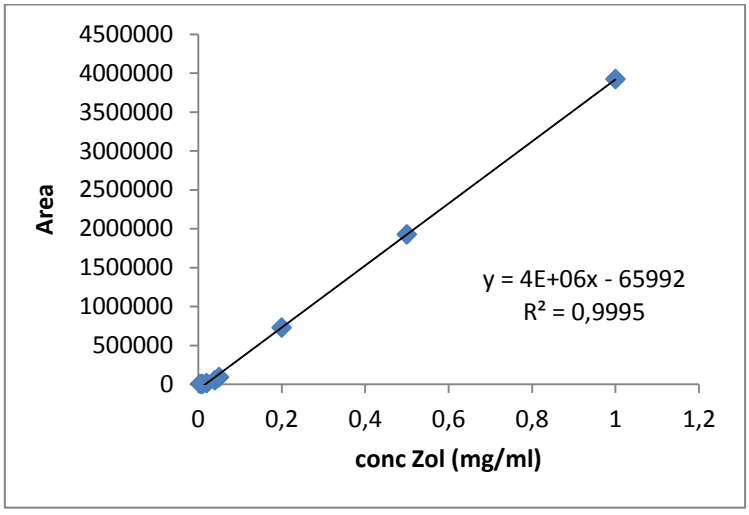

Figure 5.4.4.1: Calibration line of Zol obtained by chromatographic analysis.

In table 5.4.4.1, the amount of Zol encapsulated, expressed as Zol actual loading and Zol encapsulation efficiency (EE) in the SANPs-HA-Zol is reported. All the formulations were characterized by a high Zol encapsulation efficiency, ranging from about 72% to 83%.

Formulation	Theoretical concentration (mg/ml)	Concentration Zol in SANPs (mg/ml) ± sd*	EE (%) Zol ± sd*
SANPs-HA1600-Zol	0.238	0.17110±0.002*	72±0.8*
SANPs-HA1437-Zol	0.238	0.19451±0.002*	82±0.8*
SANPs-HA803-Zol	0.238	0.19565±0.003*	82±0.7*
SANPs-HA200-Zol	0.238	0.19840±0.002*	83±0.8*
SANPs-HA180-Zol	0.238	0.19674±0.003*	83±0.7*

*standard deviation calculated on average of three batches

Table 5.4.4.1: Zol encapsulation efficiency.

5.4.5 HA associated to the SANPs

For the dosage of HA, the modified uronic acid carbazole reaction of Bitter *et al*. [Bitter 1962] based on DISCHE's carbazole reaction [Dische, 1947] was used. Firstly, all the samples were centrifugated at 80000 rpm, at 4 °C, for 40 minutes and analyzed by Zetasizer Nano Ultra Pro (Malvern, UK) several times until the disappear of the peak related to PLs, which interfered with the assay. Supernatants were then used to perform an indirect test to calculate the encapsulation efficiency of HA in SANPs-HA and SANPs-HA-Zol.

The concentration of each HA was obtained by carbazole assay and was calculated by a calibration curve in H_2O (Figure 5.4.5.1).

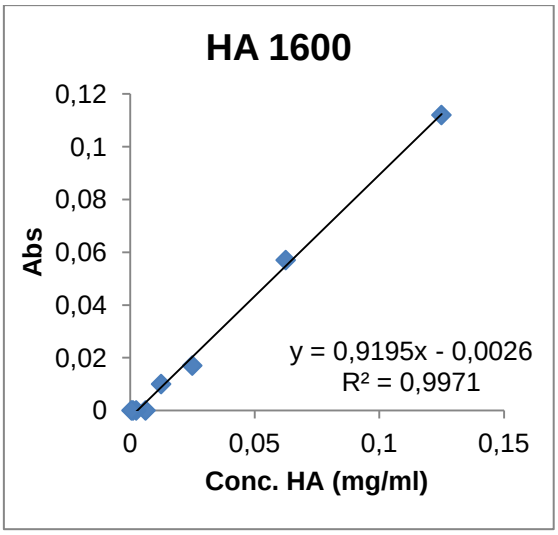
HA 1600
Abs
0,12
0,1
0,08
0,06
0,04
0,02
0
0
0,05
0,1
0,15
Conc. HA (mg/ml)
y = 0,9195x - 0,0026
R² = 0,9971

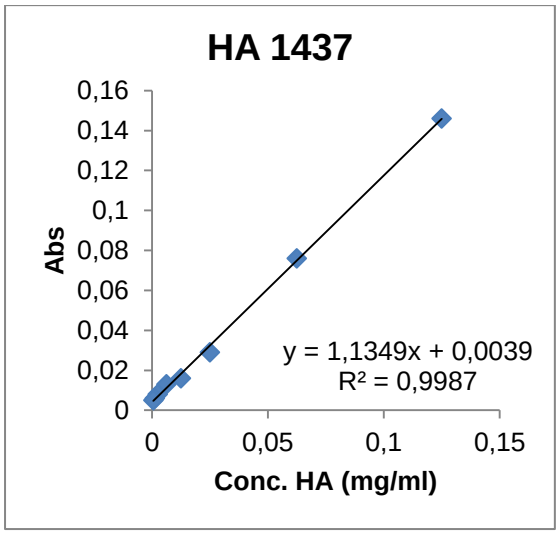
HA 1437
Abs
0,16
0,14
0,12
0,1
0,08
0,06
0,04
0,02
0
0
0,05
0,1
0,15
Conc. HA (mg/ml)
y = 1,1349x + 0,0039
R² = 0,9987

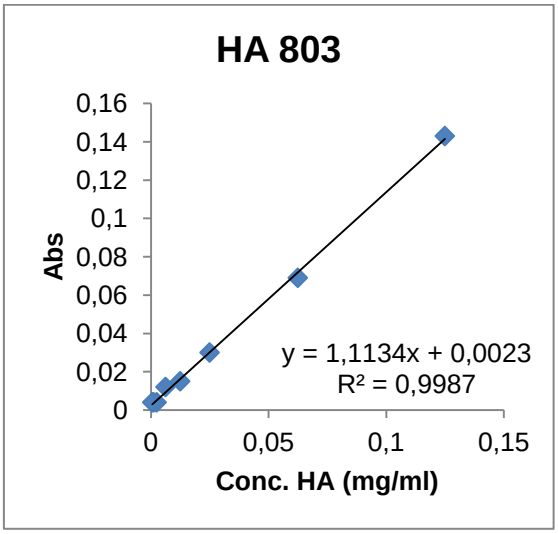
HA 803
Abs
0,16
0,14
0,12
0,1
0,08
0,06
0,04
0,02
0
0
0,05
0,1
0,15
Conc. HA (mg/ml)
y = 1,1134x + 0,0023
R² = 0,9987

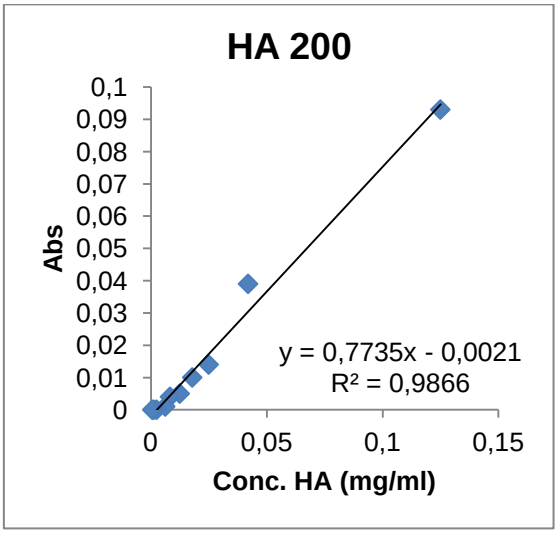
HA 200
Abs
0,1
0,09
0,08
0,07
0,06
0,05
0,04
0,03
0,02
0,01
0
0
0,05
0,1
0,15
Conc. HA (mg/ml)
y = 0,7735x - 0,0021
R² = 0,9866

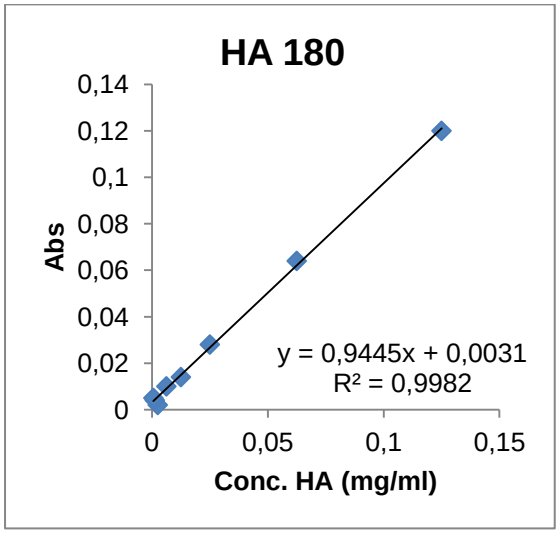
HA 180
Abs
0,14
0,12
0,1
0,08
0,06
0,04
0,02
0
0
0,05
0,1
0,15
Conc. HA (mg/ml)
y = 0,9445x + 0,0031
R² = 0,9982

Figure 5.4.5.1: Calibration line of HA obtained by photometric analysis.

The absorbance of samples was measured by spectrophotometric analysis at λ=530 nm against water.

In table 5.4.5.1, the amount of HA, expressed as HA actual loading and HA degree of association (DA) (expressed as percentage of HA associated to the SANPs respect to the HA initially used in the formulations) in SANPs-HA and in SANPs-HA-Zol is reported.

Formulation	Concentration supernatants (mg/ml) ± sd*	Concentration HA in SANPs (mg/ml) ± sd*	DA (%) HA ± sd*
SANPs-HA1600	0.0015±0.0001*	0.012±0.0001*	89±0.7*
SANPs-HA1600-Zol	0.0000±0.0000*	0.014±0.0000*	100±0.0*
SANPs-HA1437	0.0010±0.0001*	0.013±0.0001*	93±0.6*
SANPs-HA1437-Zol	0.0032±0.0003*	0.011±0.0002*	77±0.7*
SANPs-HA803	0.0006±0.0000*	0.013±0.0001*	96±0.2*
SANPs-HA803-Zol	0.0024±0.0002*	0.012±0.0002*	83±0.8*
SANPs-HA200	0.0034±0.0003*	0.011±0.0002*	76±0.9*
SANPs-HA200-Zol	0.0000±0.0000*	0.014±0.0000*	100±0.0*
SANPs-HA180	0.0045±0.0003*	0.013±0.0002*	89±0.8*
SANPs-HA180-Zol	0.0055±0.0005*	0.011±0.0004*	82±0.7*

*standard deviation calculated on average of three batches

Table 5.4.5.1: Calibration line of HA obtained by photometric analysis. The theoretical HA concentration was 0.014 mg/ml.

All the formulations were characterized by a very high HA association to the SANPs, ranging from about 76% to 100%. Furthermore, the Zol addition incremented the encapsulation efficiency of HA, but only in the case of formulations based on the inclusion of HA 1600 and HA 200. These findings are in agreement with the previously hypothesized interference of Zol on HA interaction with SANPs lipid shell.

5.4.6 Cytotoxicity of SANPs-HA and SANPs-HA-Zol

Once selected SANPs-HA-Zol with optimal physical-chemical characteristics, the ability to deliver Zol was investigated on two cell lines. In particular, the ability of the bisphosphonate to inhibit cell proliferation was measured.

In particular, the cytotoxicity of the SANPs-Zol and SANPs-HA-Zol at different Zol concentrations, namely from 1×10^{-7} M to 1×10^{-4} M, were tested. This part of the study was carried out in collaboration with the research group coordinated by Prof. S. Arpicco at the University of Turin. SANPs were tested on two cell lines, e.g. MDA MB231, characterized by an overexpression of CD44 (CD44+), and A2780, not characterized by overexpression of CD44 (CD44-). The experiments were carried out at 24, 48 and 72 hours following the incubation with the formulations. Also the plain SANPs-HA (SANPs-Zol) were tested at the same concentration. The preliminary results of this study showed no cytotoxicity for the SANPs-HA, SANPs-Zol and a slight cytotoxicity for SANPs-HA-Zol. The results are reported in Figures 5.4.6.1 (SANPs-Zol), 5.4.6.2 (SANPs-HA) and 5.4.6.3 (SANPs-HA-Zol) and also summarized in Table 5.4.6.1. More in detail, SANPs-Zol showed no toxicity on both cell lines at all times considered; SANPs-HA showed no toxicity on MDA MB231 (CD44+) at 24, 48 and 72 hours and on A2780 (CD44-) at 24 hours; whereas, SANPs-HA on A2780 (CD44-) showed 20% and 40% of cytotoxicity at 48 and 72 hours, respectively. In all these cases the IC50 was not observed at the SANPs concentration used.

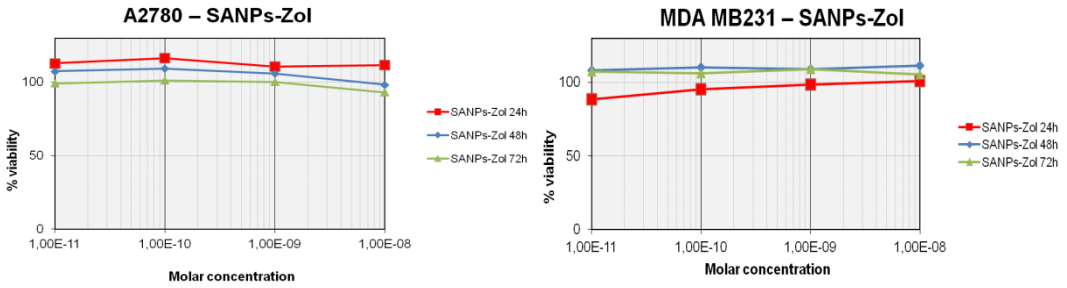

Figure 5.4.6.1: Cytotoxicity of SANPs-Zol at 24, 48 and 72 hours on A2780 (left) and MDA MB231 (right).

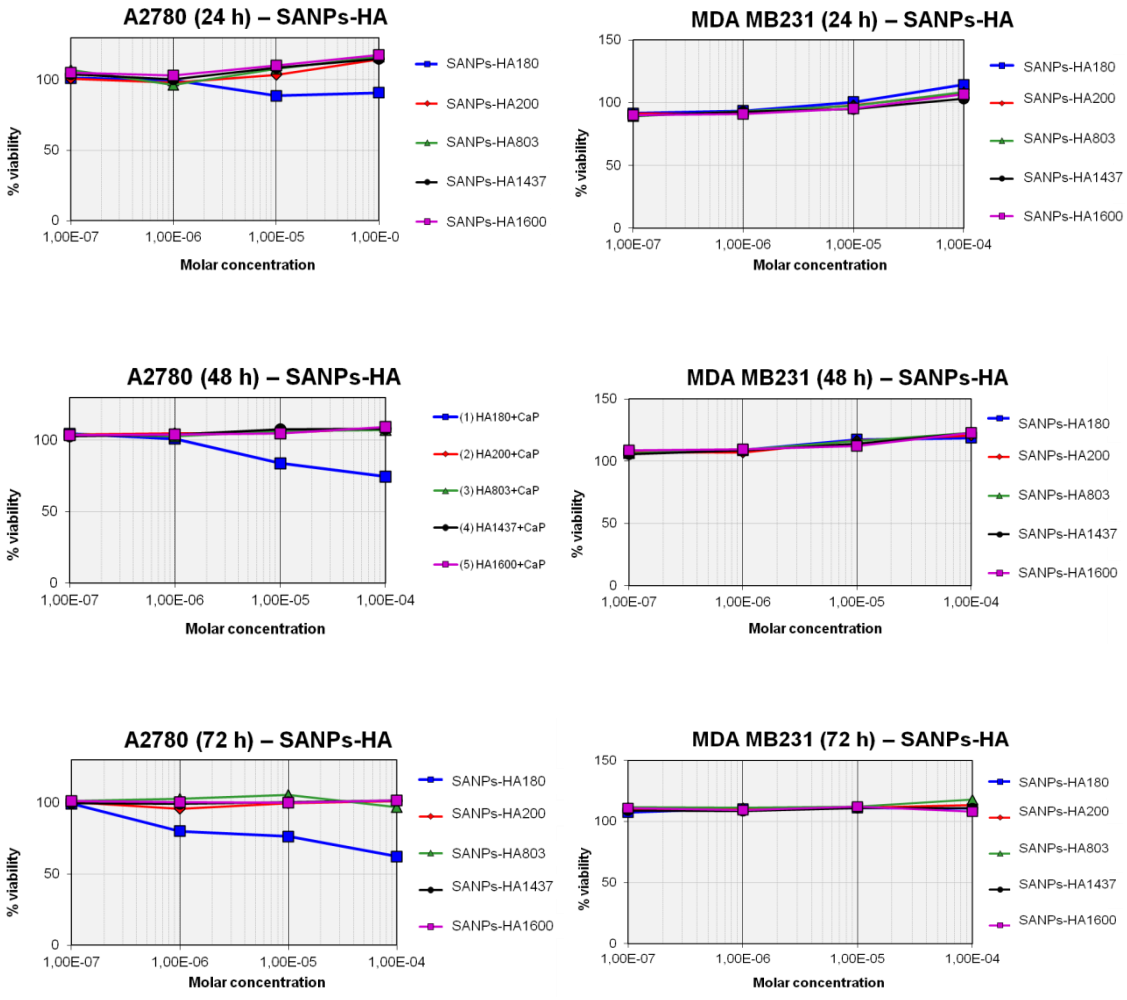

Figure 5.4.6.2: Cytotoxicity of SANPs-HA at 24, 48 and 72 hours on A2780 (left) and MDA MB231 (right).

On the other hand, the inclusion of HA on SANPs encapsulating Zol lead to increase of Zol cytotoxicity. In particular, SANPs-HA-Zol showed no toxicity on MDA MB231 (CD44+) and slight toxicity (20%) on A2780 (CD44-) at 24 hours. At 48 hours, a slight toxicity was showed for SANPs-HA-Zol based on HA 180 and HA 803 (10%) and for SANPs-HA-Zol based on HA 200 (25%) and a moderate toxicity was showed for SANPs-HA-Zol based on HA 1600 (32%) and HA 1437 (40%), on MDA MB231 (CD44+). The IC50 was obtained at 48 hours on A2780 (CD44-), namely 4.5×10^{-5} M, 4.5×10^{-5} M, 5×10^{-5} M and 8×10^{-5} M, in the case of SANPs-HA-Zol based on HA 180, 200, 803 and HA 1437, respectively; IC50 was not obtained for SANPs-HA-Zol prepared with HA 1600. Finally, at 72 hours, the IC50 was obtained for all SANPs-HA-Zol on both cell lines. In particular, the IC50 obtained on A2780 (CD44-) corresponds to 3×10^{-5} M for all SANPs-HA-Zol; the IC50 obtained on MDA MB231 (CD44+) corresponds to 2.5×10^{-5} M for SANPs-HA-Zol based on HA 1600 and HA 1437, to 3×10^{-5} M for SANPs-HA-Zol based on HA 200 and to 3.2×10^{-5} M for SANPs-HA-Zol based on HA 803 and HA 180. These preliminary results suggested that the inclusion of HA into the formulation increases Zol cytotoxicity independently on the CD44 overexpression. From our previous experience, we know that A2780 are cells more sensitive to chemotherapeutics agents. Here, we found that the inclusion of HA on SANPs lead to an increased Zol cytotoxicity reasonably for the higher Zol uptake into the cells; the presence (although at low levels) of CD44 on A2780, together with the higher sensitivity of these cells, could be responsible to the higher cytotoxicity of SANPs-Zol-HA on these cells. Despite a lower sensitivity to chemotherapeutics, the enhanced cytotoxicity of SANPs-Zol when targeted with HA should be due to the highest level of CD44 receptors characterizing these cells. The relationship between HA on SANPs and the higher cytotoxicity is also suggested by the slight increase of the toxicity when the HA molecular weight increases. Further studies should confirm these finding and clarify the dependence of HA molecular weight and SANPs-HA uptake.

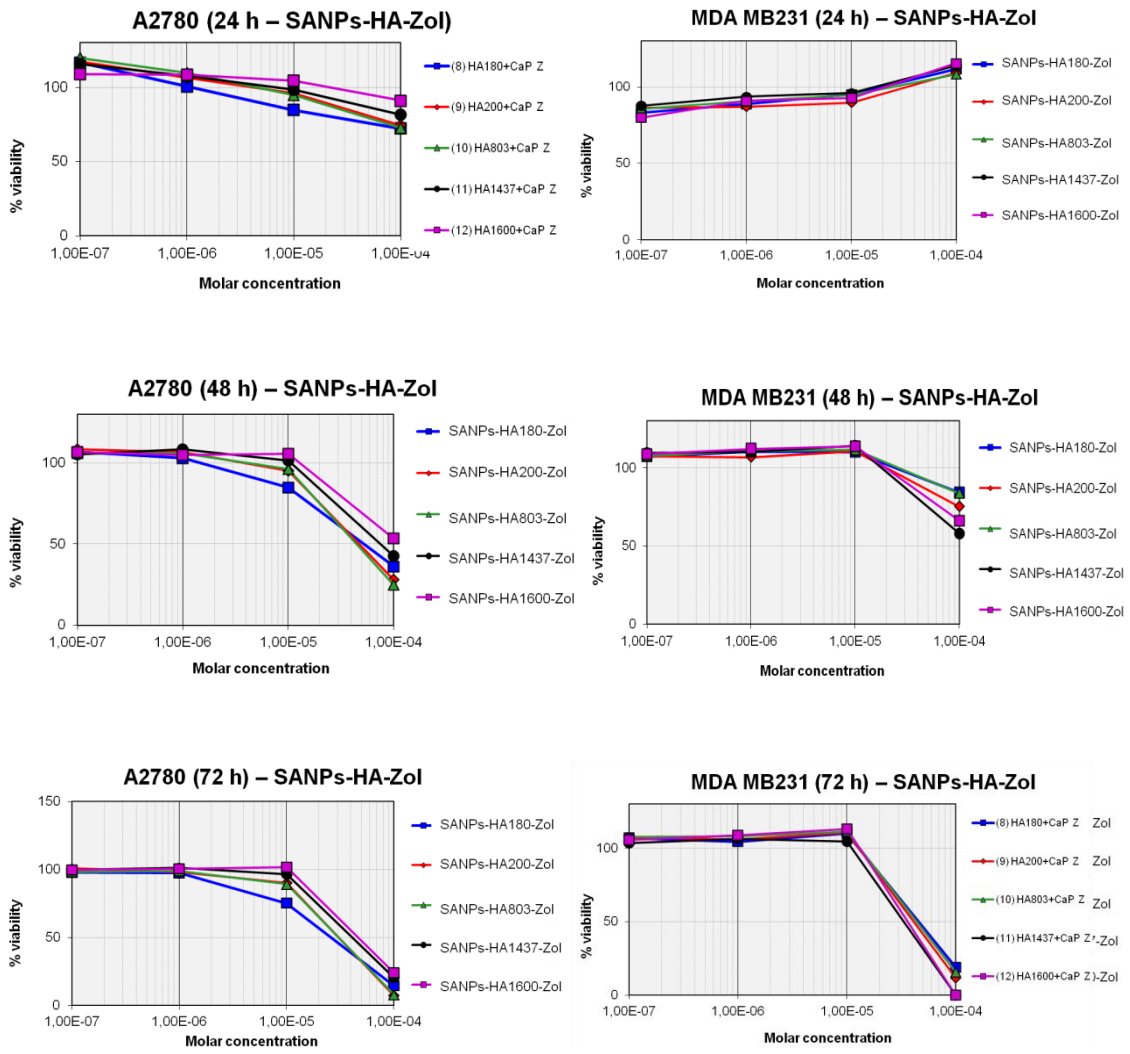

Figure 5.4.6.3: Cytotoxicity of SANPs-HA-Zol at 24, 48 and 72 hours on A2780 (left) and MDA MB231 (right).

Cytotoxicity - IC50 (M)						
Formulation	MDA MB231 (CD44+)			A2780 (CD44-)		
	24 hours	48 hours	72 hours	24 hours	48 hours	72 hours
SANPs-Zol	-	-	-	-	-	-
SANPs-HA180	-	-	-	-	-	-
SANPs-HA200	-	-	-	-	-	-
SANPs-HA830	-	-	-	-	-	-
SANPs-HA1437	-	-	-	-	-	-
SANPs-HA1600	-	-	-	-	-	-
SANPs-HA180-Zol	-	-	3.2×10^{-5}	-	5×10^{-5}	3×10^{-5}
SANPs-HA200-Zol	-	-	3×10^{-5}	-	4.5×10^{-5}	3×10^{-5}
SANPs-HA803-Zol	-	-	3.2×10^{-5}	-	4.5×10^{-5}	3×10^{-5}
SANPs-HA1437-Zol	-	-	2.5×10^{-5}	-	8×10^{-5}	3×10^{-5}
SANPs-HA1600-Zol	-	-	2.5×10^{-5}	-	-	3×10^{-5}

Table 5.4.6.1: Cytotoxicity of SANPs-Zol, SANPs-HA and SANPs-HA-Zol.

5.5 Conclusions

This study demonstrated the possibility to adapt the protocol previously developed to prepare self-assembling nanoparticles conjugated with HA for targeting of CD44 overexpressing cells. HA with different molecular weight were conjugated to the SANPs, leading to particles with physical-chemical characteristics suitable for i.v. injection. Some of the prepared formulations resulted stable until 1 month at 4 °C. Furthermore, the zoledronic acid was also loaded as model drug. Although the presence of HA and Zol influence the physical characteristics of SANPs, a high Zol encapsulation efficiency was also obtained. Finally, SANPs-HA and SANPs-HA-Zol, based on the inclusion of PEGylated liposomes and HA 1600 kDa, HA 1437 kDa, 803 kDa, 200 kDa and 180 kDa, were selected for the following *in vitro* studies to evaluate the efficiency of these formulations on cell lines. In preliminary result on two cell lines, a slight increase of the cytotoxicity on MDA MB231 observed with the highest HA molecular weights suggests a targeting effect of SANPs-HA-Zol on CD44-overexpressing cells.

REFERENCES

Alaniz, L., Cabrera P.V., Blanco G. Interaction of CD44 with different forms of hyaluronic acid. Its role in adhesion and migration of tumor cells. Cell Commun Adhes 9:117–30 (2016).

Arpicco S., Lerda C., Dalla Pozza E., Costanzo C., Tsapis N., Stella B., Donadelli M., Dando I., Fattal E., Cattel L., Palmieri M. Hyaluronic acid-coated liposomes for active targeting of gemcitabine. European Journal of Pharmaceutics and Biopharmaceutics. Volume 85, Issue 3, Part A, Pages 373-380 (2013). doi.org/10.1016/j.ejpb.2013.06.003.

Bitter T., Muir H.M., A modified uronic acid carbazole reaction Anal. Biochem. 4 330–334 (1962).

Brigger I., Dubernet C., Couvreur P. Nanoparticles in cancer therapy and diagnosis. Adv Drug Del Rev, 54:631-651 (2002).

Byrne J.D., Betancourt T., Brannon-Peppas L. Active targeting schemes for nanoparticle systems in cancer therapeutics. Adv Drug Deliv Rev, 60:1615-1626 (2008)..

Cho K., Wang X., Nie S., Chen Z.G., Shin D.M. Therapeutic nanoparticles for drug delivery in cancer. Clin Canc Res, 14:1310-1316 (2008).

Chen Z., Chen J., Wu L., Chen J., Cheng H., Pan J., Cai B. Hyaluronic acid-coated bovine serum albumin nanoparticles loaded with brucine as selective nanovectors for intra-articular injection. International Journal of Nanomedicine. 8, Issue 1, 3843-3853 (2013). doi: 10.2147/IJN.S50721.

Choi K.Y., Chung H., Min K.H., Yoon H.Y., Kim K, Park J.H., Kwon I.C., Jeong S.Y. Self-assembled hyaluronic acid nanoparticles for active tumor targeting. Biomat, 31:106-114 (2010).

Cohen Z.R., Ramishetti S., Peshes-Yaloz N. Localized RNAi therapeutics of chemoresistant grade iv glioma using hyaluronangrafted lipid-based nanoparticles. ACS Nano 9:1581–91 (2015).

Dische Z., A new specific color reaction of hexuronic acids. J. Biol. Chem. 167 189–198 (1947).

Gabizon A.A. Pegylated liposomal doxorubicin:metamorphosis of an old drug into a new form of chemotherapy. Cancer Invest. 19:424–36 (2001).

Gust, K.M.; Hofer, M.D.; Perner, S.R.; Kim, R.; Chinnaiyan, A.M.; Varambally, S.; Moller, P.; Rinnab, L.; Mark A. Rubin, Jochen Greiner, Michael Schmitt, Rainer Kuefer*, Mark Ringhoffer. RHAMM (CD168) is overexpressed at the protein level and may constitute an immunogenic antigen in advanced prostate cancer disease. Neoplasia. Volume 11, Issue 9, Pages 956-963 (2009). doi.org/10.1593/neo.09694.

Han, X.; Li, Z.; Sun, J.; Luo, C.; Li, L.; Liu, Y.; Du, Y.; Qiu, S.; Ai, X.; Wu, C. Stealth CD44-targeted hyaluronic acid supramolecular nanoassemblies for doxorubicin delivery: Probing the e_ect of uncovalent pegylation degree on cellular uptake and blood long circulation. J. Control. Release 197, 29–40 (2015).

Hayward S.L., Wilson C.L., Kidambi SHyaluronic acid-conjugated liposome nanoparticles for targeted delivery to CD44 overexpressing glioblastoma cells. Oncotarget 7:34158–71 (2016).

Hertweck, M.K.; Erdfelder, F.; Kreuzer, K.-A. CD44 in hematological neoplasias. Ann. Hematol. 90, 493–508 (2011).

Huang G. and Hualiang H. Application of hyaluronic acid as carriers in drug delivery. Drug delivery. Vol. 25, no. 1, 766–772 (2018). doi.org/10.1080/10717544.2018.1450910.

Kim E., Yang J., Kim O., An Y., Lim E.K., Lee G., Kwon T., Cheong J.H., Suh J.S., Huh Y.M., Haam S. Hyaluronic acid receptor-targetable imidazolized nanovectors for induction of gastric cancer cell death by RNA interference. Biomaterials. 34, 17 4327-4338 (2013). doi:10.1016/j.biomaterials.2013.02.006.

Margalit, R. Bioadhesive liposomes in topical treatment of wounds. In: Cohen S, Berenstein H, eds. Microparticulates: preparation, characterization and application in medicine. New York: Marcel Dekker Inc., 425–61 (1996).

Misra, S.; Heldin, P.; Hascall, V.C.; Karamanos, N.K.; Skandalis, S.S.; Markwald, R.R.; Ghatak, S. Hyaluronan–CD44 interactions as potential targets for cancer therapy. FEBS J. 278, 1429–1443 (2011).

Nagano O. and Saya H. Mechanism and biological significance of CD44 cleavage. Cancer Sci; vol 95, no. 12 (2004).

Nishiyama N. Nanomedicine: Nanocarriers shape up for long life. Nature Nanothec, 2:203-204 (2007).

Ossipov D.A. Nanostructured hyaluronic acid-based materials for active delivery to cancer. Expert Opin Drug Deliv 7:681–703 (2010).

Peer D. and Margalit R. Loading mitomycin C inside long circulating hyaluronan targeted nano-liposomes increases its antitumor activity in three mice tumor models. Int. J. Cancer: 108, 780–789 (2004). doi:10.1002/ijc.11615.

Peer D., Karp J.M., Hong S., Farokhzad O.C., Margalit R., Langer R. Nanocarriers as an emerging platform for cancer therapy. Nature Nanotec, 2:751-760 (2007).

Reed, R.; Lilja, K.; Laurent, T. Hyaluronan in the rat with special reference to the skin. Acta Physiol. Scand. 134, 405–411 (1988).

Ricci M.S., Zong W.X. Chemotherapeutic approaches for targeting cell death pathways. Oncologist, 11:342-357 (2006).

Robert, L. Hyaluronan, a truly “youthful” polysaccharide. Its medical applications. Pathol. Biol. 63, 32–34 (2015).

Rosso F., Quagliariello V., Tortora C. Cross-linked hyaluronic acid sub-micron particles: in vitro and in vivo biodistribution study in cancer xenograft model. J Mater Sci Mater Med 24:1473–81 (2013).

Saravanakumar G., Deepagan V. G., Jayakumar R. and Park1 J.H. Hyaluronic Acid-Based Conjugates for Tumor-Targeted Drug Delivery and Imaging. Journal of Biomedical Nanotechnology; Vol. 9, 1–14 (2013).

Schaefer, L.; Schaefer, R.M. Proteoglycans: From structural compounds to signaling molecules. Cell Tissue Res. 339, 237 (2010).

Sironen, R.; Tammi, M.; Tammi, R.; Auvinen, P.; Anttila, M.; Kosma, V. Hyaluronan in human malignancies. Exp. Cell Res. 317, 383–391 (2011).

Sneath, R.; Mangham, D. The normal structure and function of CD44 and its role in neoplasia. Mol. Pathol. 51, 191–200 (1998).

Taetz, S.; Bochot, A.; Surace, C.; Arpicco, S.; Renoir, J.-M.; Schaefer, U.F.; Marsaud, V.; Kerdine-Roemer, S.; Lehr, C.-M.; Fattal, E. Hyaluronic acid-modified DOTAP/DOPE liposomes for the targeted delivery of anti-telomerase siRNA to CD44-expressing lung cancer cells. Oligonucleotides 19, 103–116 (2009).

Tardi P., Choice E, Masin D, Redelmeier T, Bally M, Madden TD. Liposomal encapsulation of topotecan enhances anticancer efficacy in murine and human xenograft models. Cancer Res; 60:3389–93 (2000).

Telmer, P.G.; Tolg, C.; McCarthy, J.B.; Turley, E.A. How does a protein with dual mitotic spindle and extracellular matrix receptor functions a_ect tumor susceptibility and progression? Commun. Integr. Biol. 4, 182–185 (2011).

Toole B.P., Wight T.N., Tammi M.I. Hyaluronan-cell interactions in cancer and vascular disease, Journal of Biological Chemistry, 277, 4593-4596 (2002).

Toole B.P. Hyaluronan: From extracellular glue to pericellular cue. Nature Rev Canc, 4:528-539 (2004)..

Torchilin V.P. Multifunctional nanocarriers. Adv Drug Del Rev, 58:1532-1555 (2006).

Vichai, V. and Kirtikara, K. Sulforhodamine B colorimetric assay for cytotoxicity screening. Nat. Protoc (2006). 1. doi:10.1038/nprot.2006.179.

Wayne D. Comper, Extracellular Matrix Volume 2 Molecular Components and Interactions. Harwood Academic Publishers (1996).

Widjaja L.K., Bora M., Chan P.N. Hyaluronic acid-based nanocomposite hydrogels for ocular drug delivery applications. J Biomed Mater Res A 102:3056–65 (2014).

Yang L., Song X., Gong T., Jiang K., Hou Y., Chen T., Sun X., Zhang Z. and Gong T. Development a hyaluronic acid ion-pairing liposomal nanoparticle for enhancing anti-glioma efficacy by modulating glioma microenvironment, Drug Delivery, 25:1, 388-397 (2018). Doi: 10.1080/10717544.2018.1431979

Yerushalmi N., Arad A., Margalit R. Molecular and cellular studies of hyaluronic acid-modified liposomes as bioadhesive carriers for topical drug delivery in wound healing. Arch Biochem Biophys 313:267–73 (1994).

Zoller M. CD44 - Physiological expression of distinct isoforms as evidence for organ-specific metastasis formation, J. Molec. Med.-JMM, 73 425-438 (1995).

CHAPTER 6

Summary and future perspectives

The use of nanomedicine is today a pillar for the development of innovative therapeutics. However, the technology transfer and the scale-up often represent limiting steps for a more extensive use of nanovectors. SANPs technology has been developed and proposed as a tool able to fill the gap between an efficient drug delivery and a prototype suitable to be prepared in an industrial setting. However, this represented only a hypothesis without any validation out of a research lab. On the other hand, one of the peculiarities of SANPs is represented by versatility of this system that can be adapted for encapsulation of drugs different than bisphosphonates and for the targeted delivery.

The Ph.D. activity described in this thesis provided insight on SANPs technology investigating some issues related to the technology transfer to an industrial plant and exploring novel delivery applications for SANPs.

The study started from a formulation consisting on Zol-encapsulating nanoparticles with very promising effects in the treatment of glioblastoma, previously demonstrated *in vitro* and *in vivo*. The promising results were obtained with a formulation in which Zol was encapsulated in hybrid self-assembling nanoparticles by mixing four components. The reason of the development of this formulation was to start from components already present on the market or readily available to avoid the step of scale-up, generally encountered when trying to move nanomedicine-based formulations from the bench to the industry. The first research project reported in this thesis was focused on the optimization of a nanomedicine-based product with therapeutic potential in glioblastoma, to adapt the preparation of the components to the manufacturing plant of a pharmaceutical company. Moreover, some preparation methods, i.e. to prepare liposomes and CaP NPs, were changed for future scale up of the formulation. Briefly, this part of the work was focused on an additional development of the formulation that has been planned to adapt the SANPs preparation to the industrial manufacturing process. In this perspective, the single characteristics of the four components were studied and the preparation protocol of each component of the SANPs was modified to adapt the

formulation to an industrial plant. Finally, the first kit of the industrial formulation, named EDROMA, was set up and then assembled to obtain the first EDROMA.

On the other hand, a strategy to freeze-dry SANPs-Zol was studied to simplify their preparation protocol. In particular, the inclusion of different cryoproctectants in the formulation and their influence on the characteristics of the formulation were evaluated to select the additives able to protect the product during the lyophilization. The freeze-dry strategy set up allowed to obtain a product composed by only two components: the dried product and the ampoule with water useful to resospend the dried product. This strategy allows to reduce the mistakes during hospital preparation and to stabilize the product.

Finally, preliminary *in vitro* and *in vivo* studies showed that the dried product has a high efficacy due to the inhibition of GBM cell viability at low concentration and due to the promotion of tumor's regression in an orthotopic model of GBM.

The second research project reported in this thesis was focused on the optimization of the nanomedicine-based product with therapeutic potential in glioblastoma. In particular, the SANPs formulation has been modified for encapsulation and delivery of new nucleic acids, namely microRNA (miRNA), with potential use in therapy of GBM.

More in details, a specific miRNA, e.g. miR603, wild type or methylated, was used as model miRNA for its potential to revert chemoresistance in the treatment of GBM. To this aim, lipid composition, namely the type of cationic lipid, the presence of a neutral lipid and the type of PEGylated lipid, was optimized.

All the prepared SANPs were characterized in terms of size, zeta potential and efficiency of miRNAs encapsulation. Stability of SANPs have been tested in bovine serum albumin (BSA) or plasma; moreover, hemolytic activity of the formulations on red blood cells was investigated. Cytotoxicity of the different prepared SANPs was also tested on two different GBM cell lines. Then, formulations selected in the previous studies were tested for the delivery of the miR603 in two GBM cells. Finally, the biodistribution of the miRNA, when administered with SANPs, was studied in different organs in an orthotopic model of GBM.

The findings underline that the use of the cationic lipid into SANPs is not only mandatory for anchoring the lipid shell to the core, but also able to influence

SANPs architecture, physical and biological stability, and the delivery process. Among the neutral lipid used here, the DOPE provided a slight toxicity in some formulations, thus only SANPs based on DOTAP and DOTAP/chol were selected. Finally, the use of cer-PEG, only in SANPs-miR603 (the uptake of miR603 O-Met was found negligible) provided the highest delivery efficiency, compared to the DSPE-PEG_{2000}. Biodistribution study underlined that such SANPs are able to deliver miRNA 603 in different organs but allowing also accumulation of significant levels of the nucleic acid in the brain in an orthotopic model of GBM. Further studies will clarify if the amounts of miRNA 603 delivered in the different organs, e.g. into the brain, will allow to achieve a pharmacological effect.

Finally, a novel application of SANPs and their preparation strategy has been investigated. In particular, the formulation has been modified with hyaluronic acid at several molecular weights. More in details, this study has allowed to obtain a suitable formulation protocol to prepare self-assembling nanoparticles conjugated with several HA with different molecular weight at established concentration of 0.0125% (p/v). These formulations resulted in good physical-chemical characteristics, which makes them stable until 1 month at 4 °C. Furthermore, zoledronic acid was added in these formulations as model drug. The inclusion of Zol did not affect the SANPs characteristics, showing also a high Zol encapsulation efficiency into the SANPs. On the other hand, the HA determination carried out on both SANPs-HA and SANPs-HA-Zol, allowed to find out a high conjugation efficiency of HA in both complexes. Then, SANPs-HA-Zol, based on the inclusion of PEGylated liposomes and HA 1600 kDa, HA 1437 kDa, 803 kDa, 200 kDa and 180 kDa, were selected to evaluate the efficacy of these formulations on cell lines. In the experimental conditions used here, SANP-HA-Zol showed an increase of the cytotoxicity when increasing the HA molecular weight. These preliminary experiments suggest that HA-targeted SANPs could be a further strategy to use SANPs technology in cancer targeting, although a careful optimization of the SANPs-HA design is still needed.

Therefore, it is possible conclude that this study opens a novel strategy for targeted anticancer treatment modalities and that different ligands could included on SANPs. Taken together, the data obtained in this work could

contribute for additional development of nanomedicine in cancer therapy, demonstrating that optimization of the formulation should also be carried out not only for a more efficient drug delivery but also to facilitate the future industrialization and clinical development of nanotechnology-based products.

From this experience, future use of SANPs technology should focus on novel applications in the delivery of nucleic acid. The first product on the market for the delivery of a siRNA, e.g. ONPATTRO, as well as the approval of the RNA-based vaccines by EMA and FDA against the COVID-19, represent a breakthrough for future development of pharmaceutical products based on nucleic acids. In this context SANPs technology could represent an opportunity to accelerate the industrialization phase of formulation based on nanotechnology and nucleic acids or other anionic drugs.

ACKNOWLEDGEMENTS

This work was carried out thanks to the kind and professional collaboration of Dr. Silvia Zappavigna, Dr. Marianna Abate and Prof. Michele Caraglia (cell culture experiments in Chapter 3 and 4) – University of Campania Luigi Vanvitelli (Naples); Dr. Manuela Porru and Dr. Carlo Leonetti (*in vivo* experiments in Chapter 3 and 4) – Regina Elena National Intstitute for Cancer Treatment and Research (Rome); Dr. Daniele Zonari, Dr. Valeria Bincoletto and Prof. Silvia Arpicco (cell culture experiments in Chapter 5) – University of studies of Turin (Turin); Dr. Nicola Ottolina, Dr. Paolo di Lascio, and Dr. Ivano Morlacchi (activities carried out at the Lisapharma s.p.a. and Sirton s.p.a. plants reported in Chapter 2 and 3) – Lisapharma S.p.a and Sirton Pharmaceutical S.r.l. (Como). I would like to pay my special regards to my friend and colleague, Dr. Virginia Campani – University of studies of Naples Federico II (Naples) – whose assistance was a millestone both before and throughout the whole Ph.D. project. Finally, a special thanks to the tutor of my project, Prof. Giuseppe De Rosa – University of studies of Naples Federico II (Naples) – for providing invaluable guidance and feedback which allowed me to grow both professionally and personally.